

Material Characterization, Modelling and Simulation of Epoxy Moulding Compounds under High Temperature Storage and Temperature Cycling Thermal Ageing

M. Sc.-Ing. Bingbing Zhang

Vollständiger Abdruck der von der Fakultät für Luft- und Raumfahrttechnik der
Universität der Bundeswehr München zur Erlangung des akademischen Grades eines
Doktor-Ingenieurs (Dr.-Ing.)

genehmigten Dissertation.

Gutachter:

1. Univ.-Prof. Dr.-Ing. habil. Alexander Lion
2. Prof. Dr. Ing. Ph.D. Iva Petriková

Die Dissertation wurde am 14.11.2020 bei der Universität der Bundeswehr München
eingereicht und durch die Fakultät für Luft- und Raumfahrttechnik am 09.02.2021
angenommen. Die mündliche Prüfung fand am 18.03.2021 statt.

Acknowledgements

The present work was developed as a scientific employee at the Institute of Mechanics at the Department of Aerospace Engineering of the Universität der Bundeswehr München. At this point, I would like to thank everyone for the support and assistance which was given to me during the study of this work.

My outstanding thanks first go to my doctoral thesis supervisor Prof. Dr.-Ing. habil. Alexander Lion who accompanied me during my work at the Institute. Moreover, I would like to thank Prof. Dr.-Ing. habil. Alexander Lion and Dr.-Ing. Michael Johlitz for the excellent academic education given to me, for their outstanding support, for their great interest in my work. Meanwhile, I would also like to thank Prof. Dr. rer. nat. habil. Günther Dollinger and Prof. Dr. Petriková for great supports to my PhD thesis and defense.

My special thanks also go to Dr. Laurens Weiss and Dr. Khoi Vu from Infineon Technologies AG for financing and technical support of this project.

Furthermore, I would like to thank Prof. Dr. Ir. Jansen, K.M.B and Prof. Dr. Ir. Leo. Ernst for their great supports and special interest in my work.

Apart from this, I would also like to thank all my colleagues at the Institute of Mechanics as well as at Infineon for the great support during my research work.

Finally, I would like to thank my parents and family, especially my wife, Yuanyuan Zhang and my daughter Xuechen Zhang for the great support they provided me during the development of this work.

München, im März 2021

Bingbing Zhang

Kurzfassung

Um dem Gesetz des „Time-to-Market“ zu genügen muss die Halbleiterindustrie die Zuverlässigkeit ihrer elektronischen Produkte in möglichst kurzer Zeit testen. Die experimentelle Testung ist nicht nur zeitaufwändig sondern auch kostspielig. Daher wird häufig ein virtueller Prototyp in Kombination mit der Finiten Elemente Methode (FEM) und passenden Modellierungsmethoden eingesetzt. In [1] wird berichtet, dass etwa 65% der Fehlermodi in elektronischen Gehäusebauteilen aus thermo-mechanischen Ursachen resultieren. Für die Zuverlässigkeit elektronischer Gehäusebauteile spielen die Epoxy Moulding Compounds (EMCs) eine wichtige Rolle als Vergussmaterial. Um die FEM zur Vorhersage und zum Verständnis des thermo-mechanischen Verhaltens elektronischer Gehäusebauteile unter verschiedenen Lastbedingungen nutzen zu können, sollten die Materialeigenschaften der EMCs sorgfältig charakterisiert und passend modelliert werden.

Immer häufiger werden elektronische Gehäusebauteile herausfordernden Umweltbedingungen, wie hohen Temperaturen, hohem Feuchtegehalt, etc. ausgesetzt. Von diesen können besonders die Hochtemperatur-Umgebungen zu irreversiblen Veränderungen der EMCs führen, da es sich bei den EMCs um polymerbasierte Materialien handelt. Diese Veränderungen können auf chemische Prozesse wie die Thermo-Oxidation zurückgeführt werden, und können zu einer Degradation des verwendeten Epoxidharzes führen, welche wir hier als thermische Alterung bezeichnen. Als Folge der thermischen Alterung ändern sich die thermo-mechanischen Eigenschaften von EMCs stark.

Experimentelle Untersuchungen zeigen, dass sich während des thermischen Alterungsprozesses an der Oberfläche der EMCs eine dünne Schicht bildet; die Dicke dieser Schicht scheint sowohl von der Alterungstemperatur als auch von der Zeitdauer der Alterung abzuhängen. Als Ergebnis der Alterung ändert sich das Verhalten des gesamten EMCs (inklusive der dünnen Schicht) über der Dauer der Alterung. Da kein passendes repräsentatives Modell der Materialeigenschaften der langsam wachsenden Oxidationsschicht in EMCs vorhanden ist, ist es schwierig, die Zuverlässigkeit eines Gehäusebauteils für Langzeitanwendungen vorherzusagen. Wegen dieser Limitierung fokussiert sich die vorliegende Dissertation auf die experimentelle Charakterisierung und auf die numerische Modellierung der Alterung von EMCs während der Hochtemperaturlagerung (High-Temperature Storage, HTS) und während Temperaturzykeltests (Temperature Cycling, TC). Letztendlich kann die Änderung der thermo-mechanischen Eigenschaften von EMCs während der thermischen Alterung durch numerische Methoden angemessen modelliert werden. Zusätzlich werden die Änderungen der thermo-mechanischen Eigenschaften von EMCs unter HTS und TC Last-Bedingungen untersucht. Ein Zusammenhang zwischen dem Einfluss von HTS und TC auf die Änderung der Materialeigenschaften von EMCs wird ebenfalls hergestellt.

Auf Grundlage der oben beschriebenen Sachverhalte muss eine passende Modellierungsmethode, einfach und effizient, entwickelt werden um Effekte der

thermischen Alterung von EMCs simulieren zu können und später die Langzeit-Zuverlässigkeit von elektronischen Gehäusebauteilen bewerten zu können. Zunächst sollten für die thermo-mechanische Modellierung die Materialeigenschaften, beispielsweise der elastische Modul oder die thermische Ausdehnung, angemessen charakterisiert werden. Gleichzeitig muss ein geeignetes konstitutives Modell gefunden oder eingeführt werden, um das mechanische Verhalten der Materialien von Interesse unter definierten Belastungszuständen zu beschreiben beziehungsweise zu repräsentieren. Als nächstes müssen geeignete Verifikationsexperimente aufgebaut und durchgeführt werden, um zu beweisen, dass die konstitutiven Gleichungen und die charakterisierten Materialparameter korrekt sind. Letztendlich können die charakterisierten Materialparameter und die Modellierungsmethode für die Simulation echter Produkte eingesetzt werden.

Allerdings ändern sich die thermo-mechanischen Eigenschaften der EMCs während des thermischen Alterungsprozesses signifikant. Die Änderung der Materialeigenschaften hängt nicht nur von der Dauer der Alterung sondern auch von der Alterungstemperatur ab. Um diese Änderung der thermo-mechanischen Eigenschaften zu modellieren, wird eine Zweischicht Modellierungsmethode vorgeschlagen, die das Konzept der äquivalenten Dicke einer oxidierten Schicht enthält. Es wird angenommen, dass die mechanischen Eigenschaften teilweise gealterter EMCs mit ausreichender Genauigkeit modelliert werden können, indem eine vollständig gealterte äquivalente Schicht und ein ungealterter Kern modelliert werden. Dieser Ansatz wird mithilfe einer Reihe speziell entworfener Experimente bewiesen. Gemäß dieser Modellierungsmethode müssen die Materialeigenschaften des ungealterten sowie des vollständig gealterten EMCs umfassend und akkurat charakterisiert werden. Zusätzlich wird die äquivalente Dicke der vollständig gealterten Schicht als eine Funktion der Alterungsdauer beschrieben, indem experimentelle Ergebnisse und numerische Analysen von sorgfältig ausgewählten Proben kombiniert werden. Mithilfe der Zweischicht Modellierungsmethode zusammen mit der eingeführten äquivalenten Dicke und den charakterisierten Materialeigenschaften des ungealterten Kerns sowie der vollständig gealterten Schicht können die Gesamteigenschaften eines teilweise gealterten EMCs zu jeder Zeit vorhergesagt werden. Letztendlich werden die Modellierungsmethode und die charakterisierten Parameter von nicht gealtertem sowie vollständig gealtertem EMC durch Bi-Material-Proben verifiziert.

Abstract

Due to time-to-market law, the semiconductor industry needs to evaluate the reliability of the electronic product in a short time. The experimental method is not only time consuming but also costly. Therefore, the virtual prototyping method is generally used by combining the Finite element Method (FEM) and properly modelling methods. As a report in [1], around 65% of failure modes in electronic packages is coming from thermo-mechanical related issues. Among them, the Epoxy Moulding Compounds (EMCs) plays an essential role in the reliability of the electronic package as encapsulation material. In order to use the FEM to predict and understand the thermo-mechanical behaviour of electronic packages under different loading conditions, the material properties of EMCs should be carefully characterised and properly modelled.

Currently, more and more electronic packages are exposed to severe environments, such as high temperature, high moisture, etc. Among them, high-temperature conditions can lead to irreversible changes in EMCs since it is polymer-based material. These changes can be attributed to chemical processes such as thermo-oxidation and can lead to degradation of the applied epoxy resin, which we refer to here as thermal ageing. As a result, the thermo-mechanical properties of the EMCs change severely due to thermal ageing. Due to ongoing changes in the ageing of EMC of a package, the stress and strain distribution in the package change significantly concerning ageing time, while embrittlement also affects the fracture strength. As a consequence, the long-term reliability of a package is severely affected.

The experiment showed that a very thin layer generates on the EMCs surface during the thermal ageing process; the thickness of this skin layer appears to depend on both ageing temperature and ageing time. As a result, the overall properties of the EMC (with skin layer) changes with the storage time. Since an appropriate constitutive representation of the material properties of the slowly growing oxidation layers in EMC is not available, it is cumbersome to predict the reliability of a real package for long-term applications. Due to this limitation, this thesis focuses on the experimental characterization as well as on the numerical modelling of ageing of EMCs at high-temperature storage (HTS) and Temperature Cycling (TC). In the end, the thermo-mechanical properties change of EMCs during thermal ageing can be appropriately modelled by numerical method. Besides that, thermo-mechanical properties change of the EMCs under HTS and TC loading conditions is studied. The relationship between HTS and TC impacts on material properties change of the EMCs is also established.

Based on the above descriptions, an appropriate modelling method, simple and efficient, needs to be developed to simulate thermal ageing effects of EMCs and later can be used to evaluate the long-term reliability of the electronic package. First of all, for the thermomechanical modelling, the material properties should be adequately characterised, such as elastic modulus and thermal expansion. At the same time, a proper constitutive model needs to be found or established to describe or represent the

mechanical behaviour of the interested materials under a defined loading condition. Second, to demonstrate that the constitutive equation and the characterised material parameters are correct, a proper verification test needs to be built and performed to prove that. In the end, the characterised material parameters and the modelling method can be then used in the simulation of a real product.

In this thesis, the thermo-mechanical properties of the EMCs before thermal ageing is systematic characterisation firstly, such as modulus, coefficient of thermal expansion and curing shrinkage. Secondly, based on the measurement data, the responded material constative equation and material parameters are established for modelling. Furthermore, several verification tests are also build up and performed to check the characterised material parameters as well as the modelling method. Finally, the simulation results compare with the verification test.

However, the thermo-mechanical properties of EMCs are changing significantly during the thermal ageing process. The material properties change not only depend on the ageing time but also on ageing temperature. In order to model this thermo-mechanical properties change, a two-layer modelling method is proposed with an equivalent thickness of an oxidation layer concept. It is assumed that the mechanical properties of partly aged EMC can be modelled with sufficient accuracy, by modelling a fully aged equivalent layer and unaged core. This proposal is proved by a series of specially designed experiments. According to this modelling method, the material properties of the unaged and fully aged EMC need to be fully and accurately characterised. Moreover, the equivalent thickness of fully aged layer as a function of ageing time is established by combining experimental results and numerical analysis of properly chosen samples. Combining the two-layer modelling method, established equivalent thickness and characterised material properties of the unaged core and fully aged layer, the overall material properties of a partly aged EMC can be predicted at any time. In the end, the modelling method and characterisation parameters of unaged and fully aged EMC are verified by designed bi-material samples.

Table of Contents

1	Introduction	1
1.1	Motivation.....	1
1.2	Current state of research	4
1.3	The objects and outline of this thesis.....	8
2	Linear Viscoelasticity	11
2.1	Introduction.....	11
2.2	Linear viscoelasticity	12
2.2.1	Relaxation and Creep	12
2.2.2	Constitutive Model: spring-dashpot approximations	15
2.2.3	Dynamic Mechanical Analysis	18
2.2.4	Time-Temperature superposition principle	20
2.2.5	Relation between stress and strain in 3D model.....	24
3	Sample Preparation and Instrumentations	27
3.1	Introduction.....	27
3.2	Sample Preparation	28
3.2.1	Moulding compound	28
3.2.2	Bi-material sample	30
3.3	Testing Machines	31
3.3.1	Dynamic Mechanical Analysis (DMA).....	31
3.3.2	Thermomechanical Analysis (TMA).....	32
3.3.3	Thermal oven.....	34
3.3.4	Profilometer	35

3.3.5	Fluorescence Microscopy	36
4	Characterization and Simulation for Unaged Moulding Compound.....	39
4.1	Introduction.....	39
4.2	DMA testing and verification	41
4.2.1	Temperature Calibration	41
4.2.2	Experimental Results of DMA	45
4.2.3	Viscoelastic model of EMC.....	47
4.2.4	Verification	49
4.3	TMA Measurement	50
4.4	Curing Shrinkage determination.....	52
4.4.1	Measurement	53
4.4.2	Simulation and Discussion	54
4.5	Warpage Measurement of bi-material sample	56
4.5.1	Introduction of test method and sample preparation	57
4.5.2	Warpage measurement and Discussion	58
4.5.3	Simulation	60
4.6	Conclusion	61
5	Thermal Ageing of EMC under HTS and TC Conditions.....	63
5.1	Introduction.....	63
5.2	Modelling approach and Demonstration.....	66
5.2.1	A proposed modelling approach	66
5.2.2	Hypothesis Verification	68
5.3	Fluorescence Microscopy	73
5.4	DMA test for aged samples.....	77

5.4.1	DMA results for Ageing at 175°C	77
5.4.2	DMA results of Ageing at 150°C	80
5.4.3	Comparison between 175°C and 150°C.....	84
5.5	TMA measurement of aged EMC.....	86
5.5.1	TMA measurement of Ageing at 175 and 150°C.....	87
5.5.2	Comparison and Discussion	89
5.6	Thermal ageing shrinkage of EMC.....	91
5.7	Equivalent thickness of the Oxidation layer	93
5.8	Model verification and simulation.....	96
5.8.1	Ageing shrinkage measurement and determination	96
5.8.2	Model verification (175°C and 150°C)	99
5.9	Conclusion	105
6	Conclusion of project	107
6.1	Limitations and Recommendations	108
7	Appendix.....	109
7.1	List of Figures.....	109
7.2	List of Table	115
7.3	Symbols	116
7.4	Abbreviation	117
8	Reference.....	119

1 Introduction

1.1 Motivation

Microelectronics technology is one of the most crucial competitive area as well as the fastest-growing field in the world. The total value of the semiconductor industry in 2017 reached more than 430 billion dollars. Of course, it will dramatically grow in the future because semiconductor products are widely used in many application fields, including computing, communication, entertainment, automotive, aerospace, and so on.

It is well known, that the microelectronic industry is originated from the invention of the transistor in 1947 at Bell laboratories, and the integrated circuit (IC) build independently at Texas Instruments and Fairchild Company 12 years later. After that, significant trends in microelectronics were the drives for smaller, faster, more reliability and less expensive IC's. A previous president of Intel found a trend of chip development: The number of transistors in a single chip doubles every 18-24 months. It is the so-called 'Moors law'. Up to now, this law is still a good indicator for the semiconductor industry for the trend in chip development.

Typically, an electronic package consists of an integrated circuit (chip), a lead frame, bond wires, adhesive and encapsulated material as shown in Figure 1-1.

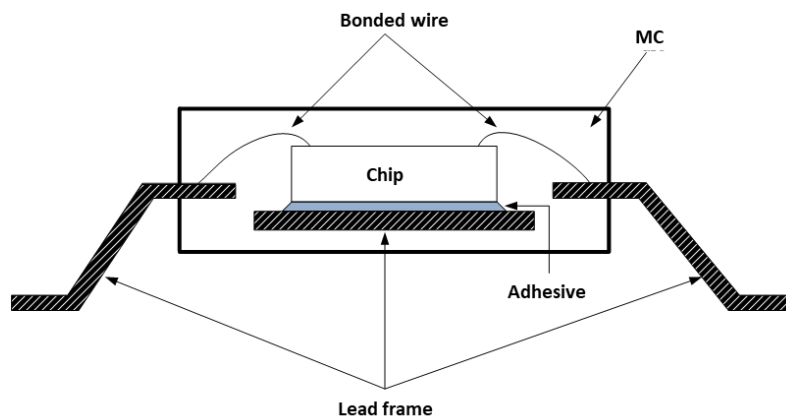


Figure 1-1: Typical structure of semiconductor product

The chip provides the fundamental function of the semiconductor product. The lead frame gives mechanical support for the chip as well as the connection between the chip and the external environment. The bond wires connect the chip to the lead frame for signal transfer. The adhesive connects the chip to the lead frame as well as transfers heat from the chip to the lead frame in order to reduce the junction temperature of the chip itself. The encapsulation material gives the protection of the product to thermal,

mechanical and chemical hazards. The functions of the electronic packaging are to protect, power, and cool the IC chip and to provide the mechanical and electronic connection between the IC chip and the external environment [2].

Based on the encapsulation material, the electronic products are classified into two main types: ceramic and plastic packages. The earliest IC's were packaged in ceramics, which military needed for many years for their reliability and small size [3]. However, those types of packages are not only time consuming to produce, but are also costly. It was too expensive to use them commercially. Since 1960, the manufacturers encapsulated their devices mostly with polymer-based materials because of the low cost and shorter production time. Until now, less than 1% of packages are encapsulated by ceramics due to specific applications, such as for military and aerospace field. They need high performance and high reliability. However, of course the price of those packages is prohibitive. The plastic encapsulation is used for more than 99% of the semiconductor devices in the world. Plastic encapsulation has many advantages, for instance good formability, flexibility, less expensive, low weight and so on. As a result, plastic encapsulation is widely used in the semiconductor industry at the moment.

Epoxy Moulding Compounds (EMCs) are the most popular encapsulation materials in the semiconductor industry. It is typically a thermoset (cross-linked) polymer. It is used for protecting the semiconductor chips from the external environment, for example external mechanical forces and external chemical and physical influences such as moisture, heat and ultraviolet radiation, such that the electrical insulation property is maintained. Also the EMC facilitates the creation of semiconductor packages with a form that allows for easier mounting on a printed circuit board [4]. EMC is made up from various ingredients, such as epoxy resin, silica filler, coupling agent, curing promoter and a release agent, to meet requirements for the reliability, physical properties, and de-mould ability. A general composition, as well as their benefits for EMC, are listed in Table 1-1.

As introduced before, an electronic component includes a chip (silicon), a lead frame (copper alloy), wire bonds (gold, copper or alumina), EMC, etc. These materials have different properties. As a result, the mismatch in material properties will cause reliability issues in the device during thermo-mechanical loading. Thermo-mechanical loads inducing reliability-related issues of electronic packages is one the primary concern in the semiconductor industry. For instance, interface delamination, chip cracking, encapsulated material cracking, solder joint cracking are observed phenomena. There is a report showing that the thermo-mechanical related failures in the product are around 65% of the total failures in the product [1]. Currently, this situation is becoming more critical than before due to further miniaturisation and the integration of multi-functions in the microelectronic packages.

Meanwhile, packages require to remain functional at high temperatures for a very long time. Especially for automotive applications, the reliability requirements are becoming quite high, while more and more components are used in a car, such as for tire pressure sensors, engine control systems and automatic control. The electric components are required to operate at temperatures of 175°C to 200°C (or even higher in the future, according to [5]).

Table 1-1: Typical ingredient of EMC as well as their benefits

Major components	Percentage	Benefits
Epoxy resin	5-10%	High adhesion strength, superior chemical resistance, moisture resistance, superior electrical properties, low curing temperature and son on
Filler	70-90%	Reduces the coefficient of thermal expansion and moisture absorption, low cost, high thermal conductivity
Coupling agent	<1%	Strengthens the adhesion at the interface between filler and resin matrix
Cure promoter	<1%	Reduces the curing time
Flame retardant	<1%	Prevents flammability
Release agent (wax)	<1%	Increases the mould-release ability

The electric component operating at such a high temperature, which is usually larger than the glass transition temperature of the moulding compound, could lead to reliability issues of the package itself. Known are wire bond degradation [6]–[8], moulding compound degradation [9]–[11], solder joint degradation [12]–[14], and interface degradation [15]–[18]. Regarding the above issues, most of the reliability problems are coming from the degradation of the EMC. Firstly, EMC is a polymer-based material, whose mechanical properties will experience irreversible changes during high-temperature storage (HTS). These changes can be attributed to chemical processes such as oxidation and degradation of the applied epoxy resin. Meanwhile, the volume of EMC will decrease during HTS. Due to changes in the material properties and shrinkage of the EMC, the state of stress and strain in a package changes significantly. Secondly, the EMC contains several components, among which halogens or halogen-containing molecules being split-off from the epoxy resin during HTS. These could result in corrosive reactions with intermetallics, weakening the bonds mechanically. In the end, the bonds can fail. Thirdly, the degradation at the interface between EMC and lead frame will reduce its adhesion properties and will finally lead to delamination in the package. All in all, the degradation of EMC under HTS is a complex process, which includes physics, chemistry and thermo-mechanics. Therefore, it is a challenging topic for the investigation due to its multidisciplinary character.

Due to its complexity, many researchers are focusing on the topic of environmental

effects on the package reliability to understand the mechanisms behind those issues for future improvement. In this thesis, the primary concern is being able to predict the thermo-mechanical behaviour of EMC after thermal ageing. To achieve this goal, three things need to be done. The first thing to be done is the characterization of the thermo-mechanical properties of the EMC during ageing. The second thing is the development of a proper modelling method to take the thermal ageing effects into account. The third thing is combining the characterization parameters and the established modelling method to predict or simulate the package behaviour during thermal ageing. An adequate material property characterization and model description forms an important input for simulations and thus are essential to achieve high quality and high accuracy simulation results. The next section will give an overview of the current state of research on this topic.

1.2 Current state of research

The term ageing denotes changes in physical and chemical properties with respect to a reference case. There are, actually, many different ageing mechanisms depending on the materials and the ageing conditions, for instance, the ageing temperature and the oxygen pressure. Meanwhile, ageing includes physical and chemical ageing. Physical ageing reflects a molecular arrangement over time (it is reversible) because the polymer is not in a state of thermodynamic equilibrium below its glass transition temperature [19]. However, chemical ageing reflects irreversible changes in the molecular chains of polymer-based materials, such as chain rupture, additional cross-linking, etc. [20]. In the present research, chemical ageing is only of concern, because the ageing temperature is higher than the glass transition temperature of the concerned EMCs.

Because of the thermo-mechanical properties mismatch of adjacent materials inside the package, during the assembly process and the application phase, the changing behaviour of the EMC significantly impacts the package reliability. In order to quantify the effect of the EMC on the package reliability, experimental qualification and finite element (FEM) simulations are typically used. However, experimental analyses are not only time consuming and costly, but also do not give detailed information of the impact of the EMC on the package reliability. The FEM gives the possibility to improve or solve the above issues. The characterisation of each material, as well as proper material models to describe the material behaviour during the various loading conditions, form an essential part of FE analyses. Besides, engineering skills and engineering judgement are required to well execute and interpret the FEM simulations. By using the Finite Element (FE) method the state of strain and stress inside the package for various loading conditions can be analysed as a function of time. The behaviour of the whole package can be explored by FE simulation and the risks for damage (such as chip cracking, delamination risk, package warpage, etc.) can be considered. In this manner, the package reliability can be optimized already in the design phase, before the actual production phase.

For using the FEM to predict or simulate the effects of EMC-ageing on the package

reliability, the material characterisation has to be done first, and then a proper material model should be constructed to describe the mechanical behaviour of the aged EMC. Understanding how the mechanical behaviour of the EMC changes during thermal ageing is a vital part of the present thesis.

As we know, EMC is a polymer-based material which has strong time- and temperature-dependent mechanical properties like other polymeric materials. Hence, the creep and relaxation behaviour of EMC in the package during the assembly process and/or the application phase will cause a redistribution of stress and strain inside the package. However, due to the limitation of computing resources or just for simplicity, in the past for most of the thermo-mechanical simulations of packages an elastic material model was used for the EMC. As a result, the simulation results, such as the state of stress and strain, generally are not representing reality. [21]–[23] show how the simulation results differ if an elastic model is used instead of a more realistic viscoelastic model of EMC. For instance in [23], significantly lower die stresses are found when the viscoelastic model of EMC is used for package assembly process.

To obtain an accurate viscoelastic model of EMC for simulation purposes, two categories of methods to characterise the viscoelastic properties are typically used. One is time domain testing (relaxation or creep testing), and another is frequency domain testing, the so-called Dynamical Mechanical Analysis (DMA). Based on the measurement results and the assumption of a thermorheologically simple material the master curve was constructed by using the time-temperature superposition method [24]–[26]. Many researchers report on how to generate the viscoelastic model of EMC based on the above methods ([27], [28], [29]). It leads to a more accurate prediction and more realistic results regarding stress or warpage assessment through simulations ([30], [31]).

For most application cases of EMC in packaging, the strains in the EMC remain relatively small, such that the linear viscoelasticity theory can be used [32]. However, in some exceptional cases, when the strains in the EMC are relatively large, the linear viscoelasticity theory will not be suitable. In such a case, a nonlinear viscoelastic model has to be established and used in FE modelling ([33]–[36]). In the present work, a linear viscoelastic material model of EMC is used. In addition to linear viscoelasticity models, several researchers are focusing on establishing a cure-dependent viscoelastic model of EMC. Such a model facilitates the prediction of the stress- and strain field in a package during the moulding process [37].

A standard mechanical characterisation of the materials of interest in a package could be sufficient for the FE simulation to analyse the package stress- or strain fields during the assembly process as well as for the application phase. However, in many cases the packages will service for years and are exposed to environments with high temperatures and high humidity levels. As a consequence, the EMC will face material degradation, which in turn can strongly change the state of stress- and strain in a package. Therefore, more and more attention is given to the effect of environmental and operational conditions, in particular on the performance of the encapsulation materials ([38], [39]). Because high-temperature conditions can lead to irreversible changes in EMCs, these changes can be attributed to chemical processes such as oxidation and can

lead to degradation of the applied resins, which we will refer to as ageing. As a result, the thermo-mechanical properties of the EMCs change severely with time. Due to ongoing changes in the EMC of a package, the stress- and strain distributions change with time, while possible embrittlement could affect the fracture strength. As a consequence, the long-term reliability of a package is severely affected by ageing.

Long-term storage of EMCs under temperatures above its glass transition temperature has a significant effect on the thermo-mechanical properties mainly due to degradation of the polymer system. It has been widely studied in the past, that this can lead to severe reliability issues of a package ([5], [37], [40]). Here, the EMC plays an essential role, because the degradation of the EMC not only changes the thermo-mechanical properties but also releases some destructive substances, for instance halogens.

[41] reported that the ingredients of compounds have a more significant influence on the device reliability than other factors that should be taken into account during HTS condition. [42] shows that EMC aged at 200°C will undergo carbonisation, decreasing the insulation resistance. As a result, the insulation between wires and leads provided by the EMC is significantly reduced. [43] and [44] found that after long-term HTS, the dielectric strength of the EMC drops significantly of 60-70%. [9], [45] and [46] used FEM simulations to check the stress state of a package once the EMC is aged. They found that the stress inside the package increases dramatically. Based on the above analysis, the thermal ageing is not only changing the mechanical properties of the EMCs but also changes the chemical properties as well as the electrical properties.

Mechanical property changes of aged EMCs, such as the coefficient of thermal expansion, the modulus and the glass transition temperature, will lead to significant stress- and strain changes inside the package due to changing material property mismatches. For quantitative analyses, the thermo-mechanical properties should be characterized before and after the thermal ageing treatment. [6], [7], [10], [45], [47]–[50] are using thermo-mechanical analysis (TMA) equipment and dynamic mechanical analysis (DMA) equipment to measure the mechanical property changes of the EMC during thermal ageing. All measurement results show that the modulus, especially in the rubbery state increases significantly compared to the unaged state. Moreover, the glass transition temperature obtained at the peak of $\tan\delta$ from 1 Hz DMA measurements is shifting to higher temperatures with increasing ageing time. However, the CTE does not show a trend of change such as seen for the modulus. Above the glass transition temperature (of the unaged EMC), the CTE decreases about 10-20% in [8]. While in [10], [45] and [47] the CTE value above T_g (of the unaged EMC) is increasing. The CTE value below T_g (of unaged EMC) is more or less constant.

The mechanical property changes of EMCs must be related to the chemical composition change during thermal ageing. [11] reports the degradation mechanism of EMC at 200°C HTS by using various test setups. The increase of both the modulus and the T_g during thermal ageing is due to the additional cross-linking being generated. Meanwhile, the (relative) percentage of oxygen and silicon is increasing at the outer layer of the EMC (or aged layer), and the percentage of carbon is reducing. The ageing will also increase the modulus of the EMC. However, the CTE is not discussed in this

paper. Based on the analysis in [11], the CTE is expected to be reduced because the silicon content is increased. It is well known that higher silicon content will decrease the CTE of EMCs.

Recent requirements from the semiconductor industry show that there is a pronounced need for the development of a reliable, predictive mechanistic and efficient model to describe the effects of isothermal ageing at elevated-temperature on the package reliability. Because the electric components, for example in automotive or aerospace applications, are often used in harsh environments, such as high temperature and/or high moisture. Electronic components working in those conditions could be easier experience reliability issues, and then the performance function of those components could get lost. Once there is adequate ageing modelling available, it will be possible to perform proper ageing simulations, already in the design phase. This in turn will result in proper design choices, such that the realized package will most probably pass the required test qualification at once.

[51] analyses the degradation of an epoxy adhesive under various thermal ageing conditions, for instance, non-isothermal and isothermal, within air and vacuum ovens, respectively. They found that the degradation of the epoxy adhesive occurs in two stages. In the first stage, molecular chain scission occurs by thermolysis. During this process, the system is thermally stable due to molecular (re-) arrangement. The mechanical properties of the adhesive remain stable in this stage, without any change. In the second stage, thermo-oxidation occurs only in oxygen environment. This leads to severe changes in the mechanical properties of the adhesive material. However, the adhesive remains relatively stable in nitrogen environment as well as in vacuum even for long-term storage.

[52] proposes a degradation mechanism based on some assumptions on the thermoset matrix. The degradation firstly occurs by thermolysis. Free radicals and volatiles are generated in this process. Then, the free radicals undergo a chemical reaction with the diffused oxygen. This reaction process is finished after a stable oxide is created. Based on this degradation mechanism, Colin et., ([53]–[56]) develop a kinetic model to predict the oxidation layer growth in a poly-bismaleimide material during thermal ageing under various temperatures. This kinetic model is based on a differential equation in which oxygen diffusion and consumption are coupled. In order to accurately predict the thickness of the oxidation layer, growing into the neat resin material, the parameters of the oxygen diffusivity, solubility and the reaction rate are required and need to be determined by experimental measurements. Meanwhile, this model could also allow for the prediction of the density change and weight loss during thermal ageing. By using this kinetic modelling method, [57] could also accurately predict the shrinkage in volume of a polymer sample.

Besides that, several modelling methods are developed based on different polymer types to simulate the thermal ageing process of specified materials. [58], [59] apply a micromechanical method to predict the oxidation layer growth of PMR-15 reinforced composites during thermal ageing. [60] uses a multiscale homogenization theory together with the finite element method to describe the microstructural change and degradation of polymer matrix composite materials during high-temperature ageing. A

multiscale model based on micromechanical analysis combined with continuum damage mechanics is developed in [61]. This model can be used to predict the lifetime of fibre/matrix composites.

As described in [62], the degradation mechanisms of polymer-based material under high-temperature conditions are of multidisciplinary character, which involve physics, chemistry and thermo-mechanics. From the analysis point of view, a coupled modelling method, such as mechanistic modelling of chemical reactions, thermodynamics of continuous media, homogenisation, fracture mechanics, damage, etc., should be taken into account.

However, for the EMC used asapsulation material for electronic components, in literature there is no adequate modelling method available to take the thermal ageing effect into account in simulations. The current situation of research in this field is still in a characterisation phase just to understand the effects of thermal ageing on the thermo-mechanical properties of the EMCs. Various papers show different results of material property changes of the EMC during thermal ageing. As for modelling, no method is currently available due to the complexity of the ageing process as well as due to a lack of accurate experimental data. To be able to model the thermal ageing effects of EMC, from the simulation point of view, several questions need to be answered first:

- 1) How to accurately characterize the material properties of the EMC during thermal ageing? Because the ageing process is relatively slow, and the oxidized layer is relatively thin, around a few hundreds of micrometres. Proper measurement methods should be chosen and applied to obtain accurate material properties of the EMCs for later simulation.
- 2) How to establish a modelling method to describe the material property changes during thermal ageing? And how to simplify this process? As described before, the thermal ageing process of polymer-based material is multidisciplinary, which includes physics and chemistry. This process is complex. A simplified method should be developed to avoid too much complexity and should easily be implemented into commercial FE software.

How to verify the characterized material parameters as well as the established modelling method? The characterized material parameters and established modelling method will be finally used in simulations of thermal ageing over a long period to evaluate the effects of thermal ageing on the stress- or strain fields in the package. Before being able to do so, the identified material parameters and the modelling method should be applied to a proper sample, that excludes other possible effects during HTS, such as delamination and sample cracking.

1.3 The objects and outline of this thesis

As described before, there is no systematic characterisation method available to monitor the thermo-mechanical property changes of the EMC during HTS (and/or during high-temperature cycling). Almost all researchers focus on the

thermo-mechanical property changes of partially aged samples of EMC. Here the aged EMC is including an aged outer layer and an unaged core. Therefore, the measurement results are obtained from the combination of aged and unaged samples. It could lead to an arbitrary result that cannot be transferred from case to case. Besides, the material mismatch between the aged and unaged parts can result into confusing property results. For example, some researchers show a CTE decrease after HTS. However, other researchers found no change or even a CTE increase after HTS. The CTE measurement results are a combination of thermal expansion of both materials and the material mismatch between the aged layer and the unaged core. In addition, due to the complexity of the thermal ageing of EMC, there is no modelling method available. As a result, there is also no adequate simulation method available for package-level assessment of ageing. According to these issues, the major purposes of this thesis are focusing on:

- 1) Establishing a systematic characterisation method for the unaged and aged EMC to understand and monitor the thermo-mechanical property changes during thermal ageing under HTS as well as under high-temperature cycling (HTC).
- 2) Establishing a simple and efficient modelling method for the complex ageing process simulation
- 3) Implementing this modelling method in standard commercial finite element software to verify this method and to enable future package simulations for HTS and HTC.

In this thesis, Chapter 1 gives an introduction and discusses the goal of the research. Besides, an overview of current and past research on the topic is presented. At the end, the outline of the thesis is briefly shown. Chapter 2 gives a brief introduction of the linear viscoelasticity theory. This theory will be used for describing the thermo-mechanical behaviour of EMC. How to construct the viscoelastic model based on various characterisation methods is also shown.

Chapter 3 discusses the sample preparation and the test equipment being selected, in relation to the fact that the thermal ageing process is quite time-consuming. The sample size should be chosen wisely, such that all measurements can be performed within a limited ageing time and yet to have sufficiently robust samples to be able to well perform all necessary handling. In order to be able to measure the selected sample size with sufficient accuracy, the test setup and methods need to be carefully chosen.

Chapter 4 gives a systematic introduction on how to characterize the material properties, such as the viscoelasticity, the thermal expansion and the curing shrinkage, for the unaged (or fresh) EMC. During the measurement, some important information is given to obtain accurate measurement results. At the end, different validation samples are used to check the reliability of the material parameters and the models obtained on the basis of measurements.

Chapter 5 gives a detailed introduction of how to model the thermal ageing effects on EMC properties. Firstly, a modelling approach is proposed based on the results from a specially designed measurement method. Secondly, the systematic characterisation

process of the EMC during the thermal ageing process is introduced. Here, the model properties, such as viscoelasticity, oxidation layer growth, thermal expansion and ageing shrinkage are established. Thirdly, the proposed modelling method is applied to predict the thermo-mechanical behaviour changes of a specially designed verification sample, which was measured in parallel. Fourthly, the relationship between the material property changes due to ageing of EMC during high-temperature storage and during temperature cycling is established. Finally, a real structure of the package is used to check the accuracy of the modelling method and related input parameters.

Chapter 6 gives the conclusion of this thesis and a recommendation for further works.

2 Linear Viscoelasticity

2.1 Introduction

Thermo-mechanically related issues always occur in microelectronics because of the various materials included in a single semiconductor product, for example, plastic encapsulation, lead frame, silicon and adhesive. These materials have different thermo-mechanical properties, such as differences in elastic modulus, thermal expansion, thermal conductivity, etc. The mismatch of the properties between different materials induces internal stresses and strains during the manufacturing process, under the reliability qualification testing and in the application phase. The induced internal stresses and strains could lead to many thermo-mechanical reliability issues inside the package, such as interface delamination and material cracking. As reported in [1], around 65% of failures in packages are coming from thermo-mechanically related issues. Meanwhile, it is not an easy task to determine the thermo-mechanical stresses or strains in an electronic package due to the complexity of the structure. To be able to analyse the stresses or strains in such a complex structure during thermo-mechanical loading, the FE method is generally applied. The FE method provides a possibility to analyse the stresses and strains in a complex structure during complicated loading conditions. Detailed information on the theory and execution of the FE method can be found in various literature, f.e. [63]. However, many of the FE analyses being performed are not well executed due to a limited understanding of the principles of mechanics. Therefore, this chapter will give a brief introduction to some basics of mechanics needed for this project. In particular, the theory of linear viscoelasticity is discussed.

For a material during loading, the most interesting item for engineering is how the material behaviour under a specific loading will evolve, for instance how the stresses or strains develop with respect to loading time. For the one-dimensional case, a simple relation between stress and strain is represented by the following equation (2-1):

$$\sigma(t) = k(t) \cdot \varepsilon(t) \quad (2-1)$$

Where $\sigma(t)$ is the stress, $\varepsilon(t)$ is the strain, $k(t)$ is a material parameter, depending on the loading time t . However, in most cases, the material parameter also depends on the temperature (T), the moisture concentration (Q), etc. Therefore, the above equation can be extended as:

$$\sigma(t) = k(t, T, Q, \dots) \cdot \varepsilon(t) \quad (2-2)$$

2.2 Linear viscoelasticity

For polymer-based materials, the material behaves time-dependent under loading. It behaves between a purely elastic and purely viscous material. To understand this behaviour, a simple (1D) example is shown in Figure 2-1. A purely elastic and a visco-elastic material are elongated at a constant strain rate. After that, the loading direction is reversed with the same strain rate to see the response stress.

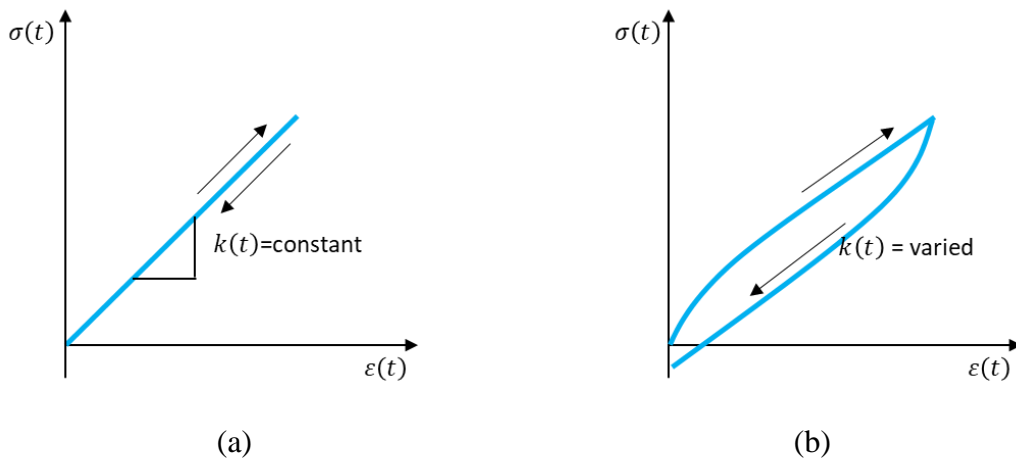


Figure 2-1: (a) Stress-Strain curve of a linear elastic material and (b) Stress-Strain curve of a viscoelastic material

For the purely elastic material (see Figure2-1a), when the strain is linearly increasing (= with constant strain rate), the responding stress also increases linearly. Once the strain reverses, the responding stress is reversed following the same loading path. The slope of the stress-strain curve is called the elastic modulus of the (linear-) elastic material. For viscoelastic material (see Figure2-1b), the material behaves significantly different compared to the (linear-) elastic case. When the strain is linearly increasing with time, the stress is not linearly increasing. When the strain is reversed, the situation becomes more confusing. The reversed curve even does not go back to the origin. Furthermore, the modulus of the viscoelastic material is not constant. It is process-dependent. From the above comparison, the viscoelastic material behaves quite different compared to the linear elastic material under the same loading condition. More tests need to be done to understand the viscoelastic material behaviour and a more complex constitutive model equation will be necessary.

2.2.1 Relaxation and Creep

For a (linear-) viscoelastic material, there are two standard test methods which are typically used to describe the time dependence of the material.

A stress relaxation test considers the decreasing stress in response to an applied

step-strain (Figure 2-2a). Here, typically, a constant strain ε_0 is applied to the material at the time t_0 . The decaying stress response is illustrated in Figure 2-2b. For a linear viscoelastic material, the stress can be expressed as:

$$\sigma(t) = E(t - t_0)\varepsilon_0 \quad (2-3)$$

Where $E(t - t_0)$ is the so-called relaxation modulus. This modulus is time-dependent.

A creep test considers the strain response as a result of a step-stress loading. A constant stress σ_0 is applied to the material at the time t_0 (see Figure 2-3a). For a linear viscoelastic material, the increasing strain as illustrated in Figure 2-3b, can be expressed as:

$$\varepsilon(t) = D(t - t_0)\sigma_0 \quad (2-4)$$

Where $D(t - t_0)$ is the so-called creep compliance, which is also time-dependent.

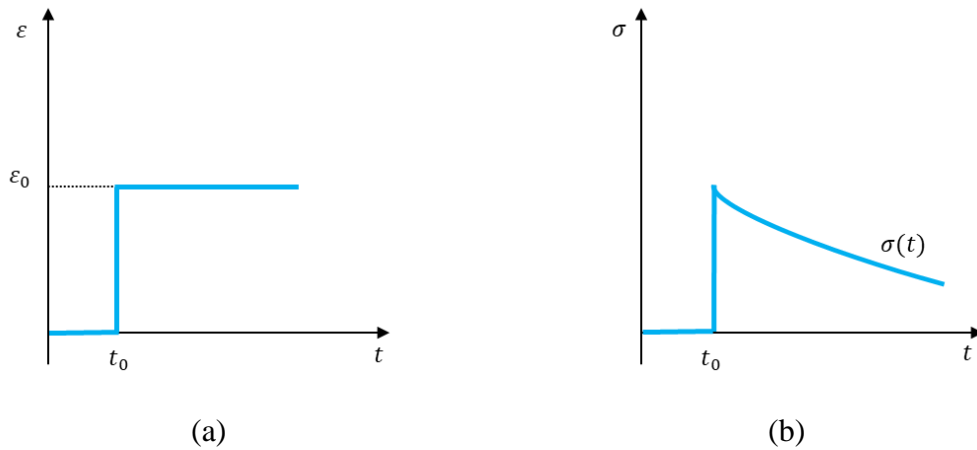


Figure 2-2: (a) Applied step strain ε_0 at time t_0 (b) Induced stress as a function of time

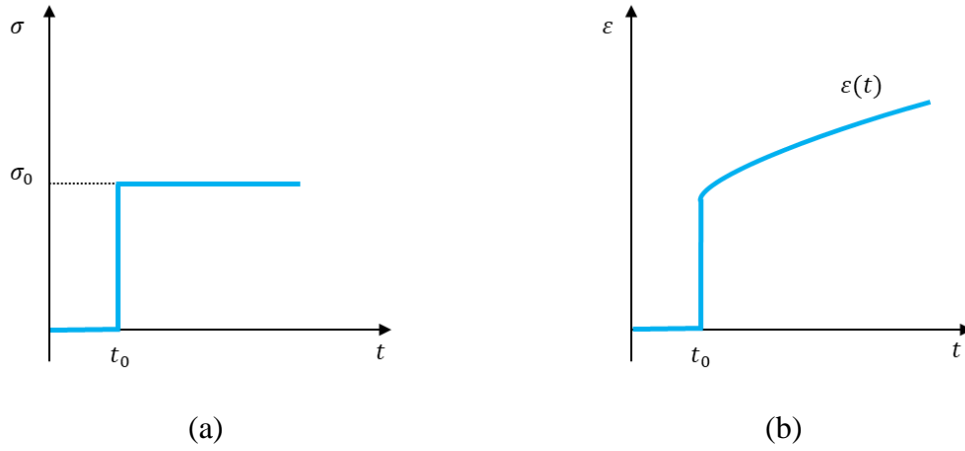


Figure 2-3: (a) Applied step stress σ_0 at time t_0 (b) Induced strain as a function of time

The Boltzmann superposition principle is widely used in formulating models and studying the rheological properties of linear viscoelastic materials. It is known that this method is reliable as long as the deformation of the material remains below its plastic yield limit [25]. This principle shows that the material response to the applied loading is a function of the whole loading history and each loading step independently contributes to the final deformation or stress of the material. Figure 2-4 schematically shows the stress relaxation response to a multi-step loading, in which the incremental strains $\Delta\epsilon_1, \Delta\epsilon_2, \dots$, are loaded at times t_1, t_2, \dots , respectively. Here, linear visco-elasticity of the material is discussed. Therefore, the total stress at the time t after multi-step strain loadings can be expressed as:

$$\sigma(t) = E(t - t_1)\Delta\epsilon_1 + E(t - t_2)\Delta\epsilon_2 + \dots + E(t - t_N)\Delta\epsilon_N \quad (2-5)$$

Where $E(t - t_i)$ is the stress relaxation modulus.

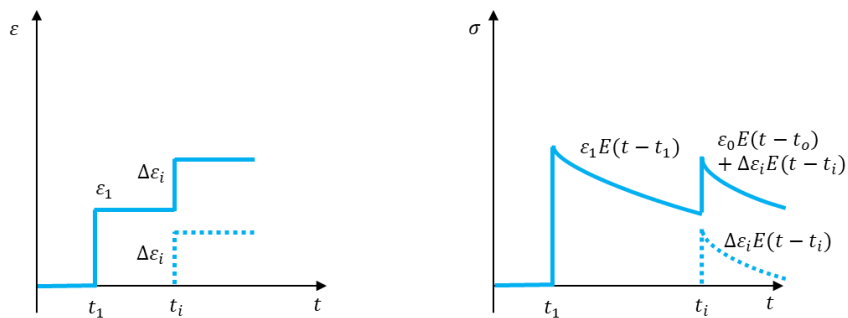


Figure 2-4: Stress relaxation response of a linear viscoelastic material to multi-step loading

By using the symbol ξ for the load application time, equation (2-5) can be expressed as:

$$\sigma(t) = \sum_{i=1}^N E(t - \xi_i) \Delta \varepsilon_i \quad (2-6)$$

By transition of equation (2-6) into an integral form, an arbitrary strain history is assumed to be made up of an infinite number of infinitesimal strain increments ($\xi_i \rightarrow 0$ and $N \rightarrow \infty$). As a result, the integral form of equation (2-6) can be expressed as:

$$\sigma(t) = \int_{-\infty}^t E(t - \xi) \frac{d\varepsilon(\xi)}{d\xi} d\xi \quad (2-7)$$

For stress-controlled loadings, a similar consideration can be modelled.

2.2.2 Constitutive Model: spring-dashpot approximations

The mechanical response of (linear) visco-elastic materials is partly viscous and partly linear elastic dependent on the time scale of the experiment. For a short loading time, the visco-elastic materials behave mainly elastic. The constitutive equation for a purely elastic material is the following Hooke's law:

$$\sigma = E\varepsilon \quad (2-8)$$

Where E is the elastic modulus of the material. An ideal spring would respond similarly. However, for a long-term loading the viscoelastic material behaves (partly) viscous. The corresponding constitutive equation for a viscous material is the following Newton's law:

$$\sigma = \eta \frac{d\varepsilon}{dt} \quad (2-9)$$

Where η represents the viscosity and $d\varepsilon/dt$ is the strain rate. A dashpot would respond similarly.

Typically, linear viscoelasticity can be expressed in principle by models consisting of a combination of a purely elastic spring and a purely viscous damper as visualised in Figure 2-6a and Figure 2-6b. The linear viscoelastic material behaviour under applied loading can be illustrated with a combination of linear springs (such as given in Figure 2-5a) and dashpots (such as given in Figure 2-5b).

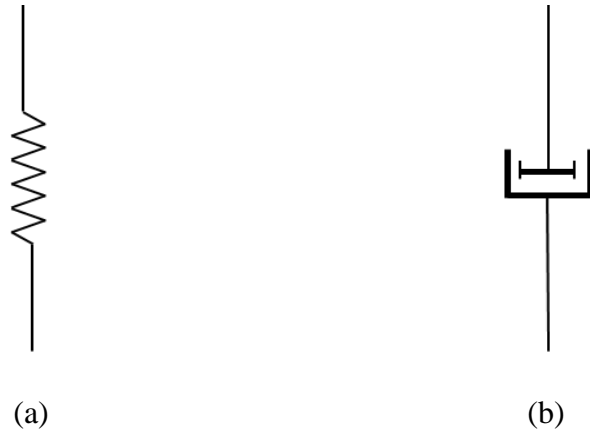


Figure 2-5: (a) spring and (b) dashpot element

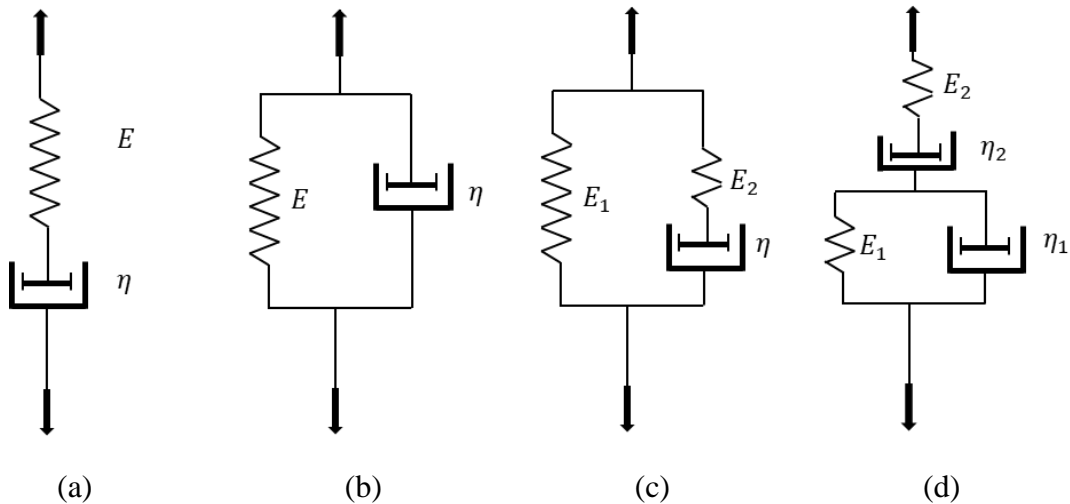


Figure 2-6: simple models: (a) Maxwell model; (b) Kelvin-Voigt model; (c) the standard linear model; (d) the Burgers model

Based on these two simple models of spring and dashpot, some simple but important models are generated by combining these two elements (see Figure 2-6).

Here, only two of them are introduced, the Maxwell model and the Kelvin model. The Maxwell model consists of a spring and a dashpot in series. The Kelvin-Voigt model consists of a spring and a dashpot in parallel. The constitutive equations for the Maxwell as well as for Kelvin-Voigt model are expressed as follows:

Maxwell model:
$$\frac{d\varepsilon}{dt} = \frac{1}{E} \frac{d\sigma}{dt} + \frac{\sigma}{\eta} \quad (2-10)$$

Kelvin-Voigt model:
$$\sigma = E\varepsilon + \eta \frac{d\varepsilon}{dt} \quad (2-11)$$

The Maxwell model (2-10) can also be written in the following manner:

$$\frac{d\varepsilon}{dt} \eta = \frac{\eta}{E} \frac{d\sigma}{dt} + \sigma \quad (2-12)$$

The ratio of η/E is often replaced with the symbol τ , where τ is a characteristic time of the material, the so-called relaxation time of the Maxwell element. For relaxation times much shorter than τ the whole system will respond as being elastic. While for times much longer than τ the whole system responds as a viscous material (the dashpot then determines the response). Therefore, considering a stress relaxation test in the Maxwell model (2-12), with the boundary condition $\sigma = \sigma_0$ at time $t = 0$, equation (2-12) can be solved. The decaying stress can be given by:

$$\sigma = \sigma_0 \exp\left(-\frac{t}{\tau}\right) \quad (2-13)$$

However, the Maxwell model can describe the stress relaxation of real materials as a first approximation. It is unable to describe real creep behaviour. More complex relaxation behaviour cannot be described, since only one relaxation time τ is present in equation (2-13). Similarly, the Kelvin-Voigt model can describe creep behaviour as a first approximation, only. More complex creep behaviour cannot be described. In order to describe real relaxation or creep behaviour of viscoelastic materials, a more complicated model can be constructed by adding more Maxwell elements or Kelvin-Voigt elements together. The most popular model is a generalized Maxwell Model (see Figure 2-7). This model consists of a series of Maxwell elements in parallel. The relaxation function of this generalized Maxwell model can be expressed as follows:

$$E(t) = \sum_{n=1}^N E_n \exp\left(-\frac{t}{\tau_n}\right) \quad (2-14)$$

Here E_n and τ_n are the modulus of the spring and the relaxation time of the n^{th} Maxwell element. This equation is also referred to as a Prony series. The relaxation behaviour of many viscoelastic materials can be accurately described by using a sufficient number of Maxwell elements, with well-chosen relaxation times. Equation (2-20) is very convenient for numerical analysis as well as for fitting experimental relaxation data obtained from dedicated measurements.

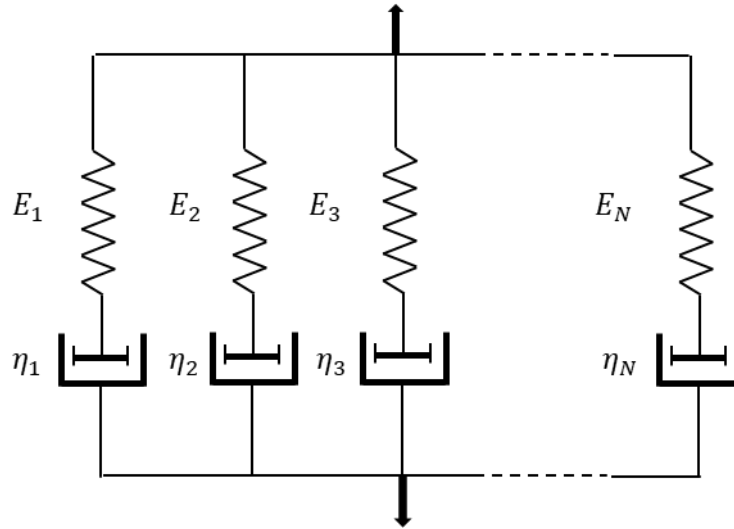


Figure 2-7: Generalized Maxwell model

2.2.3 Dynamic Mechanical Analysis

A dynamic test to obtain useful data for establishing the viscoelastic material model, will first be introduced. In this test, a sinusoidal oscillating loading (or displacement) is applied to the sample. After starting up, the sinusoidal force is measured as well. However, the responding force will be out of phase due to the energy dissipation of the viscoelastic material (see Figure 2-8). The applied loading (or strain) can be written as:

$$\varepsilon(t) = \varepsilon_m \sin \omega t \quad (2-15)$$

In which ε_m is the amplitude of the strain excitation and $\omega = 2\pi f$ is the applied radial frequency in rad/s. f is the natural frequency. The responding stress can be expressed as:

$$\sigma(t) = \sigma_m \sin(\omega t + \delta) \quad (2-16)$$

Here δ is the phase lag. By expanding the equation (2-16), the stress can be expressed to consist of two components:

$$\sigma(t) = \sigma_m \sin \omega t \cos \delta + \sigma_m \cos \omega t \sin \delta \quad (2-17)$$

In order to describe the relationship between the applied strain and the responding stress, two parameters are used. The first parameter is E' , which is the so-called storage modulus. It describes the frequency-dependent elastic properties of the material:

$$E'(\omega) = \frac{\sigma_m}{\varepsilon_m} \cos \delta \quad (2-18)$$

The second parameter is E'' , which is the so-called loss modulus. It is proportional to the dissipated energy:

$$E''(\omega) = \frac{\sigma_m}{\varepsilon_m} \sin \delta \quad (2-19)$$

The relation between E'' and E' is given by:

$$\tan \delta = \frac{E''}{E'} \quad (2-20)$$

If the phase lag δ equals 0° , then the material is purely elastic. If δ equals 90° the material is purely viscous. For viscoelastic materials, the phase lag is between 0° and 90° .

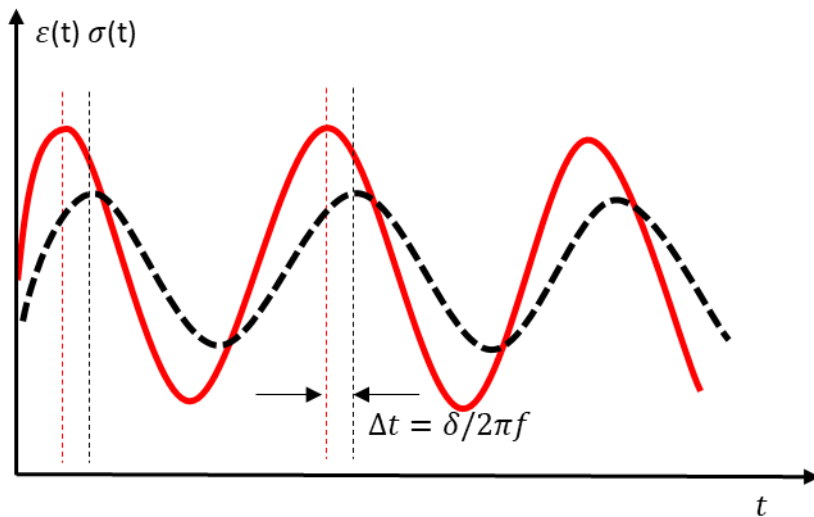


Figure 2-8: Applied dynamic strain (dashed, Black) and responded stress (Red)

As discussed before, a single Maxwell element cannot be used to describe the relaxation or creep behaviour of real polymer materials. Therefore, a generalized Maxwell model is constructed by combining a large number of Maxwell elements in parallel. A generalized Maxwell element which is subjected to a sinusoidal strain results in a storage and loss modulus equal to the following two series:

$$E'(\omega) = E_R + \sum_{n=1}^N \frac{E_n \omega^2 \tau_n^2}{1 + \omega^2 \tau_n^2} \quad (2-21)$$

$$E''(\omega) = \sum_{n=1}^N \frac{E_n \omega \tau_n}{1 + \omega^2 \tau_n^2} \quad (2-22)$$

Here E_R is the modulus in the (so-called) rubbery state. E_n and τ_n are the modulus of the spring and the relaxation time of the n^{th} Maxwell element. The measured storage and loss moduli can be numerically fitted by equation (2-21) and (2-22), respectively. The detailed fitting procedure by using Prony series to experimental data can be seen in Chapter 4. For accurately modelling the relaxation behaviour of polymer materials, normally, more than 10 Prony terms should be used for the modelling. Once the fitting is done, the time-dependent relaxation function of equation (2-14) can be obtained. Therefore, a multi-frequency mechanical loading will be used to test the samples.

2.2.4 Time-Temperature superposition principle

Before introducing the so-called time-temperature superposition method, Figure 2-9 illustrates a measured curve of the 1Hz Storage modulus versus the temperature of a typical cross-linked polymer.

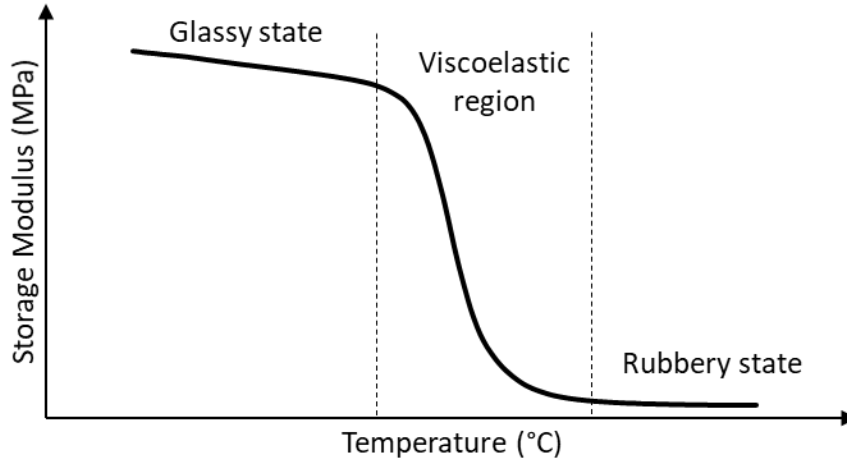


Figure 2-9: Curve of the 1Hz Storage modulus vs. Temperature

Obviously, the curve divides into three parts: Glassy state, viscoelastic region and rubbery state. At low-temperature, the material is in its glassy state and the 1Hz Storage modulus shows a relatively high value. With the temperature increase in this stage, the 1Hz Storage modulus decreases slightly. As the temperature increases, the material goes through the glass transition region and the 1Hz Storage modulus decreases significantly. This region is the so-called viscoelastic region. As the temperature is increased further, the 1Hz Storage modulus reaches the so-called rubbery state. In this state, the measured modulus almost remains constant with increasing temperature. The

Hz Storage modulus of this state depends on the crosslinking density of the material. The measured data firstly can be used to understand the material behaviour under changing temperature. Secondly, it can also be used to build the viscoelastic material model for simulation purposes with additional numerical analysis.

To build the viscoelastic material model of a polymer material, the well-known principle called time-temperature superposition is normally used. This superposition principle is used to determine the temperature-dependent mechanical properties of linear viscoelastic materials from known properties at a reference temperature. Furthermore, the principle of time-temperature superposition requires the assumption of thermorheologically simple behaviour. It implies that the mechanical response at short times or high frequencies is similar to that at low temperature [64].

For thermorheologically simple materials, the viscoelastic response at one temperature can be obtained by the parallel shifting of the viscoelastic curve at another temperature to the left or right without changing the shape of the curve (see Figure 2-10). The corresponding equation can be expressed as:

$$E(T_1, t) = E(T_2, t/a_T) \quad (2-23)$$

The function a_T is called the time-temperature shift factor, T_1 and T_2 are the temperatures. Of course, the relaxation modulus vs. with a logarithmic time axis must be constructed first before doing the shifting. This will be introduced detailed in the next section.

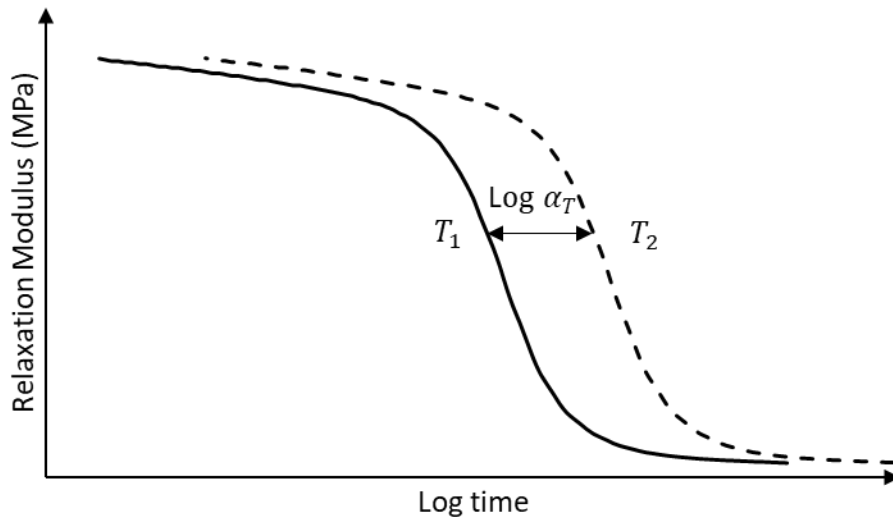


Figure 2-10: Schematic illustration of time-temperature shift

Based on the theory of the time-superposition principle, the procedure is as follows. If the relaxation modulus vs. time is known at a reference temperature, then the related curve at any other temperature can be obtained by horizontal shifting. According to the research of Williams et al., the shift factors at various temperatures are following an empirical equation called WLF equation [65]:

$$\log a_T = \frac{-C_1(T - T_{ref})}{C_2 + (T - T_{ref})} \quad (2-24)$$

The constant T_{ref} is a reference temperature. Usually, the glass transition temperature of the material is defined as the reference temperature. C_1 and C_2 are constants whose values depend on the material and choice of the reference temperature T_{ref} . Based on [65], if the glass transition temperature is used as reference temperature, then the parameters C_1 and C_2 are constant for many amorphous polymers and are equal to 17.44 and 51.6K, separately.

The WLF equation is based on the concept of free volume. This concept is based on the assumption that the polymer molecules do not fully occupy all space in a material. As a result, the total macroscopic volume V is considered as a summation of the ‘occupied volume’ V_0 (volume occupied by polymer molecules) and the ‘free volume’ V_f . Figure 2-11 shows the variation of the specific volume of a polymer with temperature on the basis of dilatometric measurement. The upper curve is the measured specific volume. And the lower blue straight line is the occupied volume V_0 . The difference in the specific volume and occupied volume is the free volume. The fractional free volume, $f = V_f/V$, at any temperature T can be written as:

$$f = f_g + \alpha_f(T - T_g), \quad T \geq T_g \quad (2-25)$$

and

$$f = f_g, \quad T < T_g \quad (2-26)$$

Where f_g is the fractional free volume at T_g , and α_f is the coefficient of thermal expansion of the free volume. The semi-empirical Doolittle equation [66] relates the flow viscosity of amorphous polymers to the free volume in the form of

$$\ln \eta = \ln A + B \frac{V_0}{V_f} \quad (2-27)$$

Where A and B are constants. Rewriting of the equation (2-27) gives:

$$\ln \eta = \ln A + B \left(\frac{1}{f} - 1 \right) \quad (2-28)$$

Thus, the shift factor can be express as:

$$\log \alpha_T = \log \frac{\eta_T}{\eta_{T_g}} = - \frac{B}{2.303 f_g} \left(\frac{T - T_g}{\frac{f_g}{\alpha_f} + T - T_g} \right) \quad (2-29)$$

The parameters η_T and η_{T_g} represent the viscosities of the polymer at the temperatures T and T_g , respectively. If $C_1 = B/(2.303f_g)$ and $C_2 = f_g/\alpha_f$, then equation (2-29) equals the WLF function (2-24). Up to now, how the WLF works is clear. However, from the above deducing, the equation is mostly working above the glass transition temperature of the polymer materials. As a consequence, the WLF equation can be applied only if the interested temperature is above the material's glass transition temperature.

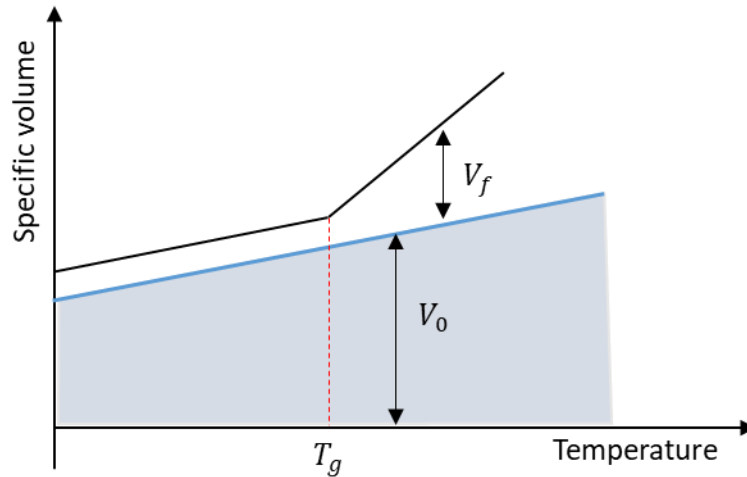


Figure 2-11: Schematic illustration of specific volume vs. temperature

Mostly, the interesting temperature range of the polymer is not only above its glass transition but also below it. Therefore, an Arrhenius equation [25] is used to describe the shifting when the temperature is below the glass transition. The shift factor can be express as:

$$\log a_T = \frac{\Delta H}{2.303R} \left(\frac{1}{T} - \frac{1}{T_{ref}} \right) \quad (2-30)$$

Where ΔH is the activation energy and T_{ref} is the reference temperature.

Based on two equations (2-29) and (2-30), the temperature shift factor can be expressed in the more general form: the generalised Vogel equation:

$$\log a_T = \frac{C}{T - T_\infty} - \frac{C}{T_{ref} - T_\infty} \quad (2-31)$$

Here, C is a constant, T_{ref} is the reference temperature. And T_∞ is a constant temperature. If T_∞ is chosen to be $T_\infty = T_g - C_2$, the Vogel equation is the same as the WLF equation. While if T_∞ is chosen to be 0 K; the above equation is the Arrhenius equation. Therefore, the Vogel equation is capable of describing both WLF behaviour and Arrhenius behaviour. In this thesis, the shift factor is fitted by both WLF and Arrhenius equations at above and below material's glass transition temperature,

respectively. Besides, a polynomial equation is also implemented into the commercial FEM software for comparison purposes. More detailed information will be given in Chapter 4.

2.2.5 Relation between stress and strain in 3D model

The above information shows how to construct the constitutive equation based on the Maxwell element and how to obtain the related parameters for the equation. Once the constitutive equation is known, for example a Prony-series, as well as loading conditions, the stress or strain can be easily calculated.

At the beginning of this chapter, we take a look at the equation (2-1) which shows the relation between stress and strain in the one-dimensional case. In the real world, the sample usually is under multi-axial loadings; such that the stress-strain relation can be expressed in the following form:

$$\sigma_{ij}(t) = \int_{-\infty}^t C_{ijkl}(t - \xi) \frac{d\varepsilon_{kl}}{d\xi} d\xi \quad (2-32)$$

Where σ_{ij} and ε_{kl} are the elements of the stress and strain tensors, respectively. C_{ijkl} are the relaxation modulus functions. For an isotropic material, the relaxation modulus functions include only two components: shear relaxation modulus and bulk relaxation modulus expressed as $G(t - \xi)$ and $K(t - \xi)$, respectively. While the shear modulus is related to the stress response under shape changes, the bulk modulus is related to the volumetric changes. Thus, the relaxation modulus function can be expressed as:

$$C_{ij}(t - \xi) = D_{ij} \cdot G(t - \xi) + V_{ij} \cdot K(t - \xi) \quad (2-33)$$

In equation (2-1) the Voigt-notation has been used in which the stress- and strain tensors, are represented. In this notation, the relaxation modulus tensor of 4th order is represented by a 6X6 matrix.

Where D_{ij} and V_{ij} are the deviatoric and volumetric (constant) coefficient matrices, with

$$[V_{ij}] = \begin{bmatrix} 1 & 1 & 1 & 0 & 0 & 0 \\ 1 & 1 & 1 & 0 & 0 & 0 \\ 1 & 1 & 1 & 0 & 0 & 0 \\ 0 & 0 & 0 & 0 & 0 & 0 \\ 0 & 0 & 0 & 0 & 0 & 0 \\ 0 & 0 & 0 & 0 & 0 & 0 \end{bmatrix} \quad (2-34)$$

and

$$[D_{ij}] = \begin{bmatrix} 4/3 & -2/3 & -2/3 & 0 & 0 & 0 \\ -2/3 & 4/3 & -2/3 & 0 & 0 & 0 \\ -2/3 & -2/3 & 4/3 & 0 & 0 & 0 \\ 0 & 0 & 0 & 2 & 0 & 0 \\ 0 & 0 & 0 & 0 & 2 & 0 \\ 0 & 0 & 0 & 0 & 0 & 2 \end{bmatrix} \quad (2-35)$$

The strain can be divided into the volumetric component and the deviatoric component. Then the stress can be rewritten as:

$$\sigma_{ij}(t) = \int_{-\infty}^t \left[2G(t - \xi) \cdot \frac{d\varepsilon_{ij}^d}{d\xi} + K(t - \xi) \cdot \frac{d\varepsilon_v^{eff}}{d\xi} \right] d\xi \quad (2-36)$$

Where ε_v^{eff} and ε_{ij}^d represent the effective volumetric strain and the deviatoric strains. They can be written as:

$$\varepsilon_v^{eff} = \sum_{i=1}^3 [\varepsilon_{ii} - \varepsilon_{ii}^*] \quad (2-37)$$

$$\varepsilon_{ij}^d = \varepsilon_{ij} - \frac{1}{3} \varepsilon_v^{eff} \quad (2-38)$$

Here, ε_{ii}^* is the initial strain.

As equation (2-36) shows the stress as a function of strain is based on the shear and volumetric relaxation modulus. In the experiment, the storage and loss moduli are measured. As we know the mechanical behaviour of a viscoelastic isotropic material can be completely described by two of four material functions namely: the elongation modulus $E(t)$, the shear modulus $G(t)$, the bulk modulus $K(t)$ and the Poisson ratio $\nu(t)$. Once the elongation modulus and Poisson ratio are known, then the shear and bulk modulus can be calculated according to Table 2-1 [67]. For linear viscoelastic materials, these relation use only valid in the frequency domain.

Table 2-1: Relation between elastic constants

Material constant	Combination of constants					
	G and E	G and ν	E and ν	K and E	K and ν	G and K
K	$\frac{GE}{9G - 3E}$	$\frac{2G(1 + \nu)}{3(1 - 2\nu)}$	$\frac{E}{3(1 - 2\nu)}$			
G			$\frac{E}{2(1 + \nu)}$	$\frac{3KE}{9k - E}$	$\frac{3K(1 - 2\nu)}{2(1 + \nu)}$	
E		$2G(1 + \nu)$			$3K(1 - 2\nu)$	$\frac{9KG}{3K + G}$
ν	$\frac{E}{2G} - 1$			$\frac{1}{2} - \frac{E}{6K}$		$\frac{3K - 2G}{6K + 2G}$

3 Sample Preparation and Instrumentations

3.1 Introduction

This chapter provides a brief introduction of the experimental setups and the measurement techniques adopted during this work. In order to model the effects of thermal-ageing on the thermo-mechanical behaviour of the moulding compound (EMC), the material characterisation procedure constitutes an aspect of utmost importance. The cross-section of an EMC sample which has been aged for several weeks under high temperature is shown in Figure 3-1. Two distinct areas are visible, the outer layer (oxidised layer) and the inner core (unaged core). To model the changes of the EMC, the material properties of both areas must be known. Nevertheless, the characterisation of the oxide layer is a critical aspect, as only few micrometres of oxide are formed after a long ageing period at high temperature. Not only special testing setups and methods need to be developed, but also the sample preparation needs to be seriously considered, in particular the optimal sample geometry should be identified.

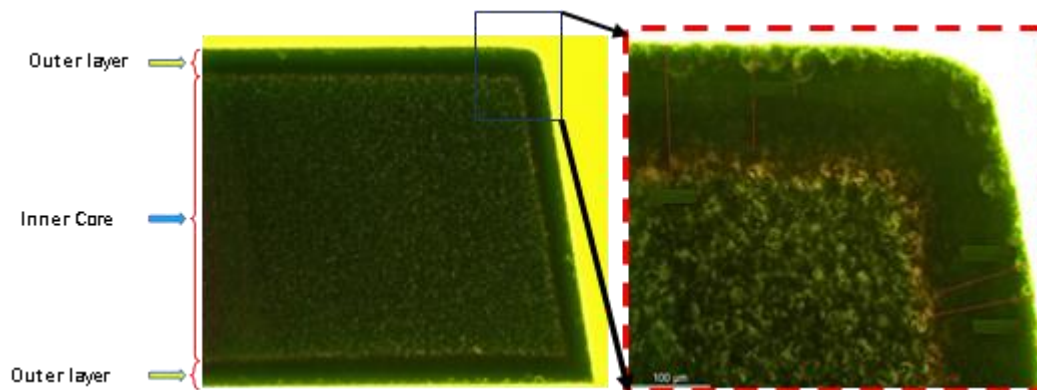


Figure 3-1: Cross-section of aged EMC

Section 3.2 discusses the production and preparation of the samples required for the material characterisation of the moulding compound. In section 3.3, the experimental tools used are briefly introduced.

3.2 Sample Preparation

3.2.1 Moulding compound

As an encapsulating material, the EMCs not only protect the micro-chip against impacts from the external environment but also ensure the mechanical support to the chip-lead-frame system. To meet the stringent customer requirements as well as to save manufacturing costs, an EMC is typically composed of several ingredients: epoxy resin, filler, curing agent, coupling agent, flame retardant, etc. Due to the presence of an epoxy resin, chemical reactions are triggered when the EMC is exposed to high temperature. In order to understand this phenomenon and to model the thermal ageing effects, the material properties of EMCs before and after thermal ageing have to be fully characterised. Based on the above requirements, samples with different geometries are prepared for different purposes. Since the thermal ageing process of an EMC is very slow, the ideal sample and the ageing procedure should fulfil the requirements listed below:

- 1) The sample must be thin enough such that the required ageing time is not too long, but not that thin that the size of the filler particles will influence the measurement results.
- 2) The sample shape should be such that the experimental characterization in the available testing machines is accurate enough.
- 3) The ageing time should be long enough to ensure the stability of the material properties.

In our laboratory, thicker and medium thick EMC strips were moulded by a moulding tool. Normally, the thicker EMC is used in order to perform dynamic mechanical analysis (DMA) using the three-point bending mode while the medium thick sample is used for DMA tests in the tension mode. However, as introduced before, the sample for thermal ageing should be thin enough for saving ageing time. Therefore, the sample geometry should be optimized. Unfortunately, a very thin sample could not be directly moulded by the moulding tool at this moment. As a result, additional setups, cutting and a polishing machine (Figure 3-2), are applied to get the required geometry.

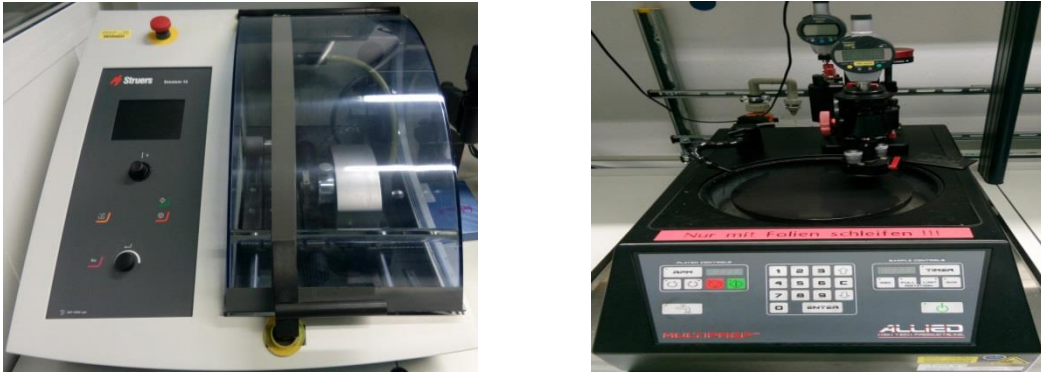


Figure 3-2: Diamond saw and polishing machine

The fresh and medium thick sample is clamped into the cutting machine where the required width is obtained. Subsequently, the sample was installed in the polishing machine for grinding to the desired thickness. As shown in Figure 3-3, four different types of samples were fabricated for different purposes.

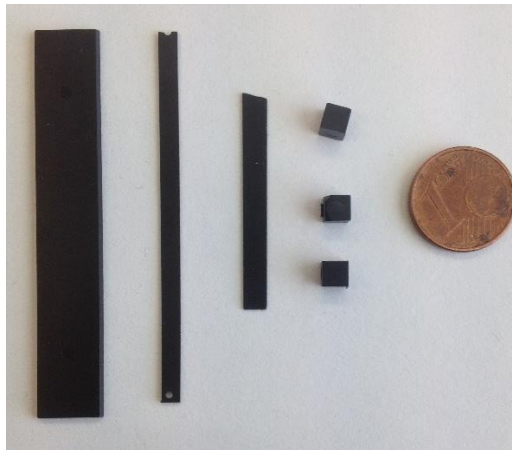


Figure 3-3: Four types of EMC samples

The thicker sample is used to perform a DMA test for deriving the viscoelastic model of the EMC as well as to carry out thickness measurements of the oxide layer via fluorescence microscopy. The medium thick sample is also used to perform DMA tests for creating the viscoelastic model after thermal ageing. The thin sample is used to carry out the DMA tests for creating the viscoelastic model as well as to perform TMA testing for obtaining the coefficient of thermal expansion (CTE) after thermal ageing. The cubic sample in Figure 3-3 is used to do TMA testing for obtaining the CTE values of fresh samples.

3.2.2 Bi-material sample

The material properties and parameters for modelling could be directly obtained from related experimental tests. However, the material model should be checked carefully before applying it to a real package simulation. Based on this, some special specimens are prepared and fabricated. Afterwards, the verification test and the corresponding simulation have to be done to verify the material model and its parameters. In this study, a special bi-material sample which is called Mould Map made of EMC and copper is fabricated to verify the material model before and after thermal ageing. Again, the manufacturing process is the same as the moulding process for a real package. For fulfilling the test requirement, the mould map is cut into strips. The structure of the mould map and the cut sample are shown in Figure 3-4. By using the specially developed test method, the deformation of the bi-material strip was measured under temperature loading. More detailed information about testing and results will be shown in the next chapter.

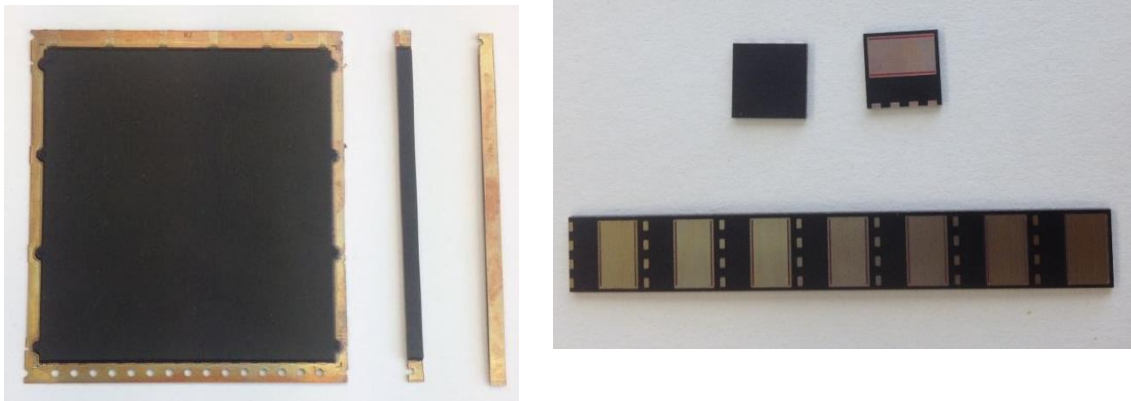


Figure 3-4: Mold Map and strip; single dummy package and strip dummy package

Besides a simple bi-material sample, a bi-material sample with a structured lead frame (see Figure 3-4) was also made for special purpose testing. The single dummy package has the same structure as a real product, but no chip has been included. The strip dummy package includes six single dummy packages. Under temperature loading, the deformation of specimens will be measured and then compared with simulation results based on the established material model. By using these samples, the material model will be independently checked whether it is suitable to simulate a real package structure.

3.3 Testing Machines

3.3.1 Dynamic Mechanical Analysis (DMA)

Dynamic mechanical analysis is a technique used to investigate and characterize material properties as a function of frequency, time or temperature. It is a powerful tool used to study the viscoelastic behaviour of polymer-based materials. During testing a sinusoidal stress (or strain) is applied and then the resulting strain (or stress) is measured. As for polymer materials, the measured strain will have some phase lag with respect to the applied sinusoidal stress. The DMA machine used in this study is (a Q800 from TA instruments) is presented in Figure 3-5 together with the applied clamping systems. Meanwhile, the technical data is shown in Table 3-1. Besides the dynamic testing, the machine could be also used to do static testing, for example: creep and relaxation testing. Various test modes can be selected, such as the three-point bending (3PB) test mode which is normally used to measure thick and high modulus samples; while the tensile mode is normally used to measure thin and low modulus samples; the dual/single cantilever beam mode is used to measure thermoplastic and highly damped materials. In this study, the 3PB and tensile modes are chosen and used to measure the viscoelasticity of EMC samples before and after thermal ageing.



Figure 3-5: DMA machine and clamp systems

Table 3-1: Technical data of Q800 DMA

Maximum and Minimum force	18N and 0.0001N
Displacement resolution	1nm
Frequency range	0.01 to 200Hz
Temperature range	-150°C~600°C
Heating rate	0.1 to 20°C/min
Cooling rate	0.1 to 10°C/min

In this study, the linear viscoelasticity theory was considered due to the application of EMC in electronic packaging. Therefore, all experiments are performed in the regime of a small strain which belong to the geometric linear range. Thereby an amplitude of the sinusoidal load of about 10 μ m is applied for all measurements. The frequency was set from 1Hz to 20Hz and the temperature range varies from 25°C up to 300°C with 1°C/min heating rate. For obtaining good measurement results the chosen settings are very important. For example, the heating rate should not be too high or too low and the applied preload should be low enough, but not too low. In the next chapter, detailed information about how to set the testing parameters is discussed and some tests are done to show how to achieve good results.

3.3.2 Thermomechanical Analysis (TMA)

Thermal mechanical analysis is a technique of measuring the dimensional change of specimens while subjected to a temperature regime. During the testing, a negligible force is acting on the sample for contacting its surface. As a result, the (1D-) dimensional change of a sample can be monitored in real-time. Based on this principle, the TMA is frequently used to determine the coefficient of thermal expansion (CTE) as well as the glass transition temperature (T_g) of polymer materials. Apart from this, various testing modes can be used for different purposes, such as penetration (softening temperature measurement), swelling, shrinkage and so on. In this study, the TMA is mainly used to determine the CTE value of EMC before and after thermal ageing. The TMA machine used here to measure the dimensional change of EMC during heating and cooling is the SDTA841 (Figure 3-6) from METTLER. Table 3-2 shows the technical data of this equipment.

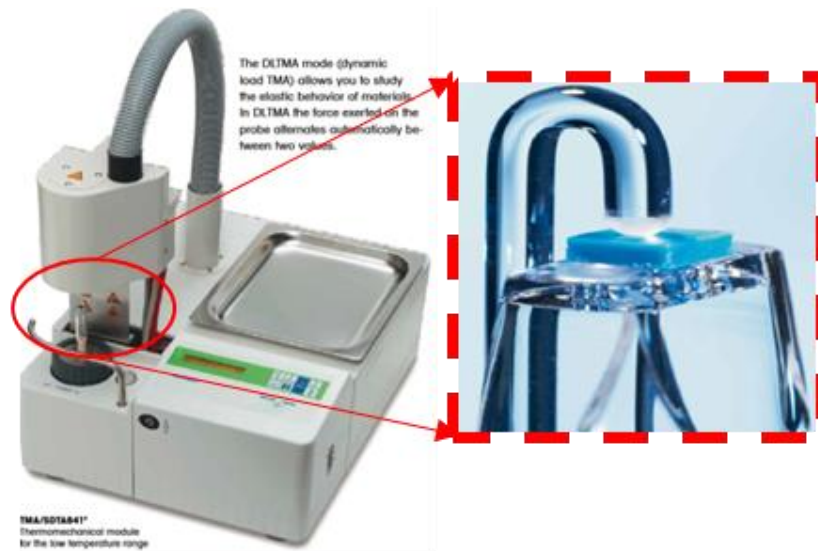


Figure 3-6: TMA machine

Table 3-2: Technical data of TMA

Temperature range	-150°C ~ 600°C
Temperature accuracy	±0.25°C
Maximum sample length	20mm
Measurement range	±5mm
Resolution	<10nm
Force range	-0.1 ~ 1N
Heating (-150°C~600°C)	<8 min

Even though there are testing standards defined for various materials, for example IPC-TM-650 for laminated materials and printed circuit boards, there is no standard yet for EMC, since different types of EMC have significantly different material properties. Therefore, for obtaining accurate results the test conditions should be properly chosen based on the sample status. Meanwhile, before the measurement a precondition should be applied to eliminate physical ageing and moisture effects. Based on some pre-testing results the following test conditions have been applied: heating and cooling rates are 3°C/min with 0.01N preload. At least two temperature cycles are performed and only the second cycle is used to determine the CTE and the T_g . The temperature range is from -30°C to 250°C.

3.3.3 Thermal oven

It is well known that thermal ageing effects the long-term behaviour of components and then could induce reliability problems of a device. The main reason is that the material properties of EMCs will change significantly while accompanied by volume shrinkage, when they are exposed to a high temperature above its glass transition. In order to understand the mechanism of thermal ageing and quantifying the changing material properties, EMCs are stored under three different temperature conditions by using three different thermal ovens which are called: isothermal oven, temperature cycling oven and vacuum oven (Figure 3-7).



Figure 3-7: Temperature cycling oven, isothermal oven and vacuum oven

The isothermal oven is used to cause the material property changes at a constant temperature during chosen ageing times. Two different constant temperatures, 150°C and 175°C, were set in two isothermal ovens. The temperature cycling oven is used to generate the material property changes after a chosen number of temperature cycles.

In the temperature cycling oven there are two parts, the upper part is a hot chamber and the lower part is a cold chamber. When the tested box with the samples is leaving from hot to cold chamber the temperature inside it will change immediately. The temperature profile in the TC oven is chosen as follows: 15min at 150°C and 15min at -55°C.

The vacuum oven is used to investigate the mechanism of material property changes during high-temperature storage in vacuum condition. The temperature in the vacuum oven is kept constant. Two different temperatures are tested: 175°C and 200°C.

After a certain period of ageing in an isothermal oven or a vacuum oven, or after a chosen number of temperature cycles in a temperature cycling oven, a small part of samples is taken out for mechanical testing. Test results will be presented in Chapter 4, together with comparisons between the results from different types of ovens.

3.3.4 Profilometer

The profilometer is used to measure a surface profile of an object. Generally, two types of profilometers are existing, one is the contact profilometer with a diamond stylus used as a surface scanner, the other is contact-free, using an optical sensor. In the present work, a non-contact profilometer (the CT100 from Cyber) with a high resolution down to 3nm and up to 12mm is selected to measure the warpage (out-of-plane deflection) before and after thermal ageing. This comparison is used to verify the material parameters used in the simulation model. The setup is shown in Figure 3-8.



Figure 3-8: Profilometer

The system can scan a maximum area of 150mm width and 150mm length. The samples are located on a granite platform that can move in X- and Y-direction. Above the granite platform the fixed head, equipped with a chromatic white light sensor, is positioned. The sensor is based on the confocal measurement principle and works using chromatic depth scanning. It consists of a light point and a spectrometer. During the testing, different wavelengths from light are projected on different height levels. The spectrometer analyses the wavelengths to calculate the height of the sample.

The sample was measured at room temperature. For each test, at least, three samples need to be measured to check the reproducibility of the measurement results. This setup can also measure the warpage of a sample under temperature loading if an additional

temperature chamber is installed on the granite platform. However, this option was not applied.

3.3.5 Fluorescence Microscopy

In order to visualize chemical changes in the sample during thermal ageing, the fluorescence microscopy technique is used. The principle of fluorescence microscopy is that the sample is illuminated with light of a special wavelength which is absorbed by the fluorophores, causing them to emit light of longer wavelength. More details about this technique can be found in [68]. Based on this technical a colourful image could be visualized from the sample cross-section under the microscope. Before the measurement, the sample must be embedded in a fluorescent material. It is not only to support the sample but also to exhibit the high-quality image of the sample cross-section. The setup and a tested sample are presented below (see Figure 3-9 and Figure 3-10). This microscope not only can show the image of the cross-section of the sample, but also can measure the thickness of the oxidation layer with high resolution. Later on, the oxidation layer growing with respect to ageing time will be measured and plotted in a later chapter.



Figure 3-9: Microscope

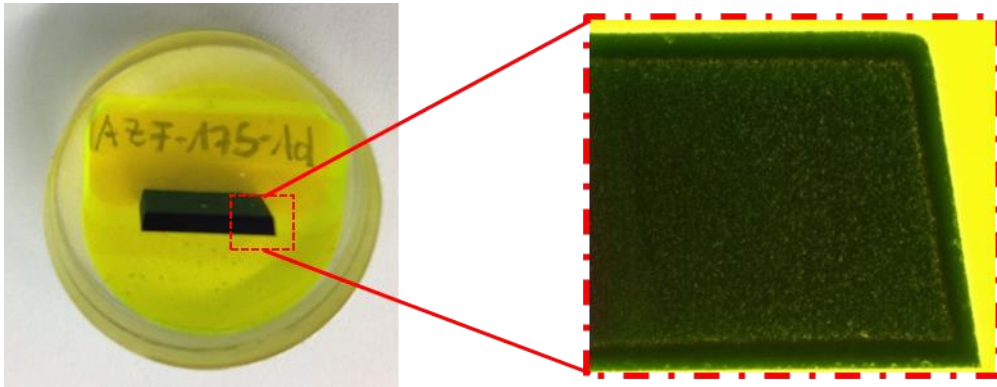


Figure 3-10: Embedded sample and cross-section of aged sample

4 Characterization and Simulation for Unaged Moulding Compound

4.1 Introduction

At the beginning of the transfer moulding process, an uncured epoxy moulding compound (EMC) pellet is heated up to the moulding temperature and then is injected into the moulding tool under hydraulic pressure. After de-moulding, an additional process is applied. This is the so-called Post-Mould Curing (PMC). This PMC is performed to improve the physical properties of the MC, such as strength, glass transition temperature and so on. The importance of the PMC for MCs has been investigated by many researchers in the past [69]–[71]. As a result, some researchers developed a cure dependent material model of MCs during the curing process to evaluate the influence on package reliability [72]. In the present thesis, only cured MC is considered.

In order to be able to predict the mechanical behaviour of a package under physical loading through FEM simulations, the material properties and parameters should be well characterized and defined. As we know, the material properties of EMCs are time- and temperature-dependent and generally have to be described by a viscoelastic model. However, in the past, an elastic model of MCs was used to evaluate the stress state inside the package during temperature loading. This generally leads an overestimation of the stress inside the package as reported by some researchers [73]–[75]. In the present work, a more adequate linear viscoelastic model for the MC was established and further used. Besides the linear viscoelastic model, other material parameters, such as the thermal expansion and the curing shrinkage, are also crucial for obtaining accurate simulation results. For example, without curing shrinkage the stress and warpage of a package will generally be underestimated [76], [77].

In this thesis, the goal is to develop a material model, describing the effects of thermal ageing of the EMC such that the ageing influence on the reliability of packages can be evaluated. Before doing this, a material model for unaged EMC should be established first. To this end, the characterization methods should be properly selected. If these methods and produces are proven to be correct and reasonably accurate, the material model of aged EMC can subsequently be established by using the same methods and procedures.

In this chapter, the characterization methods and procedures are introduced and the results are discussed in detail. Based on the experimental data, numerical analyses are applied to establish a material model for simulation. A special test method is developed

to measure the warpage. A warpage simulation is done to verify the material model and its parameters as obtained from the characterizations. Among these, some critical issues are pointed out to accelerate the testing time while yet obtaining a sufficiently accurate test result. The following contents will be presented:

- Section 4.2 will introduce the procedure for establishing the viscoelastic model. At the beginning of this section, some critical issues will be shown and discussed. Then DMA testing was performed to establish the model parameters of the linear viscoelastic model of EMC. Finally, several relaxation tests are performed to verify the linear viscoelastic model.
- Section 4.3 will introduce the procedure for establishing the Coefficient of Thermal Expansion (CTE). In this section, an EMC and copper are considered and the CTE values are presented.
- Section 4.4 will introduce an empirical method to determine the curing shrinkage of MC, as the curing shrinkage is also necessary for package simulations.
- Section 4.5 will introduce a new, efficient and accurate method for warpage measurement. The experiment was performed with a chosen bi-material sample. A warpage simulation is done, applying the material model and parameters from section 4.2-4, to facilitate the comparison of both the experimental and the simulated warpage data;
- Section 4.6 will give a conclusion of this chapter.

4.2 DMA testing and verification

It is well known, that since MC is a polymer-based material, its thermomechanical behaviour is viscoelastic. To obtain the viscoelastic model of MC, several test methods such as Dynamic Mechanical Analysis (DMA), relaxation testing, and creep testing, are often used. Among these, DMA testing is a suitable and quick way to characterize the viscoelastic behaviour of polymer-based materials. However, before running these tests, some calibrations should be performed, such as for the sample temperature. Since the material properties of MC are highly temperature-dependent, the accuracy of the temperature control is directly determining the quality of the DMA measurement results. Therefore, firstly the “sample temperature” is carefully calibrated. Also, an additional thermocouple is used to verify the established sample temperature (= measurement chamber temperature + temperature compensation, see the next section). Further, it should be realized that with changing chamber temperature the sample temperature could lag behind. Therefore, the DMA test results for two different temperature profiles, “temperature stepping” and “temperature ramping”, are investigated and compared, to establish the acceptable temperature ramping speed and thus to obtain a safe accelerated testing time. Furthermore, how to quickly and efficiently get a test result is also a critical issue for the industrial application. Finally, the DMA tests were performed in the “multi-frequency sweep” mode with a Q-800 of TA-instruments. Based on the DMA test results, a procedure based on the Time-Temperature Superposition (TTS) principle [78] is applied to establish the viscoelastic model. In the end, relaxation tests at various temperatures were performed to verify the viscoelastic model as obtained from DMA testing and TTS.

4.2.1 Temperature Calibration

The viscoelastic behaviour of EMCs is time- and temperature-dependent. As a consequence, the accuracy of the sample temperature during testing is directly determining the quality of the measurement results. According to this point, a process of sample-temperature calibration in the DMA machine (TA-Q800) must be done in advance and should be executed according to the standard procedure. Commonly, the temperature calibration is performed by using a standard metal with a known melting point. Here, two standard metals, being Indium and Tin, are used to do the temperature calibration. The melting points of these two metals are 156.6°C and 231.9°C, respectively. Then these two metals are installed in the chamber. A heating rate of 2°C/min is selected. For this, the established melting points occurred to be 168.76°C and 240°C, respectively. Afterwards, the real and the measured values are input into the control software to calculate a temperature compensation value for the specified heating rate (=2°C/min). During testing, the real temperature of a sample is equal to the chamber temperature plus temperature compensation value. Because the real temperature of the sample has delay compared to chamber temperature under a given heating rate, it is very important to consider this to obtain accurate and reliable test results.

To verify the “measured temperature” (= the chamber temperature + temperature compensation) an additional thermocouple on the sample is used. A schematic of the testing system is shown in Figure 4-1. The detection system includes three parts: a thermocouple sensor with 0.1°C resolution, a LabVIEW device for data transforming and a PC for data processing. During the measurement, the thermocouple directly contacted to the sample surface detects the real temperature of the sample. The temperature profile includes heating and holding steps. The results from the instrument itself and the external thermocouple are plotted together in Figure 4-2. The blue solid curve is from the instrument, and the red dashed curve is from the thermocouple. Either at the holding step or the heating step a relatively large deviation between both is always existing. The difference is more than 10°C.

According to the above result, another test is performed, but this time without temperature calibration, but with a relatively low heating rate (1°C/min) to minimize the temperature lag between sample and chamber. In the same manner as before, both results are presented in Figure 4-3. The comparison shows that the deviation between both signals is around 1~2°C. Based on these investigations, the method without temperature compensation and a heating rate of 1°C/min are considered as reasonable and sufficiently reliable for DMA testing.

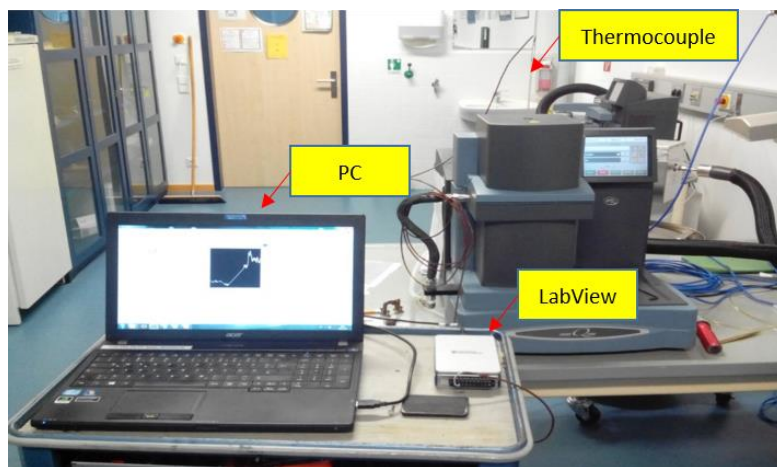


Figure 4-1: Schematic of detecting system

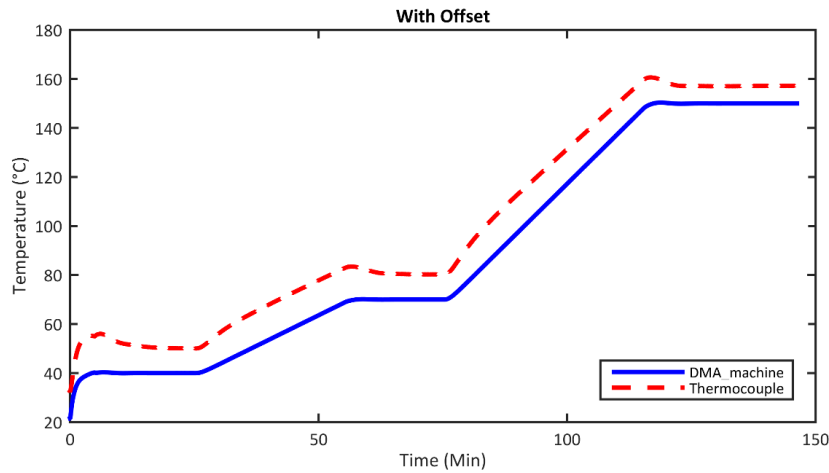


Figure 4-2: Comparison between “Sample Temperature” (= chamber temperature plus temperature compensation value) according to the DMA-machine and according to the thermocouple. *Heating rate = 2°C/min.*

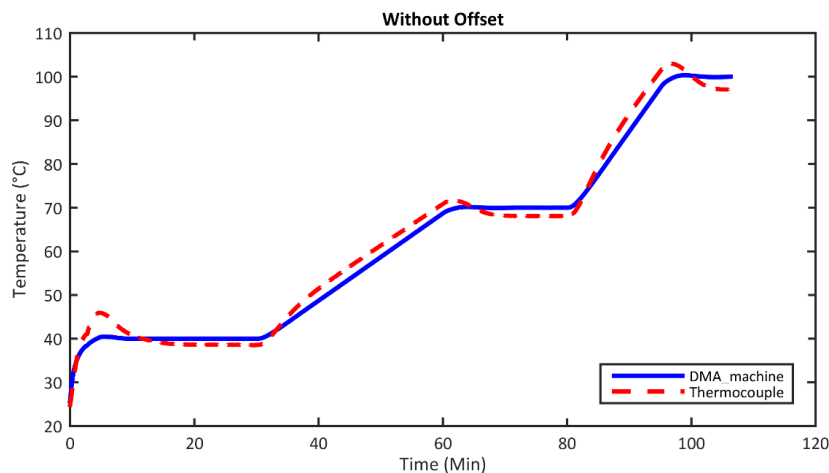


Figure 4-3: Comparison between “Sample Temperature” (= Chamber temperature) according to the DMA-machine and according to the thermocouple. *Heating rate = 1°C/min.*

To verify whether the method without temperature compensation and a heating rate of 1°C/min are indeed sufficiently reliable for the further DMA testing, two different temperature profiles are defined: One is temperature stepping, and the other one is temperature ramping.

- 1) Temperature stepping means that the DMA test will be performed after each temperature increment. A 5°C increment is chosen, followed by a hold time of 5min to reach a constant temperature in the chamber. Afterwards, the DMA test is run (No temperature compensation is applied). This procedure is repeated for each temperature step.

- 2) Temperature ramping means that the temperature is linearly increasing at a constant rate. In the ramping test, the heating rate is $1^{\circ}\text{C}/\text{min}$ (No temperature compensation is applied).

For both temperature profiles, the other measurement settings are kept the same. Figure 4-4 shows that the curves of the storage modulus and the loss modulus as a functions of temperature are quite similar for both applied temperature profiles. However, there is some more deviation at higher temperatures. The reason is that in case of the temperature stepping test the sample is at a higher temperature much longer than in the case of the temperature ramping test. The duration of the temperature ramping test is about 3 hours. However, it took 8 hours for the temperature stepping test. MC exposed to temperatures above its glass transition temperature is affected by thermal ageing, even after a few hours. For temperature ramping the exposure time above the glass transition temperature is much lower than for temperature stepping. At low temperature, there is no or just a minor thermal ageing effect. Therefore, the curves are almost the same below the glass transition temperature.

More information about thermal ageing effects on the properties of MCs will be found in the next chapter. Nevertheless, the test results confirm that the temperature ramping at $1^{\circ}\text{C}/\text{min}$ heating rate results into sufficiently reliable DMA test results.

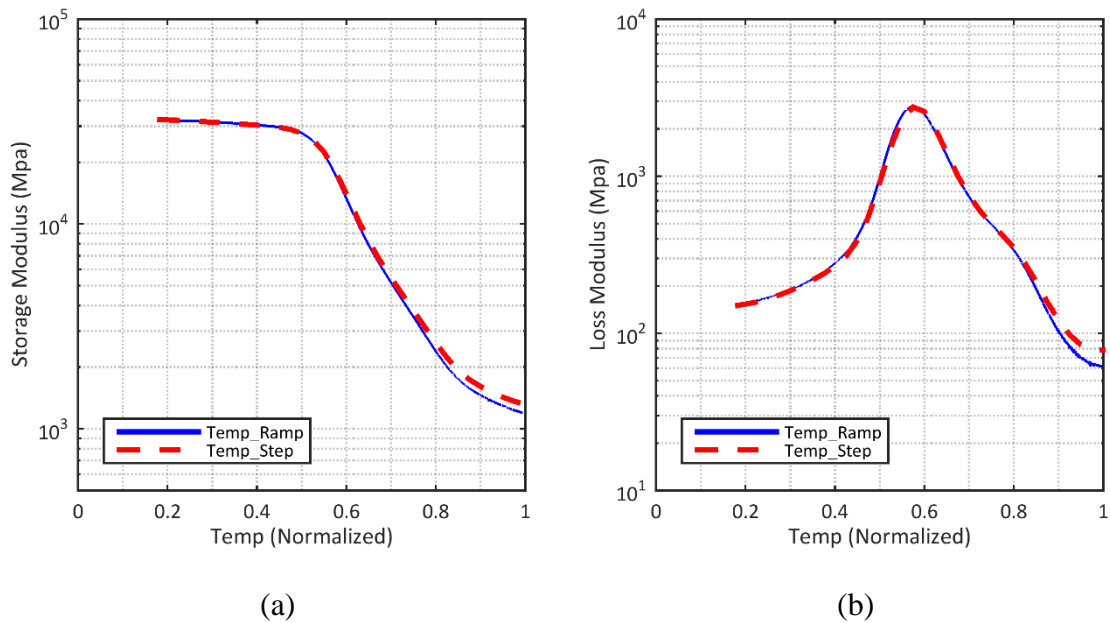


Figure 4-4: DMA test at 1HZ: Storage modulus (a) and Loss modulus (b) as functions of Temperature

According to the above investigations, in the present research, the temperature process with $1^{\circ}\text{C}/\text{min}$ heating rate is utilized in the DMA measurements. With this, the testing time is reduced, while the effect of continuing ageing is minimized.

4.2.2 Experimental Results of DMA

A DMA test is performed in tensile mode, applying the multi-frequency sweeping mode, with a heating rate of 1°C/min. The results are presented in the following figures.

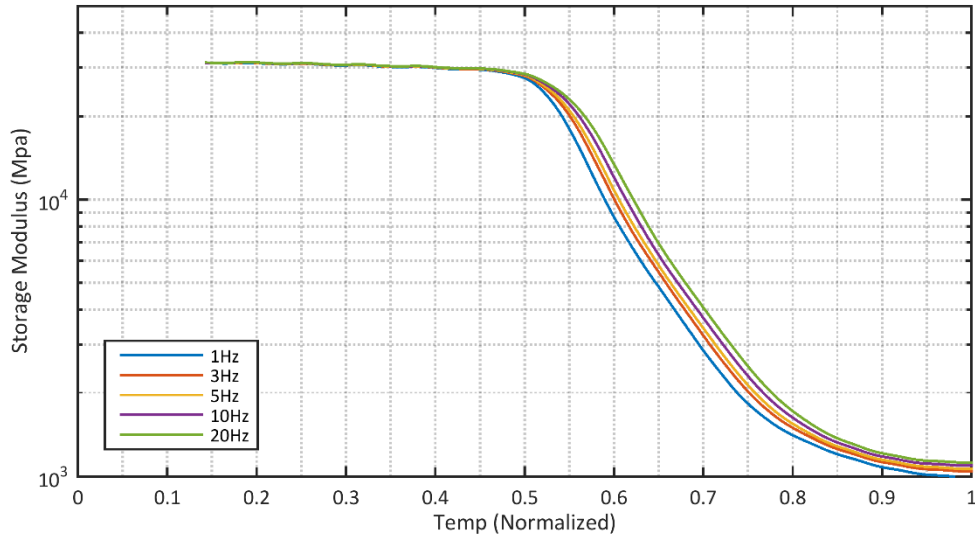


Figure 4-5: Storage modulus as a function of temperature and frequency

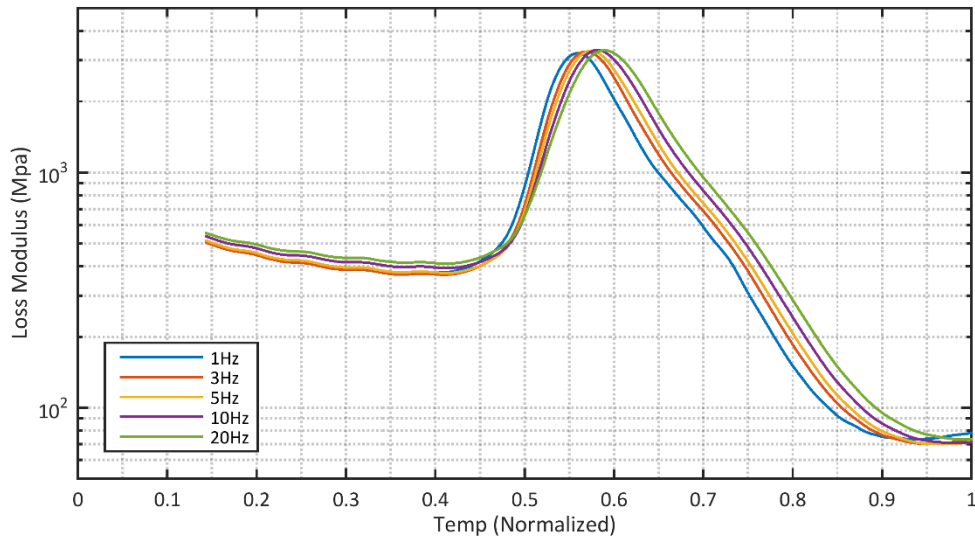


Figure 4-6: Loss modulus as a function of temperature and frequency

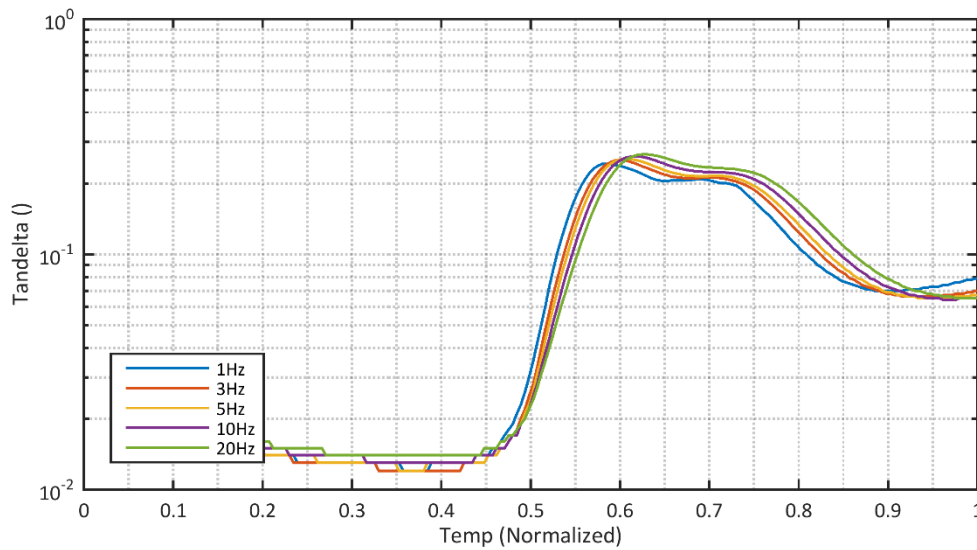


Figure 4-7: Tan delta values as a function of temperature and frequency

Figure 4-5, 6 and 7 show the storage modulus, the loss modulus and the tan-delta values as functions of temperature and frequency. The storage modulus represents how the viscoelastic material stores energy, while the loss modulus represents how the viscoelastic material dissipates energy. The tan-delta, is the ratio of loss modulus and storage modulus.

From the above Figures, it can be observed that the storage modulus, the loss modulus and the tan-delta value of this moulding compound are independent of the applied frequency below 105°C. Typically, the mechanical behaviour of the moulding compound in this region is considered to be in the glassy state (≈elastic state). Furthermore, when the temperature reaches 200°C the curves are becoming horizontal and overlap again. This region is considered to be the rubbery state. Here, the moduli are also independent of the applied frequency (≈elastic state). However, between 105°C and 200°C the moduli and tan-delta values are highly dependent on the applied frequency. This region is the so-called glass transition region. In this region, the storage modulus dramatically decreases with increasing temperature. However, the loss moduli and tan-delta values are increasing firstly, and then decreasing. The peak values are observed at various frequencies in both pictures. Mostly, the peak value of tan-delta (*versus Temperature*) or the peak value of the loss modulus at 1Hz (*versus Temperature*) are defining the glass transition temperatures (T_g) of the polymer-based material. As for the storage modulus, the temperature where it (at 1Hz) starts to change from the glassy state to the glass transition region is alternatively defined as the T_g of the EMC. According to the Figure 4-5, 6, 7, the glass transition temperatures of this moulding compound are found as: about 105°C from the storage modulus, about 120°C from the loss modulus and about 125°C from the tan-delta, respectively.

4.2.3 Viscoelastic model of EMC

In the past, an elastic model of MCs was used to evaluate the stress state inside the package during temperature loading. It leads to an overestimation of the stress inside the package as reported by some researchers [73]–[75].

Based on this drawback, a viscoelastic model of EMC is developed for package simulations. Thereby, DMA measurements are proposed and used to obtain the viscoelastic model of EMC for thermo-mechanical simulation applications. Since the EMC is a thermorheologically simple material the principle of Time-Temperature Superposition (TTS) is used to generate a viscoelastic model. The TTS avoids the challenge of measuring a polymer's behaviour over a long period at a specified temperature by utilizing the fact that at higher temperatures and long times the polymer will have the same response. To apply TTS, the sample must be in the linear viscoelastic range under the deformation of interested.

Figure 4-8 shows the storage modulus of the EMC as a function of the applied frequencies at different temperatures. For using TTS, a reference temperature should be specified first, and then the individual isothermal curves are shifted along the frequency axis to the left or to the right to form a single “master curve”. Through shifting the individual isothermal curves, the so-called master curve (for the chosen reference temperature) is constructed. It shows how the storage modulus behaves at the specified reference temperature. Finally, a generalized Maxwell model is used to fit the constructed master curve in Figure 4-9. As illustrated in Figure 4-9, the generalized Maxwell model with 20 Prony elements matches the experimental data quite well.

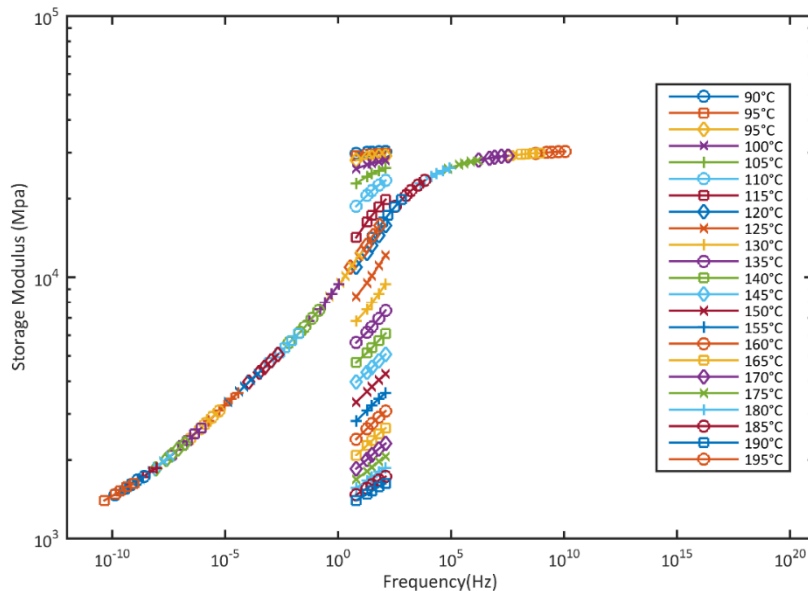


Figure 4-8: Constructed master curve after TTS

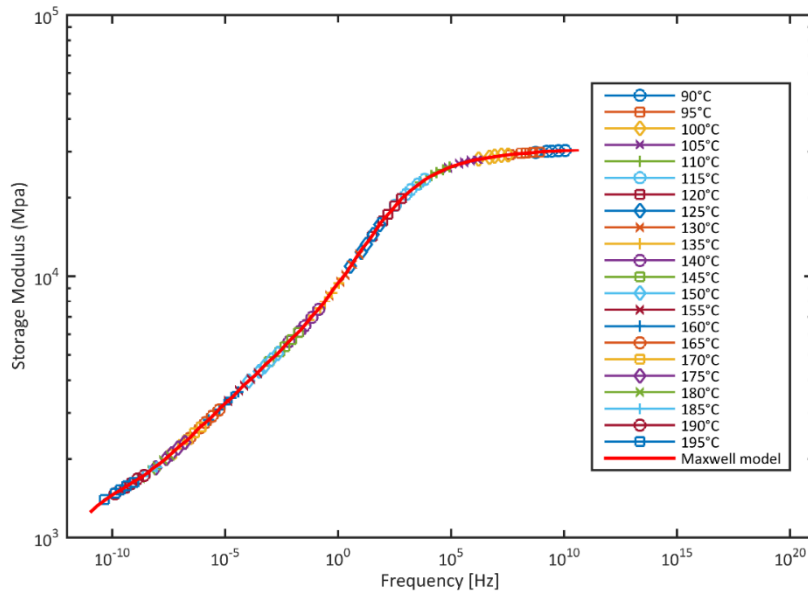


Figure 4-9: Master curve fitted by Generalized Maxwell model

In the past, lots of researchers noted that the master curves belonging to different temperatures always show the same shape. Generally, this kind of material is called a thermorheological simple material. After constructing the master curve a graphic of shift factor $a_T(T)$ with respect to temperature can be obtained (see Figure 4-10). This shift factor curve in fact serves as a key for interpreting the master curve. Based on this graphic, the master curves at various temperatures can be easily established by shifting the reference master curve from Figure 4-9 to the right or left. With this shifted master curve the viscoelastic behaviour of this material can be predicted at any temperature of interested.

Figure 4-10 illustrates the so-called shift factors as obtained by shifting the individual curves to the master curve (for the chosen reference temperature). In general, two different functions are used to fit these shift factors below and above the glass transition temperature. Below the glass transition temperature, the Arrhenius law is used because there the relaxation behaviour is activation energy driven. While above the glass transition temperature the Williams-Landel-Ferry (or called WLF) law is used because there the relaxation behaviour is mainly driven by the free volume mechanism. Detailed information, such as equations, can be found in Chapter 2. The fitting curves from both principles are shown in Figure 4-10. They are matching the experimental data quite well. However, some difficulties occur while trying to implement them in various commercial FE software. Therefore, a polynomial function with three orders was used to fit the experimental data as well. A fitted curve from the polynomial function is plotted together with experimental data in Figure 4-10. The fitted curves from WLF and Arrhenius are also plotted together with polynomial fitting. They are quite similar. In the end, the shift factor model with polynomial function is implemented in the commercial FEM software used within the present project.

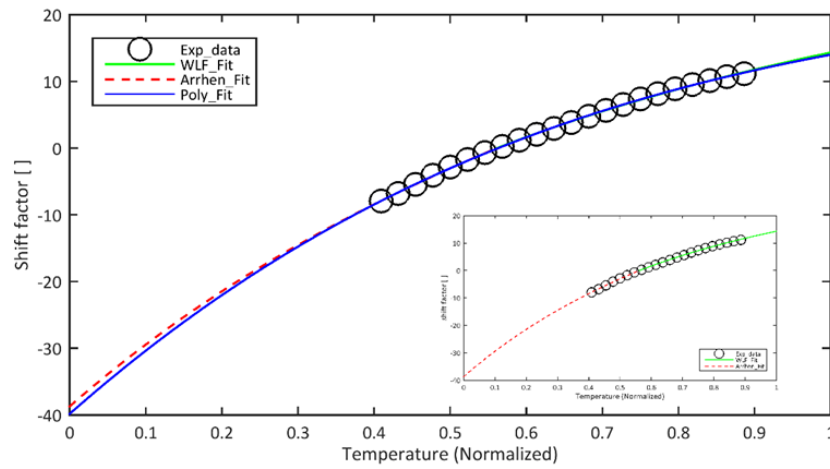


Figure 4-10: Shift factors fitted by the defined functions

4.2.4 Verification

After establishing the viscoelastic model of this EMC, the expectation is that this model could predict relaxation or creep behaviour of EMC at arbitrary temperatures under small deformations. Thus, in order to verify the viscoelastic model as constructed from DMA, a relaxation test at various temperatures by using a three-point bending clamp system is applied. The schematic of the setup and the FE model are presented in Figure 4-11.

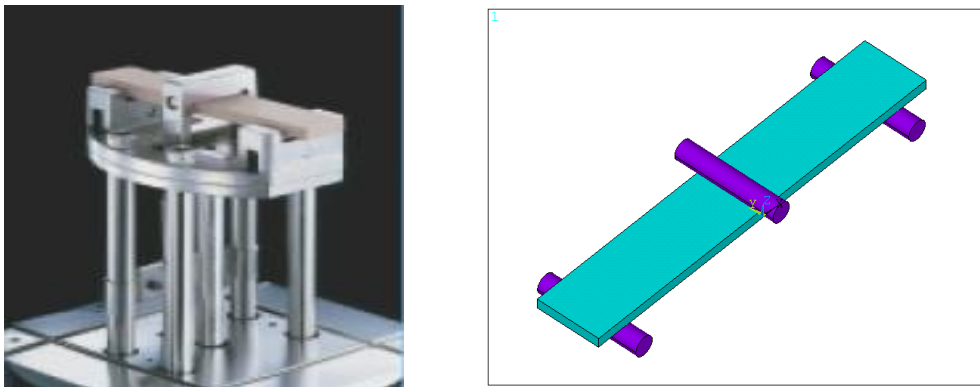


Figure 4-11: Schematic of three-point bending Relaxation test (setup and FE model)

Here, relaxation tests are performed at 30°C, 90°, 100°C, 110°C, 130°C and 150°C. During testing, a constant strain was prescribed at the top of the EMC surface for 2 hours. The relaxing stress of the sample was recorded during the measurements. At each temperature, at least, two tests were performed to check the reproducibility. Afterwards, the simulations were carried out at each temperature with the established viscoelastic model.

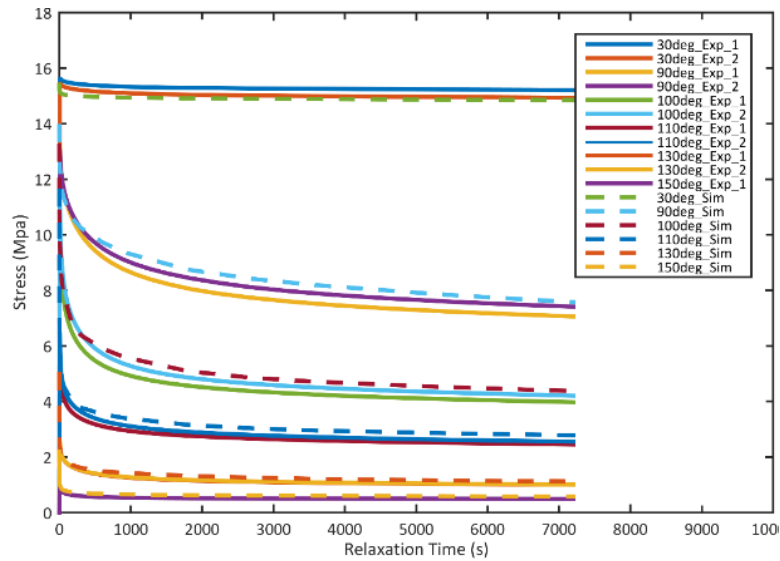


Figure 4-12: Results of simulations and relaxation tests

Figure 4-12 presents the experimental results for six different temperatures together with the simulation results. Firstly, the experimental results show that stress relaxes only slightly at 30°C. Because at 30°C the EMC is staying in its glassy state. Considerable stress relaxation was found when the measured temperature is in the glass transition range. In this region, the stresses relaxed quickly after loading setup and subsequently smoother. The simulation results match quite well with the experimental data for all temperatures. It confirms that the viscoelastic model from DMA testing is accurate.

4.3 TMA Measurement

Besides the viscoelastic model, the CTE is also a very important factor for package design simulations, since electronic packages include various materials, such as silicon, copper, MC and solder. Those materials have different thermomechanical properties. Among these, the CTE mismatch inside the package can induce internal stresses and then lead to reliability issues, such as warpage, cracking and delamination. As a result, the CTE is one of the key factors for package design. In order to simulate or predict the thermomechanical behaviour of a package under thermal loading the CTE as a function of temperature is necessary. In this research, only two materials are used, copper and EMC. Thereby, the CTE values of both materials will be characterized by a Thermomechanical Analysis (TMA) instrument. The TMA machine was introduced in Chapter 3.

A small cubic sample of EMC and a strip of copper was used for the TMA measurements. Test results of EMC and copper are presented in Figure 4-13. The temperature range is from -30°C to 250°C at a heating rate of 3°C/min. Several

temperature cycles were performed. To eliminate the moisture and physical ageing effect on the experimental data, the first heating data was not used for the CTE analysis; only the second heating segment was used for the TMA analysis.

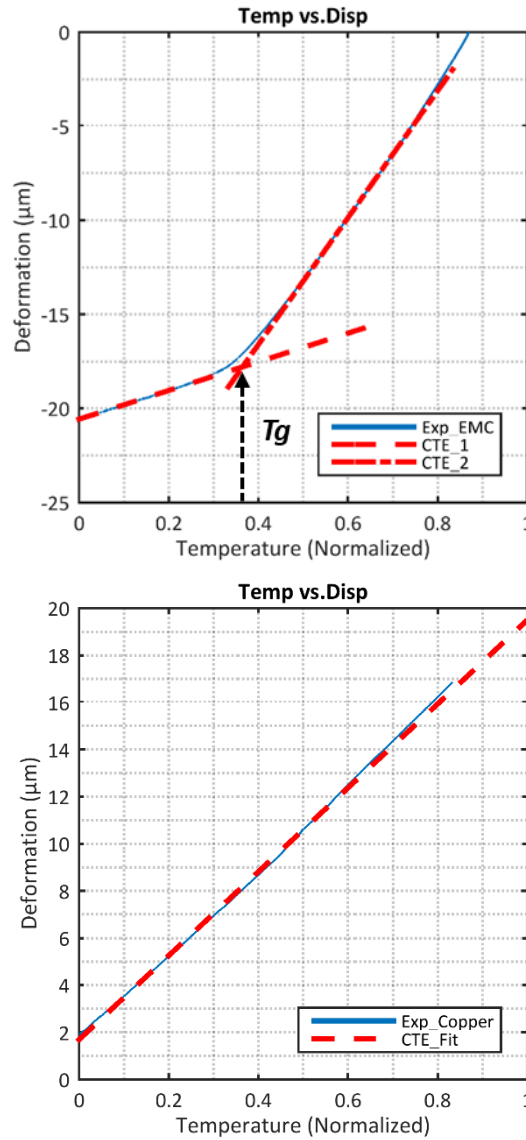


Figure 4-13: CTE measurements of EMC and copper

The two pictures show the deformation (=dimensional change) as a function of temperature. The left picture represents the measurement data of the EMC, and the right one shows the measurement data for copper. The CTE calculation is according to the following expression:

$$CTE = \alpha = \frac{\Delta L}{L * (T_1 - T_0)} \quad (4-1)$$

Here the ΔL is the change in dimension during the test; α is the CTE value; L is the

initial length of the sample; $T_1 - T_0$ is the temperature change.

From the right figure, it is seen that for the copper, the deformation versus temperature is almost linear.

However, from the left Figure, it is observed that this is not the case for the EMC. For the EMC a more or less bi-linear behaviour is found. The intersection of the two more or less linear function is near the T_g of the EMC. This intersection gives an alternative definition for the glass transition temperature of the EMC. Linear fitting was used to fit each of the parts, below and above T_g , separately (also shown in the left figure). According to the above CTE expression, from each linear fit a separate CTE value is found: CTE_1 and CTE_2 for below and above the T_g , respectively. The intersection of two fitted lines is the glass transition temperature of this moulding compound.

The CTE value of the copper is found from a linear fit of the experimental curve of the right figure.

Table 4-1 The CTE's of EMC and copper are listed.

	T_g	CTE_1 (ppm/°C)	CTE_2 (ppm/°C)
EMC	105	0.23(Normalized)	1(Normalized)
Cu	-	16.3	

When the temperature is lower than the glass transition temperature of the EMC, the CTE value of copper is higher than that of the EMC. However, when the temperature is higher than the glass transition temperature of the EMC, the CTE value of copper is lower than that of the EMC. These differences will exhibit in the warpage measurement of a bi-material sample in a later section.

4.4 Curing Shrinkage determination

For the encapsulated packages, the warpage builds up due to two processes. One is the chemical shrinkage of the moulding compound due to moulding and post-moulding curing processes. Another one is thermal shrinkage due to the material properties mismatch between respective materials during the cooling process. As a result, the total warpage of a package is coming from curing shrinkage plus thermal shrinkage (equation-4.1). [76] shows the importance of curing shrinkage of EMC in warpage and stress analyses. In order to accurately predict the warpage of an electronic package after encapsulation and cooling down, the values of both shrinkages should be well defined. As we know, the thermal shrinkage is due to the material property mismatch and it is easy to measure. However, the curing shrinkage is due to the chemical reaction during cure, and it is hard to measure directly. Therefore, an indirect method was applied. Here, an empirical method (Figure 4-14) combined with a Finite Element simulation was used to determine the curing shrinkage similar to many researchers [76], [79]. The

whole process is divided into four steps. Firstly, the curvature of a package surface is measured at a specified temperature. Secondly, by using the FE method the cure shrinkage strain was defined as a trial value in the model. Then, the cooling process from the moulding temperature to the specified temperature was simulated. Next, the trial value is updated until the simulated curvature fits with the measured curvature.

$$\varepsilon_{Total_Shrinkage} = \varepsilon_{Cure_Shrinkage} + \varepsilon_{Thermal_Shrinkage} \quad (4-2)$$

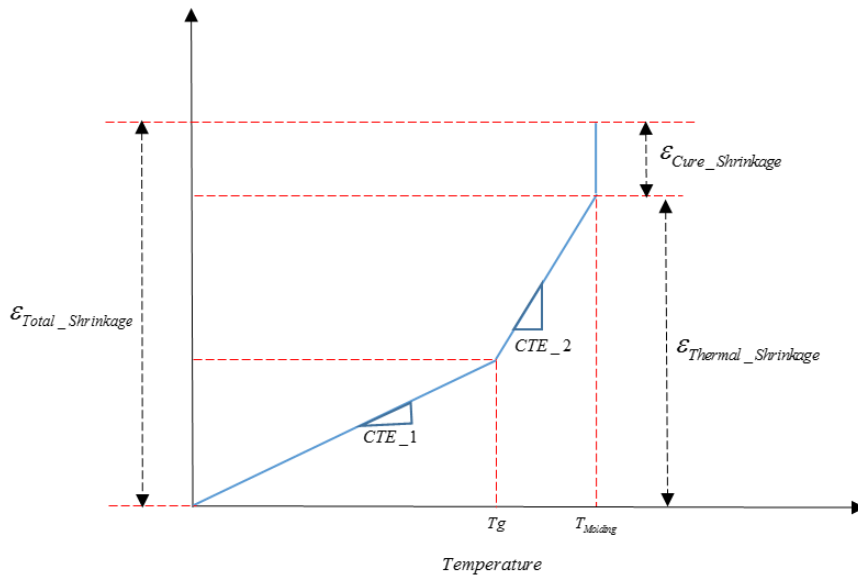


Figure 4-14: Total shrinkage of EMC

4.4.1 Measurement

As introduced before, the curing shrinkage is hard to measure directly. So an indirect method is used. Figure 4-15 shows the structure of a sample (from both sides) with diagonal warpage-measurement paths. The sample, a so-called dummy package, consists of EMC on a copper substrate. There is no chip and glue or solder inside. The curvature of the sample surface at the EMC side is measured by a Profilometer (see section 3.3.5). Several dummy packages were measured to establish the standard deviation. The measurement results are shown in Figure 4-16. Figure 4-16(a) is the out-of-plane deflection of the diagonal AB and (b) is the result of the diagonal CD. The results from the six samples are quite repeatable in both diagonals. Due to the roughness of the moulding compound surface the curves are not smooth. Therefore, the fitting procedure is done by using three coefficients of a polynomial function to represent the experimental data in order to get a smoother curve (Figure 4-16(c)) for later comparison. Figure Figure 4-16(d) shows that the measured curves in both diagonals are similar within the standard deviation since the structure of the sample is almost symmetric in the diagonal direction. Meanwhile, it is observed that the measured curves are not symmetric from the centre due to the fact that the whole

structure is not symmetric (see Figure 4-15). It is also found that the standard deviation at the edge is much higher than in the centre because of the slicing process.

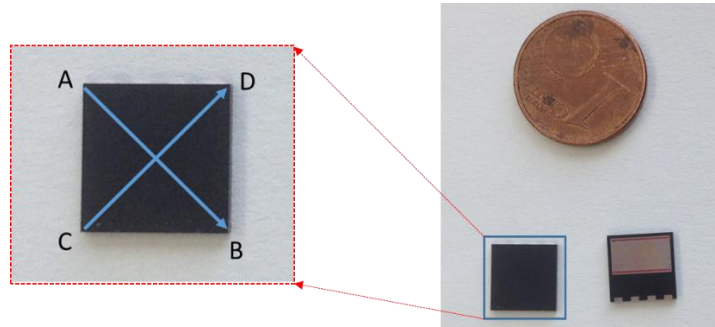
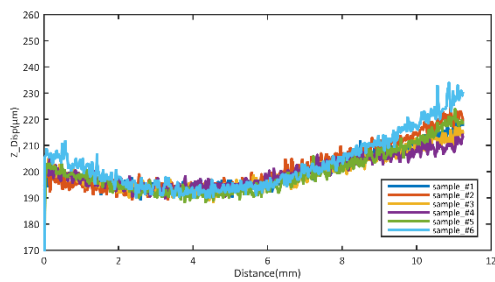
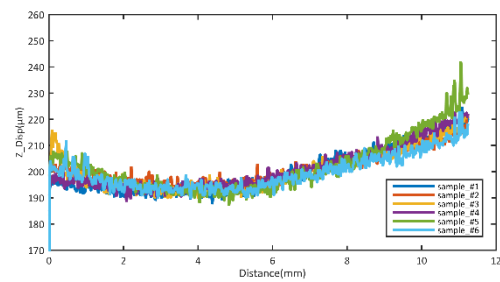


Figure 4-15: Sample structure and measured paths

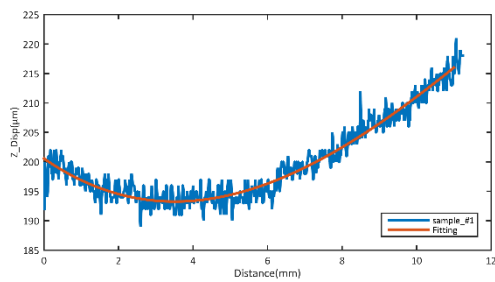
(Left: top view of package and measured path, right: top and bottom view of package)



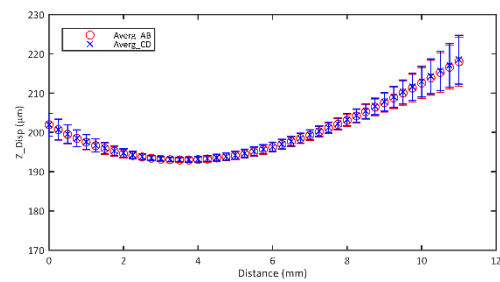
(a) measurement of diagonal A-B



(b) measurement of diagonal D-C



(c) A-B single measurement with fit



(d) fitting curves of diagonal A-B and D-C

Figure 4-16: Data processing for measurement data and simulation results

4.4.2 Simulation and Discussion

The 3D model of this dummy package is shown in Figure 4-17. It consists of the moulding compound (Blue) and the lead frame (Red). The material model and

parameters for the simulation are shown in the previous sections. Here, the simulation was done according to the procedure as described in Figure 4-14. Firstly, an initial strain for the curing shrinkage of the EMC was defined at the moulding temperature, and then the package is cooled down from the moulding temperature to room temperature. In the end, the initial strain for the curing shrinkage is updated until the simulated warpage fits the experimental data.

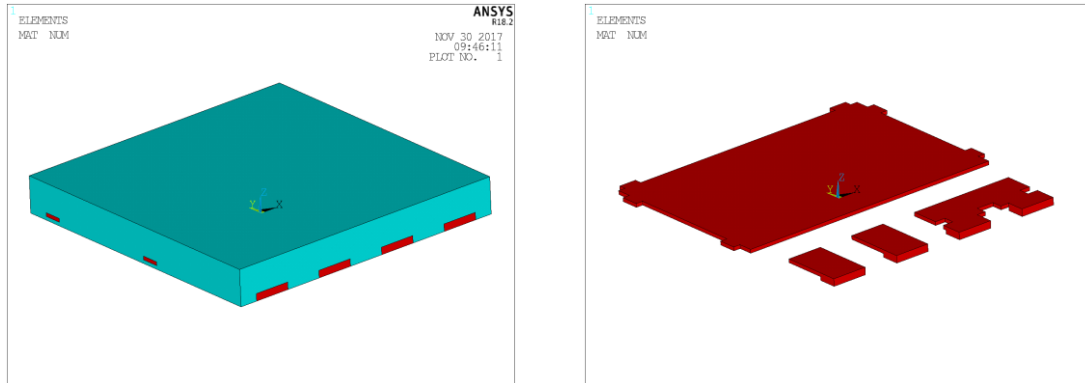


Figure 4-17: The structure of a dummy package

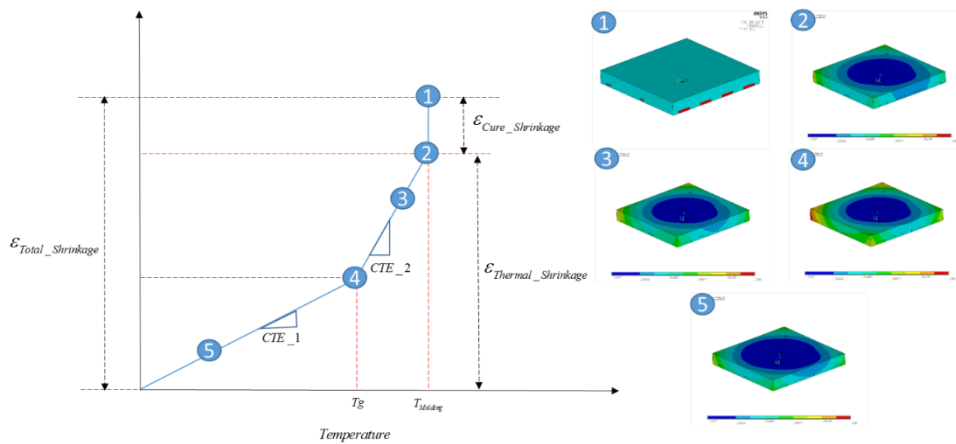


Figure 4-18: Simulation procedure and out-of-plane deflection of the dummy package

Figure 4-18 shows the simulation results of the out-of-plane deflection of the package at different loading steps. At point 1, the package (at moulding temperature) is assumed stress-free. At point 2, the simulation was done (at moulding temperature) with the curing shrinkage of the EMC (included as initial strain). At point 3, the temperature is above the T_g of the EMC; thermal shrinkage is activated (also included as initial strain). Meanwhile, the CTE of the EMC is bigger than that of copper, so the total warpage is increasing. At point 4, the temperature is equal to T_g , such that the maximum warpage is reached. At point 5, the temperature is below T_g and the CTE of copper is larger than that of the EMC. Therefore, the additional deformation of the sample is in the opposite

direction. As a result, the total warpage decreases.

Moreover, for understanding the impact of curing shrinkage on the package warpage, two simulations were done with and without curing shrinkage. The simulation results for the measurement temperature are presented in Figure 4-19 together with the measurement data. As illustrated in Figure 4-19, without curing shrinkage the warpage of the dummy package is smaller than the experimentally obtained warpage. So, the simulation cannot fit the experimental data. While with curing shrinkage, the simulation shows a good agreement with the experimental data. From this comparison, it can be concluded that the curing shrinkage is a critical value necessary to simulate the package warpage accurately. It can be concluded that this simple method provides a quick way to determine the curing shrinkage value of the EMC. In the subsequent simulations, the curing shrinkage of the EMC is always included in the FEM models.

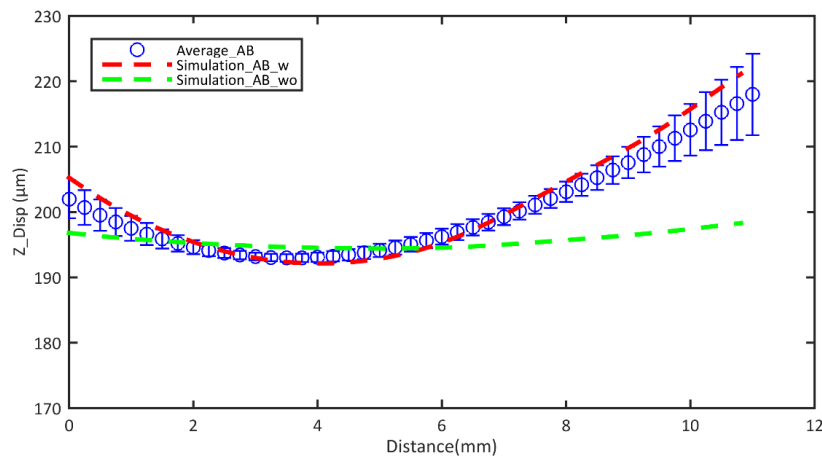


Figure 4-19: Deformation with and without curing shrinkage of EMC compared with experiment result

4.5 Warpage Measurement of bi-material sample

Warpage measurement is normally used to evaluate the thermomechanical behaviour of a package under thermal loading. Meanwhile, it is also an indirect method to evaluate the internal stress of the package by FE simulation since the internal stress of the package cannot be directly measured. The internal stress state directly corresponds to the established warpage. Many researchers reported [80], [81] how to measure a package warpage by using an optical method. However, the equipment is not only expensive, it is also not easy to operate in order to obtain a good result. Besides, an additional numerical analysis always needs to be done after testing. According to these disadvantages, a simple, efficient and cheaper approach is developed to measure the warpage of the specified sample. In this section, firstly, a new approach of warpage measurement is proposed and introduced in detail. Then a special bi-material specimen was prepared and tested by this new approach. The test results are analysed and discussed. With the material model and its parameters obtained in section 4.2-4, a

simulation was performed to predict the thermomechanical behaviour of a bi-material under temperature loading. The comparison between experimental data from the warpage measurement and the simulation is shown in the end.

4.5.1 Introduction of test method and sample preparation

Generally, the optical measurement is a so-called non-contact method. It is often used to measure the warpage of a sample. Due to the reasons as described above, a contact method (or mechanical method) is developed in this thesis based on measurements with the TA-Q800 instrument. The out-of-plane deflection of the bi-material sample under thermal loading is measured and used for the later comparison with the simulation. The schematic of this approach is sketched in Figure 4-20. The measured result is strongly dependent on the span between the two supports. When the distance between the two supports, L_0 , is small ($L_0 \sim 0$) then the (thickness) expansion of the sample is measured (state 1). When the distance between the two supports is equal to L_1 then the (thickness-) expansion and warpage of the sample are measured in total (state 2). While, when the distance between two supports is equal to L_2 (with $L_2 \gg L_1$) then the expansion and warpage of the sample are also measured in total (state 3). However, for a large L_2 the warpage value is much higher than the thickness expansion so that the value of the thickness expansion is negligible. In order to obtain a reasonable result of warpage the distance between two supports should be large enough.

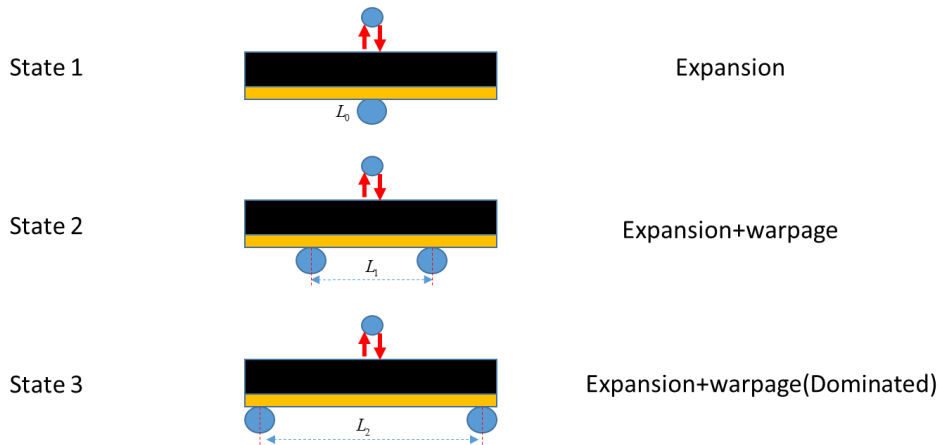


Figure 4-20: The schematic of warpage measurement by three-point bending

There are some advantages of using this method:

- 1) The principle is simple.
- 2) It is easy to use.
- 3) The measurement accuracy is high.
- 4) The results, while heating or cooling are continuous.
- 5) No additional numerical analysis needed.

Of course, there are some disadvantages of this method, for example only one point can be detected during testing and the thickness expansion of the sample is always included

in the measurement data. Therefore, the recommendation for this method is that the sample length should be large enough to limit the influence of the expansion effect. Anyway, from the simulation point of view, the expansion effect can also be simulated. This experiment is just used to verify the material model and its parameters as used in the characterizations.

Based on this, two special bi-material samples were produced in the production line with identical process conditions as for a real package (see Figure 4-21). Bi-material plates of EMC on copper, so-called mould maps, were moulded first. Both mould maps consist of EMC and copper. The difference between them is the shape of the copper substrates. One type is with flat copper, the other one with structured copper. The strip-samples were cut from these mould maps.

The warpage measurement is developed based on the TA-Q800 instrument by using the three-point-bending clamp system. The test setup is shown in Figure 4-21. The sample is placed on the roller supports and a moveable tester contacts the upper sample surface. When the sample is bending due to thermal loading, simultaneously the detection point of the movable tester can move up and down to follow the position of the contact point. In the end, the displacement as a function of temperature is recorded.



Figure 4-21: Setup and Bi-material Sample

4.5.2 Warpage measurement and Discussion

Figure 4-21 shows the construction of the test system. Apparently, the whole clamping system will expand or contract during a temperature loading, since it is made of metal. In order to investigate how much expansion comes from the clamping system, a very thin silicon sample was prepared. It is used for the system expansion and contraction measurement as well as for calibration since the pure silicon could not bend during thermal loading. The silicon strip is placed on the supports as shown in Figure 4-22. The geometry of the silicon strip is 60(L)X10(W)X0.5(T) mm. The test result is presented in Figure 4-23. The total expansion of this system is around 15 μ m in the temperature range between 25°C and 200°C. The CTE of pure silicon is around 2.6e-6 ppm/°C. In this temperature range, the expansion of this thin silicon is less than 0.5 μ m.

Therefore, the total expansion of silicon can be ignored within this temperature range. The measured expansion data will be used for the correction of the temperature-dependent warpage data of the bi-material samples,

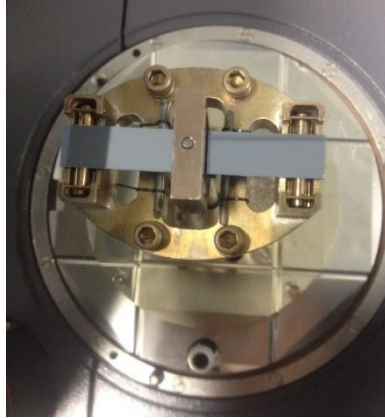


Figure 4-22: Setup for calibration measurements

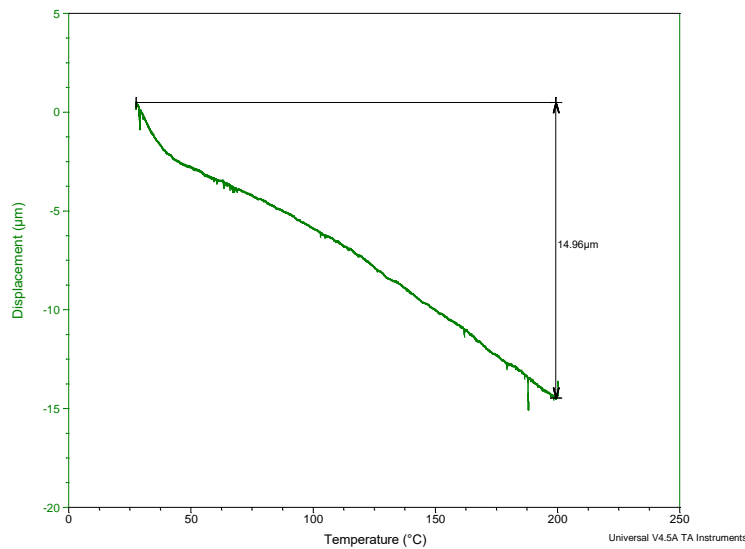


Figure 4-23: Expansion and contraction calibration result of the clamping system

After the system calibration, the real tests with the specified bi-material samples were performed to obtain their thermomechanical behaviour of this under temperature loading before thermal ageing. The sample used for the measurement is shown in Figure 4-21. The movable clamp is contacting the copper side since at high temperature the EMC will become soft. Even with the small contact force, the detected point could penetrate into the EMC and then could affect the measurement result.

In the test, the contact force is 0.005N, the heating rate is 1°C/min and the test mode is force-control. The experimental result (for the simple bi-material sample) is shown in

Figure 4-24. It is clear to see that the measured curve can be divided into two parts. The turning point is the glass transition temperature of the EMC. Compared to the glass transition temperature obtained by DMA or TMA, the T_g from TMA and storage modulus are similar to the value identified here. However, if T_g is taken from the peak value of the tan delta or loss modulus from DMA, it is much higher than the one shown here.

As illustrated in Figure 4-24, when the temperature is lower than T_g of the EMC the shape of the bi-material sample is ‘crying’; while when the load temperature is higher than T_g the shape of the bi-material sample will become ‘smiling’. The reason is that the CTE value of EMC is changing below and above T_g . Above T_g , the CTE of this EMC is higher than CTE of copper; below T_g , the CTE of this EMC is lower than copper. As a result, the shape of the bi-material is changing. In this testing, at least, three measurements are done to minimize the testing errors.

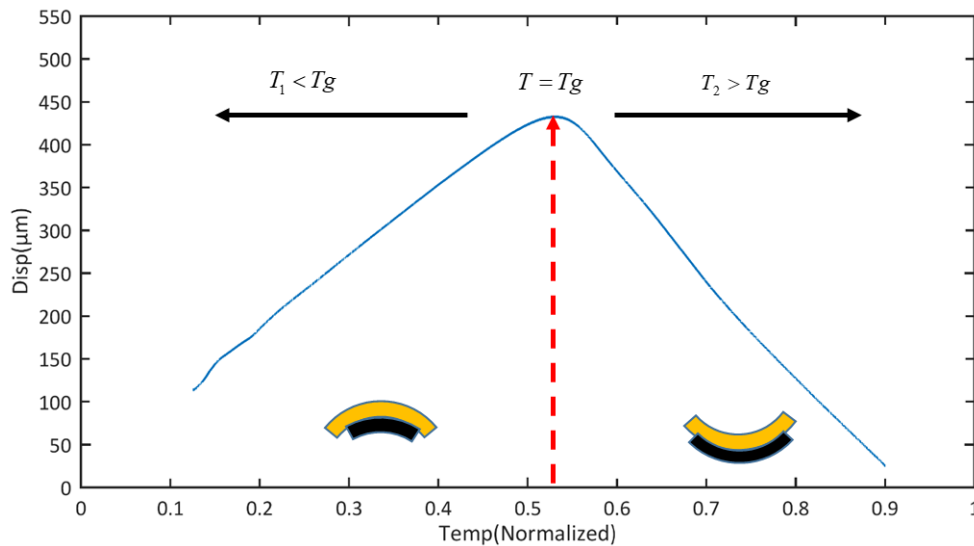


Figure 4-24: Test result of the (simple) bi-material sample

4.5.3 Simulation

In this part, the simulation was performed. The viscoelastic material model and the parameters from the characterization, the CTE and the curing shrinkage, are the inputs. The 3D models of two bi-material samples were built with the Ansys (see Figure 4-25). The boundary conditions are set the same as in the experiment. The simulation results as well as the experimental data are plotted together in Figure 4-26. The comparison shows that the FE model well predicts the thermomechanical behaviour of these two bi-material samples under temperature loading. It confirms that the characterization methods and procedures are accurate enough to obtain the material model and parameters for subsequent FE Modelling.

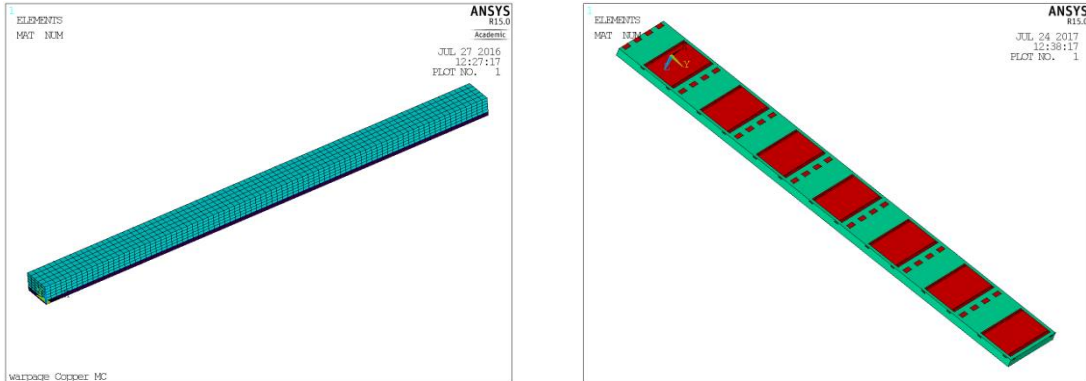


Figure 4-25: 3D models of bi-material samples

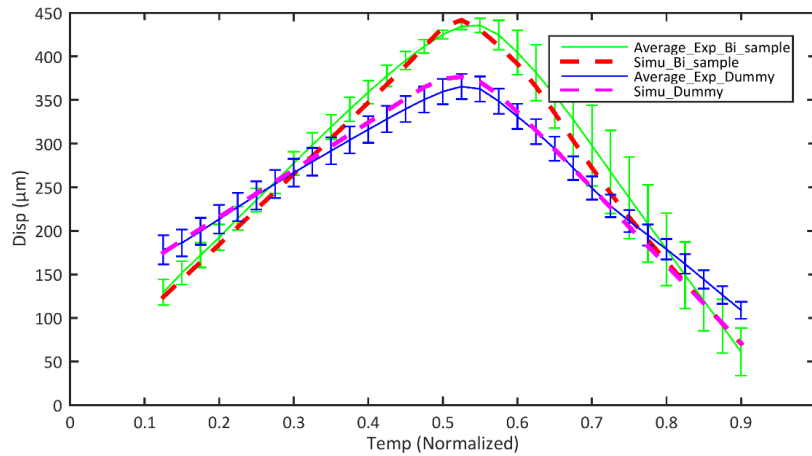


Figure 4-26: Comparison between experiment and simulation

4.6 Conclusion

In this chapter, the material properties and parameters of fully cured EMC were characterized, such as the viscoelastic model, the CTE and the curing shrinkage. Meanwhile, the corresponding simulations were done to verify the material model and its parameters. The comparison between experiment and simulation show a good agreement. According to the above work, the following conclusions are given:

- The moulding compound is a polymer-based material. Therefore, its properties are time- and temperature-dependent. In order to obtain accurate experimental results, the settings for testing should be properly chosen.
- Through combined DMA testing and numerical analysis, the viscoelastic model of the EMC can be easily established. It describes the thermomechanical behaviour of EMC under temperature loading.

- The CTEs of the moulding compound and copper were characterized by a TMA machine. From the test results it follows that the CTE of the EMC is higher than that of copper, when the temperature is higher than the T_g of the EMC. When the temperature is lower than T_g of the EMC, than the CTE of the EMC is lower than that of the copper. The effects are visualised and discussed in the warpage measurement results in section 4.5.
- An empirical method was used to determine the cure shrinkage of the EMC, since it is hard to measure directly. So, an indirect method combined with FE simulations was applied. Besides, the simulation results also show the differences in warpage with and without the curing shrinkage taken into account in the FE simulations. It shows that the curing shrinkage is a critical parameter for the simulation to get a match between the experimentally obtained and the simulated warpage.
- A mechanical method was developed for warpage measurements. The simulation model with very good approximation well predicts the thermomechanical behaviour of two different bi-material samples.

In brief, this chapter shows a systematic characterization procedure for EMC. The process will also be used to characterize the material properties and parameters of EMC after thermal ageing (see in the next chapter).

5 Thermal Ageing of EMC under HTS and TC Conditions

5.1 Introduction

Epoxy Moulding Compound as an encapsulation material for microelectronic devices has many advantages compared to other materials [82]. Presently, electronic components are frequently subject to harsh environmental conditions, such as high temperature and/or moisture. A component subjected to these harsh conditions can experience reliability problems, such as interface delamination, corrosion and material cracking [83]–[85] due to thermal ageing and/or humidity related changes of the encapsulating Epoxy Moulding Compound. Since thermal ageing impacts the long-term reliability of electronic packages, the experimental characterization and the constitutive representation of the ageing of EMCs have become an important subject for various researchers [10], [68], [86]–[91]. Meanwhile, various modelling methods for polymers were proposed and developed by various authors [92]–[94]. Nevertheless, a proper constitutive approach describing the slowly growing oxidation layer in the EMC is not available. Thus that it was cumbersome to predict the reliability of a real package for long-term applications. Further, the existing modelling methods for polymer-based materials are not only complex but also cannot be simply implemented in a standard FEM package. Therefore, an efficient and simplified modelling method and simulation process should be developed in order to improve this situation. Besides, most researchers focus on the thermal ageing under High-Temperature Storage (HTS) conditions. However, the EMCs will also be subject to ageing under Thermal Cycling (TC) conditions [95]. Obviously, ageing under these conditions is much slower than under HTS condition. Even so, it should become clear whether or not an EMC-validation sample being aged under TC shows equivalent material property changes as an EMC-validation sample being aged under HTS. Therefore, in this thesis an efficient and simplified modelling method and simulation process for EMC-ageing under HTC as well as under TC will be presented.

Three temperature processes are investigated in this chapter: HTS at 175°C and 150°C and TC from -55°C to 150°C according to the definition in Figure 5-1. For TC, the hold-times of the samples at the highest and at the lowest temperatures are both 15 minutes. The temperature changes from the highest temperature to the lowest temperature happen in a few minutes. In order to compare the ageing at HTS at 150°C with TC between -55°C and 150°C, an equivalent ageing time at 150°C is introduced. The assumption is that there is no thermal ageing or ignorable thermal ageing occurring at -55°C as well as during the temperature ramps. For example, 1000 cycles of TC than would compare to 250 hours of ageing at 150°C and 2000 cycles of TC than would compare to 500 hours of ageing at 150°C.

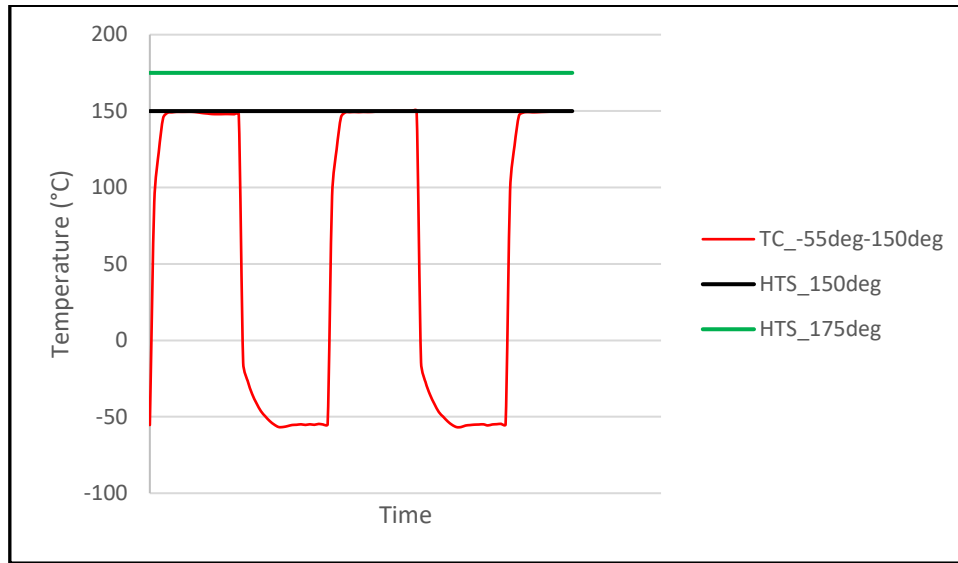


Figure 5-1: Thermal ageing temperature profiles for HTS and TC

Thermal ageing under HTS and TC conditions are considered for EMCs, since both can lead to irreversible changes in the applied EMCs. These changes can be attributed to chemical processes such as oxidation and lead to a degradation of the applied material. As a result, the thermo-mechanical properties of the EMC changes significantly. Due to the change in mechanical properties of EMC, the stress and strain distributions in a real package change with storage time as well. As a consequence, the long-time reliability of a package is severely affected. Frequently, an experimental method is used to assess the reliability of a real (already produced) package after long-term testing. However, using an experimental method on an already produced package is not only time consuming, but also costly. Therefore, for a semiconductor company, the question on how to quickly and efficiently assess the product reliability, already in the design state, is required and necessary. Compared to the experimental investigation on a real (already produced) package; the FE method is providing a quick and cheap way to improve the above situations. It is used in many industries to accelerate the design process. Quite important for FE modelling is the input of proper (correct and accurate) material models. In order to establish a correct material model input for the simulation, first of all, an appropriate material model should be selected. The material parameters for the selected model for the concerned material should then first be carefully characterized. In this chapter, the thermo-mechanical properties of EMCs after HTS and TC ageing are systematically characterized. In Chapter 4, the characterization was discussed for a fresh EMC (without ageing) by performing a series of mechanical test methods as well as numerical analyses. In the end, the FE model of fresh EMC as established could predict the thermo-mechanical behaviour of a fabricated bi-material sample during temperature loading quite well.

To be able to describe the material property changes of EMC and to predict the mechanical behaviour of an EMC-copper sample after the thermal ageing being applied, by using the FE method, much preparatory work was done in advance. First, a simple modelling method of thermal ageing on EMC is proposed, and then several special tests

are designed and performed to confirm the hypothesis. Second, based on the proposed method, a systematic characterization method is established to fully characterize and understand the material properties changes during thermal ageing. Third, according to the measurement results, the corresponding numerical analyses are applied to obtain the material model and the relevant parameters as input for the FE modelling. Finally, verification tests on bi-material samples are performed to check the accuracy of the established model. More detailed information will be presented in this chapter. Each section of this chapter starts with a short introduction, as follows:

- Section 5.2 will introduce a new idea for modelling thermal ageing effects on EMCs. Further, several tests are done to confirm the concerned hypothesis;
- Section 5.3 will show the oxidation layer growth as a function of ageing time as well as of the storage temperature by using fluorescence microscopy;
- Section 5.4 will show the measurement results of aged EMC from DMA testing;
- Section 5.5 will show the measurement results of aged EMC from TMA testing;
- Section 5.6 will introduce the ageing-induced shrinkage measurement of EMCs;
- Section 5.7 will introduce the “equivalent thickness” of the “equivalent oxidation layer” for a two-layer model
- Section 5.8 will introduce the warpage measurement of a bi-material sample as well as the simulation results;
- Section 5.9 will give a conclusion of this chapter.

5.2 Modelling approach and Demonstration

5.2.1 A proposed modelling approach

Since thermal ageing effects influence most of the critical failure modes in electronic components, such as die cracking, EMC cracking and interface delamination, research results were reported by many researchers [83]–[85], [91]. Investigations show that the thermal ageing of EMC is one of the main factors contributing to those failure modes. In order to understand the mechanisms of thermal ageing on EMC, a detailed investigation is done first.

Figure 5-2 and 5-3 show (fluorescence microscopy-) cross-sections of a strip of EMC before and after thermal ageing (in an oven with air at 175°C), respectively. As illustrated in Figure 5-2, before thermal ageing, only one colour is observed on the cross-section. However, after thermal ageing, Figure 5-3 shows layers of different colour existing in the cross-section. The outer layer is the so-called ‘aged layer’, the inner part is the so-called unaged core. In between a very small transition layer can be observed, which will be addressed later. The whole sample is the so-called ‘partly aged’ sample. The aged layer is created due to a chemical (or thermo-oxidative) reaction as previously addressed in [68]. The thickness of this layer is around a few hundred micrometers depending on storage time and ageing temperature. Because of this layer, the mechanical properties of such a partly aged EMC changed significantly, as reported by various researchers [10], [68], [96]–[99]. A severe influence on the stress and strain in packages is also reported [98], [99]. Unfortunately, there is still no good or simple modelling method available to describe the thermal ageing process of EMC during storage. Most of the researchers are still staying in the experimental analysis phase. Therefore, it is necessary to develop a simple and efficient approach to describe the effects due to thermal ageing on the mechanical behaviour of EMCs. Afterwards, this method can be applied in real packages for long-term reliability assessment under the high-temperature application.

Typically, the oxidized layer generated on the EMC’s surface is thought to be created by various effects such as oxygen diffusion, chemical reactions and possibly diffusion limiting. A full simulation model should include all these effects, including the resulting influences on the mechanical properties. However, it would be too complicated to include all effects in an applicable simulation model. Even it is not quite easy to implement the coupled diffusion and reaction process into commercial FE software. Therefore, a simple and efficient modelling method is proposed that can yet be well applied in FE-simulations. This approach is using so-called “equivalent layers”. Based on the above demands, a two-layer model is proposed based on the experimental observation and previous researches [68]. Actually, more than two layers are observed in the cross-section of aged EMC (see Figure 5-3). The outside layer is the fully aged layer (Dark colour), the middle part is the reaction layer (yellow colour) and the core is the unaged part (light yellow colour). The material properties of the reaction layer

cannot be easily established since this layer is relatively thin. Thus, a two-layer model with an “equivalent thickness” for the (fully) aged layer is proposed (see Figure 5-4).

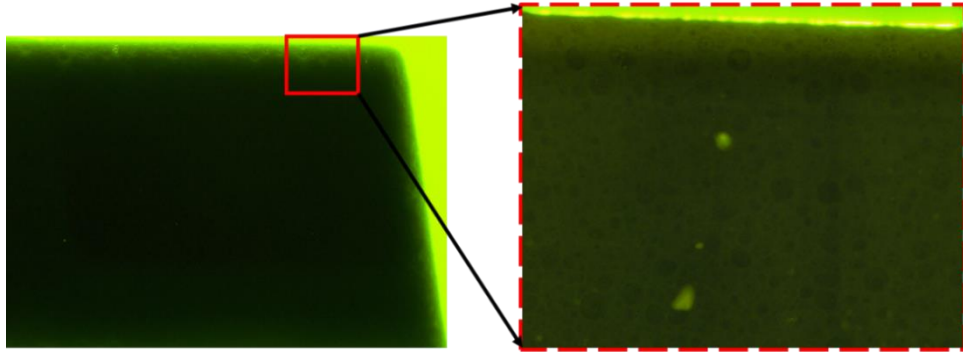


Figure 5-2: (Fluorescence microscopy-) Cross-section of unaged EMC

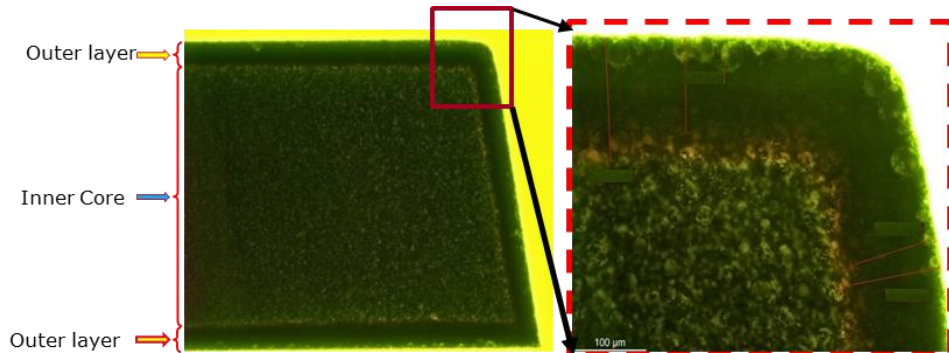


Figure 5-3: (Fluorescence microscopy-) Cross-section of aged EMC

In Figure 5-4, a schematic of this method is presented. It assumes that the mechanical behaviour of the partly aged sample can be modelled with sufficient accuracy, by modelling a fully aged “equivalent layer” and an unaged core material. The thickness of the equivalent layer as a function of ageing time should be defined such that the “overall material properties” of a strip of moulding compound are well predicted for any time during high-temperature storage. Thus, only unaged and (fully) aged EMC have to be characterized and analysed. In Chapter 4, the characterization on the unaged EMC was presented. How to characterize the material properties of the very thin oxidation layer and how to establish the equivalent thickness of the oxidation layer (aged layer) as a function of ageing time and ageing temperature are the main challenges of the present work. If the material properties of both the unaged core and the fully aged layer are established and the oxidation layer growth as a function of ageing time and temperature is known, then the “overall material properties” of a partly aged strip of Moulding compound can be predicted. Subsequently, the stress and strain state of a real package after various thermal ageing times can also be simulated and predicted.

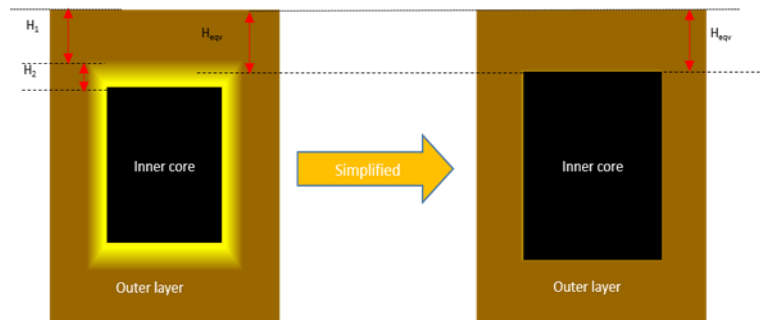


Figure 5-4: The principle of a two layers model

5.2.2 Hypothesis Verification

Obviously, before using the proposed two-layer model, several questions have to be answered in advance. For example, does the core material keep the same material properties as the (original) unaged sample? Is the core thermally stable during high-temperature storage? Another question arises on: “How thin the sample should be prepared in order to get a fully aged sample in a short time”. To answer the above questions and to enable the development of the proposed two-layer modelling method, a series of tests are performed. Samples of two different thicknesses are prepared as illustrated in Figure 5-5. The thick samples are produced directly from the production line. The thin samples are obtained from the polishing process as introduced in Chapter 3.

Firstly, the aged samples of both thicknesses are obtained through storage in a normal air oven at 175°C. The mechanical tests are subsequently performed for both types of samples before and after thermal ageing.

Secondly, samples of both thicknesses are subjected to storage at 175°C in two different isothermal ovens: One filled with air and the other under vacuum.

In addition, the cross-sections of all samples are also checked with fluorescence microscopy.



Figure 5-5: Samples of two different thicknesses are prepared for mechanical testing

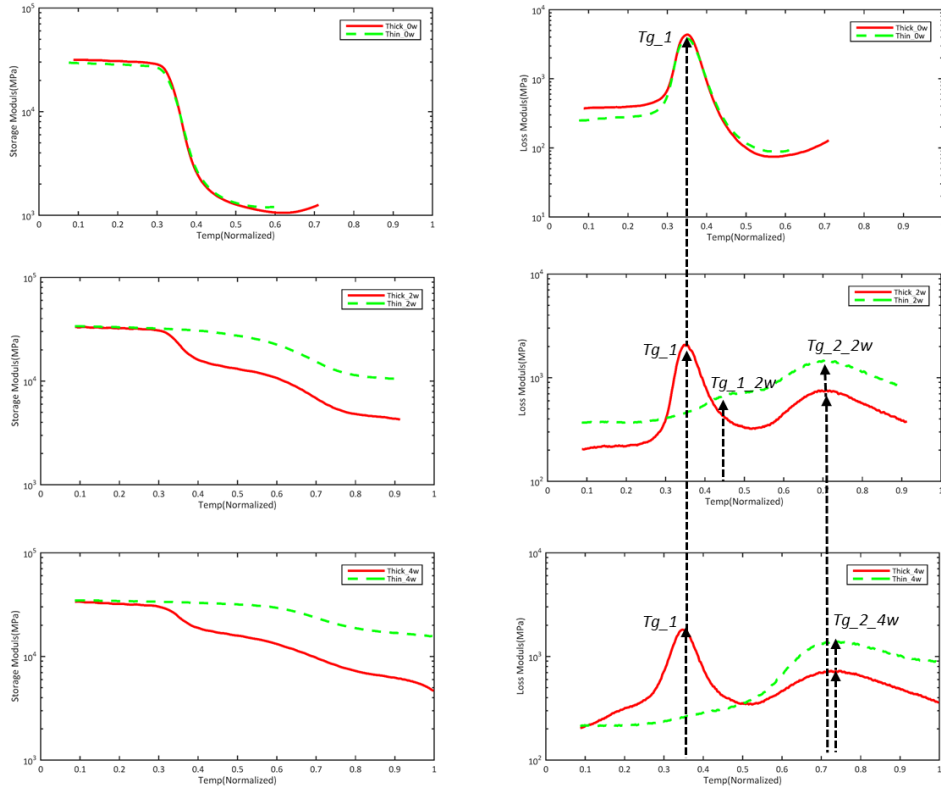


Figure 5-6: DMA test results of thick and thin EMC samples before and after ageing at 175°C: 1st row: unaged (0w); 2nd row: aged (2w); 3rd row: aged (4w)

In Figure 5-6, the storage modulus (left column) and loss modulus (right column) versus temperature (at 1Hz) are shown, before and after thermal ageing. The (left) peak value of the loss modulus represents the glass transition temperature. The measurement conditions, such as heating rate and loading amplitude, are the same for all measurements. The red curves represent the results from the thick samples, and the green curves are from the thin samples. The pictures at the 1st row are the results from the thick and thin samples before thermal ageing (0w). The pictures at the 2nd and the 3rd row are the results of the thick and thin samples after 2 weeks (2w) and 4 weeks (4w) on ageing under air at 175°C, respectively. From Figure 5-6, the following conclusions can be drawn:

- 1) Firstly, without thermal ageing, the thin sample has the same modulus and glass transition temperature as the thick sample. This indicates that after polishing the thin sample has the same material properties as the thick sample.
- 2) Secondly, after 2 weeks of thermal ageing, the storage and loss modulus (as shown in the 2nd row) appear to be thickness dependent. The storage modulus of the thin sample is much higher than that of the thick sample except in the glassy state. Meanwhile, two peaks in the loss modulus are observed in both samples. This means that two different materials (with different T_g) exist in both samples after 2 weeks of thermal ageing. Furthermore, they show different peak values for the first T_g but have the same values for the second T_g . The first T_g of the

thick sample is the same as that of the fresh (unaged) sample. It means that the core of the thick sample is unaged. However, the first T_g value of the thin sample is higher than that of the thick sample (and thus higher than that of the unaged material). The reason is that the core of the thin sample is somewhat oxidized (but not fully oxidized). As a result, there is no unaged core existing in the thin sample after 2 weeks of thermal ageing. The second T_g values from both samples are (more or less) the same, which is from the aged layer (or outside layer of the sample). Because both sample surfaces are exposed to the air, they appear to have the same degree of ageing. In other words, the material property of this oxidation layer appears to be thickness independent.

- 3) Thirdly, after 4 weeks of thermal ageing, the storage modulus of both the thick and the thin sample is increased compared to that of the 2w samples. The storage modulus is continuously increasing with ageing time, especially at the rubbery state. Also, these moduli appear to be thickness dependent. Meanwhile, two T_g values are still existing in the thick sample even after four weeks of thermal ageing. The first T_g of the thick sample still keeps the same as that of the fresh sample. The second T_g of the thick sample has the same value as that of the thin sample within the same ageing time. Meanwhile, only one T_g (the 2nd T_g) was found in the thin sample after 4 weeks of thermal ageing. This indicates that only one material remains in the thin sample. Besides that, the 2nd T_g value from 4 weeks ageing is a little bit higher than that from 2 weeks ageing. It means that after 4 weeks of ageing the thin sample is close to be at the “fully aged” state.

From the above findings, the following concluding remarks can be made: after polishing the thin sample keeps the same mechanical properties as the thick sample. The mechanical properties of aged EMC are thickness dependent as well as ageing time dependent for the defined storage temperature. If the whole thickness of the sample is oxidized, then only one T_g is observed from the measurement. Otherwise, two T_g values are always observed if the unaged core still exists. It indicates that the proposed modelling method could work if the material property of the (unaged) core is still the same as that of the fresh sample. Therefore, a second test is designed and performed to check whether or not the modulus of the inner core of aged EMC is changing.

In the second test, samples with the same thickness are divided into two groups and stored in the air oven and the vacuum oven, respectively. The storage temperature is 175°C for both storage conditions. After a certain ageing time, the mechanical test is performed to measure the modulus of EMC aged under air and under vacuum conditions. Meanwhile, fluorescence microscopy is also used to check the cross-section. Three ageing times are checked: zero, two and four weeks. All test results are shown in Figure 5-7. As illustrated in Figure 5-7, the storage and loss modulus of aged samples in two ageing conditions are plotted together with the results for the unaged sample. The results show that the material properties of EMC after being stored under vacuum conditions are the same as those of the unaged sample. However, for storing under air environment, it appears that the material properties are changing significantly with increasing storage time. In particular, the rubbery state is seriously affected or dramatically increased. Besides, two T_g values are also found after thermal ageing in

the air oven. The first T_g value remains the same as that of the fresh sample; the second T_g value is much higher than the first T_g value. It is shifting to higher temperatures with increasing ageing time. It indicates that some additional substance is generated during thermal ageing in the air oven. However, only one T_g value is observed after ageing in the vacuum oven which is the same as that of the fresh sample (or unaged sample). It means that the EMC is thermally stable under vacuum ageing conditions.

The cross-sections of samples from the vacuum oven and from the air oven with the same storage time are also checked by fluorescence microscopy. The pictures are presented in Figure 5-8. The left picture is from the fresh sample and only one colour was observed. The upper right picture is the aged sample from the air oven after two weeks of ageing time. In this (upper right) picture it can clearly be observed that an oxidized layer exists at the outside surface of the EMC. The lower right picture is from the vacuum oven after two weeks of thermal ageing. Here, only one colour is observed. There is no additional layer existing or generated. The colour of the pictures belonging to the fresh and aged samples (from the vacuum oven) is different due to the settings of the fluorescence microscopy measurement.

Combing the above findings and demonstrations, a two-layer assumption for thermal ageing modelling of EMC becomes obvious: after high-temperature storage in the air oven two parts exist in the EMC (Figure 5-3). The outer layer is the aged layer or oxidized layer and the inner layer is the unaged core. The unaged core keeps the same material properties as the fresh or unaged sample. The thermo-mechanical properties of unaged EMC are fully characterized and verified in Chapter 4. Only the material properties of the aged layer are unknown at the moment. So, if the material properties of these two states of the EMC are established, while the thickness of the oxidation layer as a function of ageing time is also known, then the “overall material properties” of partly aged EMC can be predicted for any ageing time. Therefore, the following sections will be focusing on the material characterization of the oxidation layer as well as the verification.

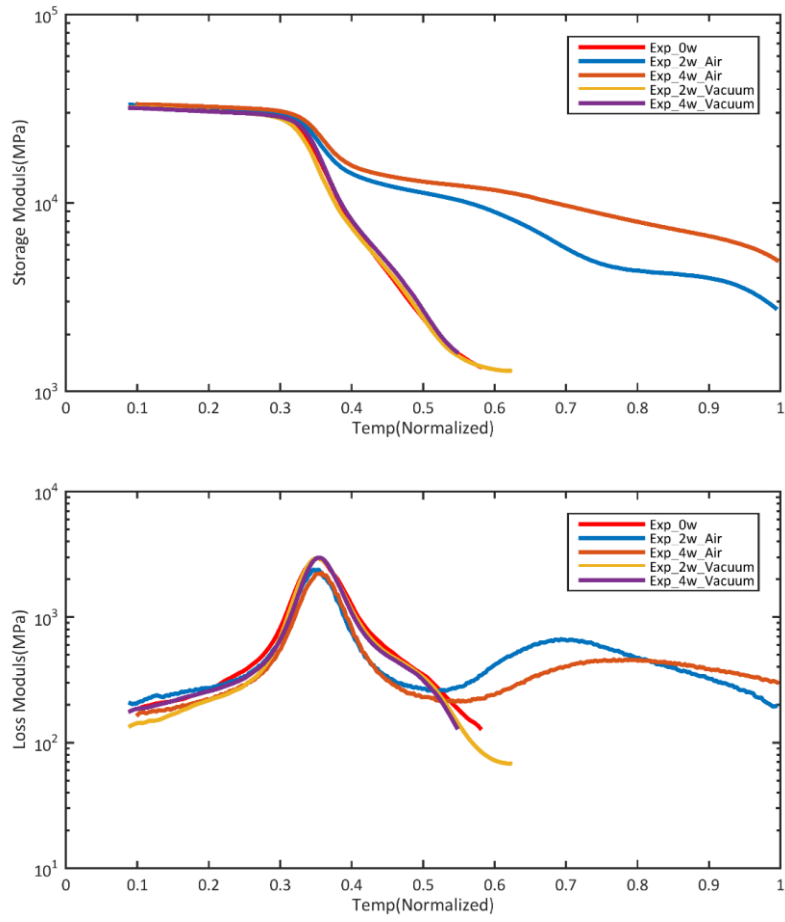


Figure 5-7: Storage and loss moduli of EMC before and after thermal Ageing under air and under vacuum environment

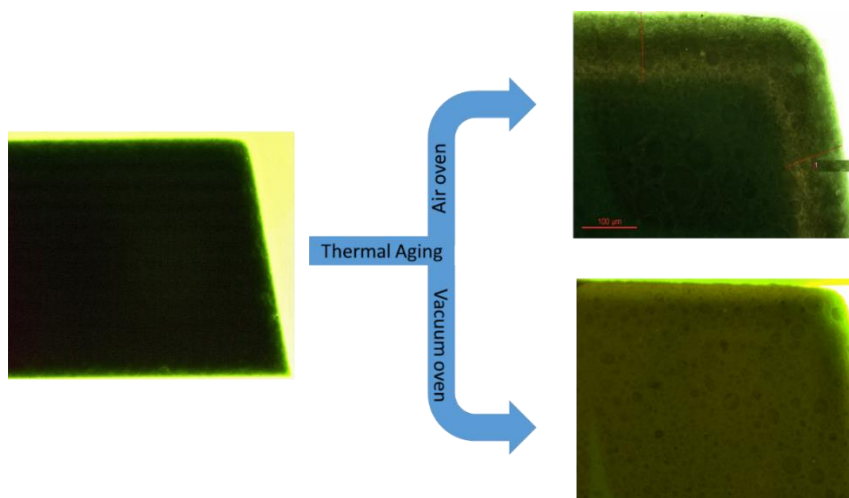


Figure 5-8: The Cross-section of EMC before and after thermal Ageing in the air and vacuum oven

5.3 Fluorescence Microscopy

From the previous section, it is observed that new material is generated below the EMC surface during thermal ageing. In order to establish the oxidation layer growth as a function of ageing time at a specific temperature, the cross-sections of samples after various thermal ageing times are visualized by fluorescence microscopy. The thickness of the aged layer is estimated for the various ageing times. These thickness estimates are performed for thermal ageing at HTS under 175°C and 150°C and also for TC at 150°C.

Figure 5-9 shows the cross-sections of EMCs being aged from 2 days up to 16 weeks at 175°C. All pictures show about three layers existing in the cross-sections. The outer layer has a dark colour. The middle layer is yellow. The dark inner part represents the unaged core. The dark outer layer is more or less fully aged, and the yellow layer is the so-called reaction zone, where the chemical reaction between EMC and oxygen takes place. With increasing ageing time, the yellow zone becomes smaller until it remains unchanged. However, the thickness of the outer dark layer is continuously increasing with ageing time. The total thickness of the aged layer (dark layer plus yellow layer) is plotted in Figure 5-11 as a red curve. The definition of the total thickness is a rough estimation from the microscopy measurement because the boundary between unaged core and reaction zone (yellow layer) is hard to distinguish.

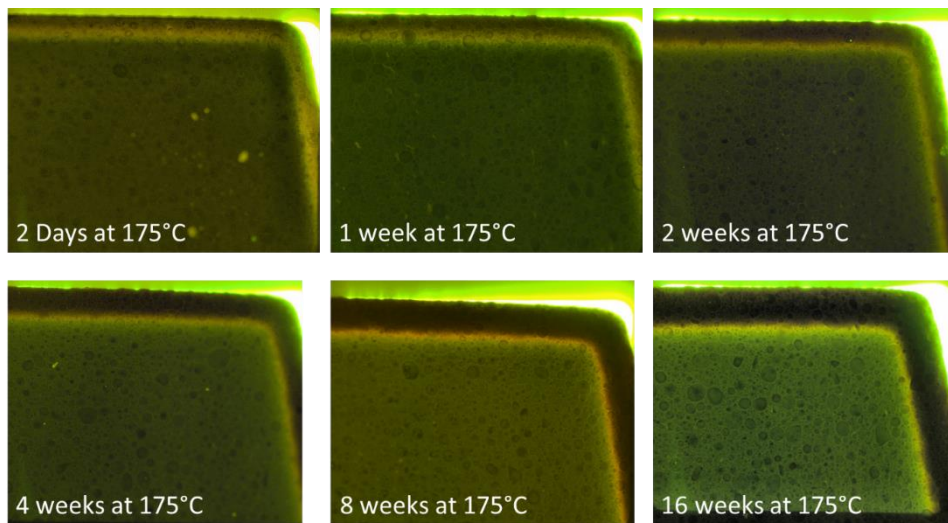


Figure 5-9: Cross-section of aged EMC after thermal Ageing at 175°C

Figure 5-10 shows the cross-sections of EMCs aged from 1 week up to 24 weeks at 150°C. The colour of the oxidation layers remains similar for the various ageing times; the thickness of the oxidation layer is growing with ageing time again. It appears that the colour of the oxidation layers for ageing at 150°C is slightly different from that at 175°C. (*Here it should be noted that it is not fully clear whether the microscope settings were the same in all cases.*) This suggests that ageing at 150°C could possibly result in a different chemical reaction process compared to that for ageing at 175°C. This is confirmed in the mechanical measurements as it will be shown later. The

oxidation layer growth as a function of ageing time for ageing at 150°C is plotted in Figure 5-11 as the blue curve.

As illustrated in Figure 5-11, the thickness of the oxidation layer at 150°C is higher compared with that for ageing at 175°C, within the same ageing time. The reason is probably that the oxidation layer generation is controlled by two processes: oxygen diffusion and reaction. When the ageing temperature is 175°C, the chemical reaction process is much quicker than the oxygen diffusion process inside the EMCs. In other words, the chemical reaction is intense between EMC and oxygen at 175°C. The reaction process will consume most of the diffused oxygen. As a result, less or no oxygen could diffuse further into the core of EMC. Meanwhile, it leads to a high level of ageing of the oxidized layer and a thin layer of the oxidized EMC. At 150°C, the oxygen diffusion process is relatively quicker than the reaction process. Therefore, more oxygen can diffuse into the EMC. As a result, more EMC reacts with oxygen and leads to a thicker oxidation layer compared to the 175°C case (within the same ageing time). But the level of ageing of the oxidation layer is lower than that of the 175°C case. This will be confirmed with mechanical testing in the next section. Within the same ageing time, the overall stiffness of a sample aged at 175°C is much higher than that of a sample aged at 150°C. The oxidation layer growth for both ageing temperatures is following the empirical power law:

$$d = \left(\frac{t}{t_0}\right)^\alpha + d_0 \quad (5-1)$$

Where, t is the ageing time and t_0 , α and d_0 are the fitting parameters. Here, α is lower than 0.5. This indicates that the ageing process is not only oxygen diffusion-controlled but also reaction controlled [98].

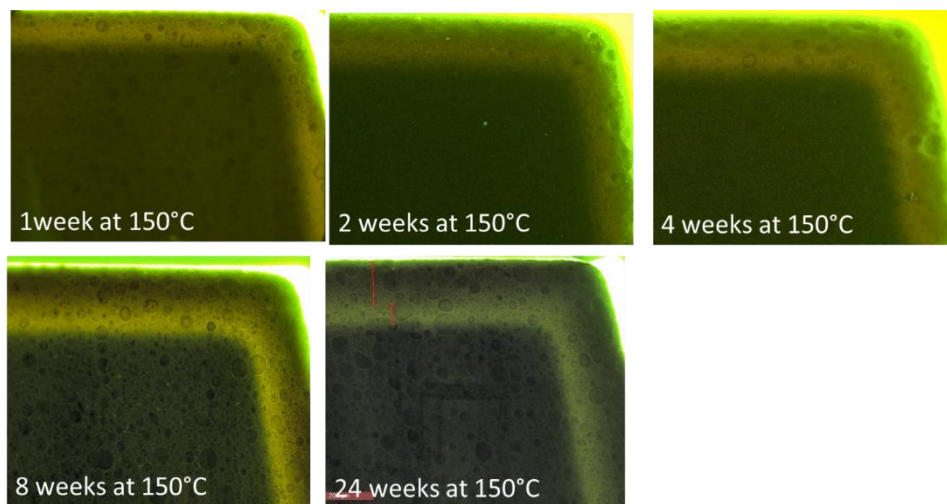


Figure 5-10: Cross-section of samples after thermal ageing at 150°C

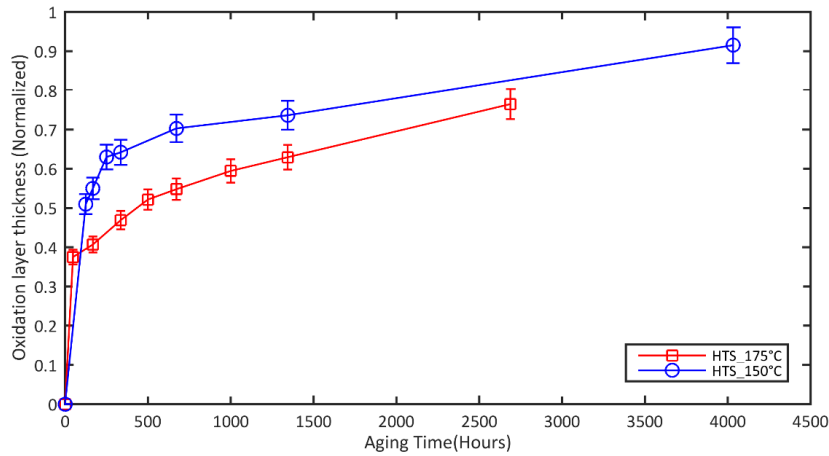


Figure 5-11: Oxidation layer growth as a function of ageing time

As shown in Figure 5-11, both curves can be roughly divided into two parts: the oxidation layer grows very quickly before 500 hours of ageing. After that, the oxidation layer growth is much slower. The same phenomenon was found in paper [5], [17], [18], [21]–[23]. According to these researches, the thermal ageing could change the density and the volume of the polymer-based material. During thermal ageing, the material density will increase, and volume will possibly shrink. Thus, the oxygen diffusion process in an aged layer is becoming more complicated compared to the diffusion in unaged EMC. As a result, less oxygen diffuses further into the EMC core once the density of the oxidized layer becomes higher and higher. Once the aged layer becomes stable or fully aged, the density or volume will not change any more. Then the velocity of oxygen diffusion in this layer will be stable again. That's the reason that the oxidation layer grows smoother and more or less follows a linear law in the second part of the curves. After the same ageing time, the ageing level of the oxidation layer is much higher at 175°C compared to 150°C. This means that the density of the aged layer is higher at 175°C. It is an explanation of the slow increase of the oxidation layer that grows at 175°C. We will come back to the above discussion after our measurements in Section 5.6.

Figure 5-12 and Figure 5-13 show the cross-section and thickness of the oxidation layer of aged EMCs after HTS and TC conditions. Two points are compared, 125 and 250 hours at a constant temperature of 150°C and 500 as well as 1000 TC cycles at -55°C-150°C, respectively. The results show that the oxidation layer measured by the microscope is the same for both types of thermal ageing conditions since the total (equivalent) ageing time at 150°C is the same for both conditions. It indicates that thermal ageing only occurs at higher temperatures. There is no or less ageing at lower temperatures. Further investigation needs to be done in order to explore whether the mechanical properties of EMCs are also the same in both conditions. This research will be shown in later sections.

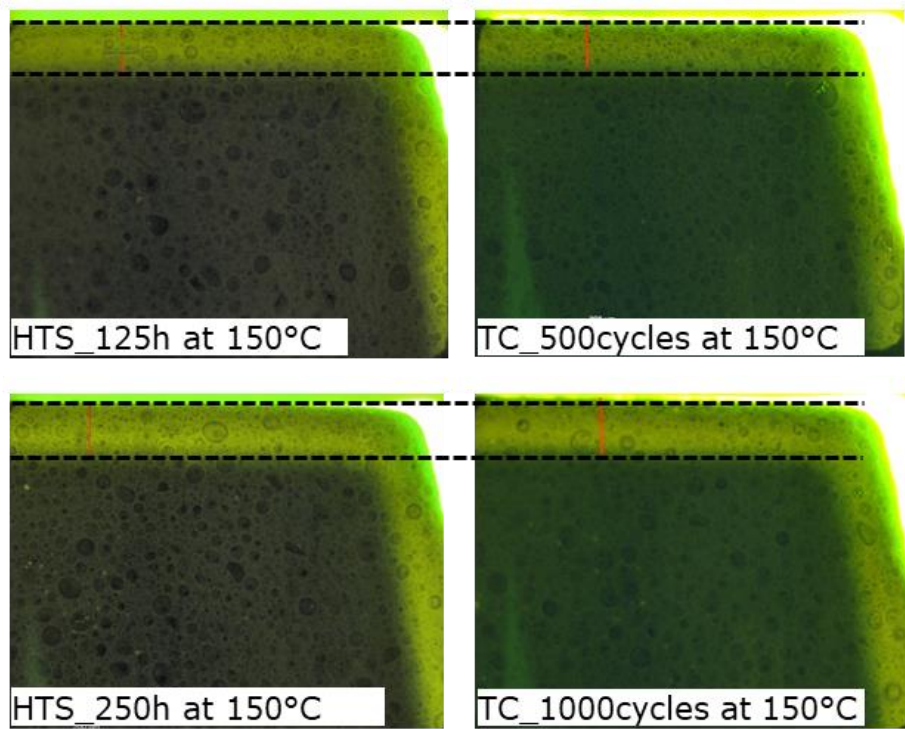


Figure 5-12: Cross-section of EMCs after thermal ageing at HTS and TC at 150°C

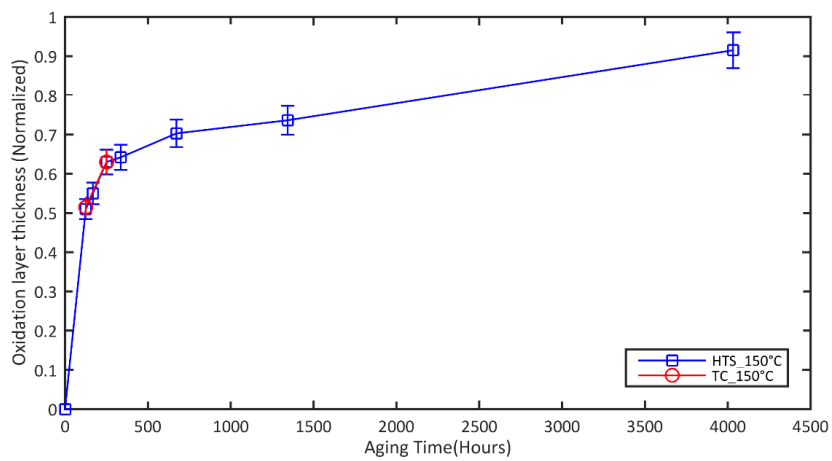


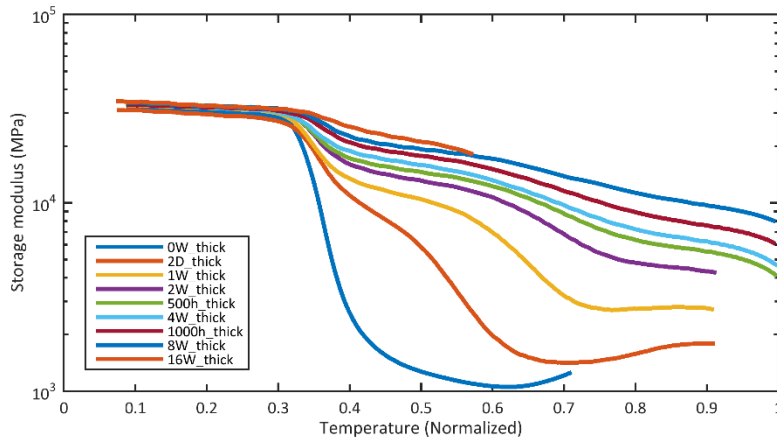
Figure 5-13: Oxidation layer growth after HTS and TC thermal ageing at 150°C

5.4 DMA test for aged samples

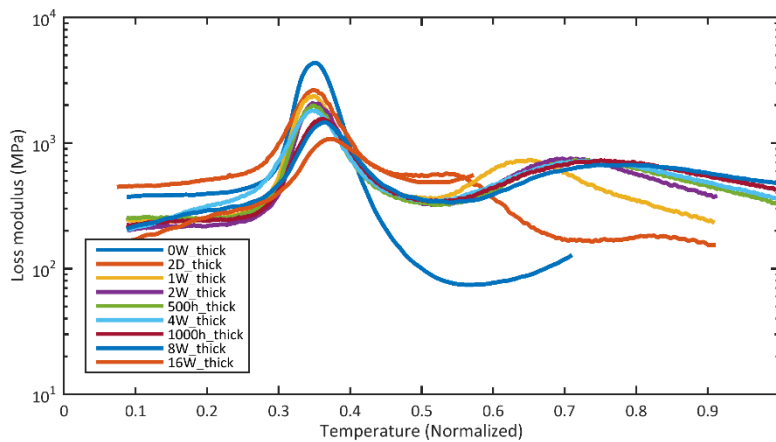
In order to generate the material model for FE simulation, DMA testing is applied to obtain the viscoelastic parameters of EMC before and after thermal ageing. Firstly the material model of aged EMC is established based on the test results. Secondly, the thermal ageing effects on the changing EMC properties could also be established. The DMA-test conditions are the same as previously used for the unaged EMC.

5.4.1 DMA results for Ageing at 175°C

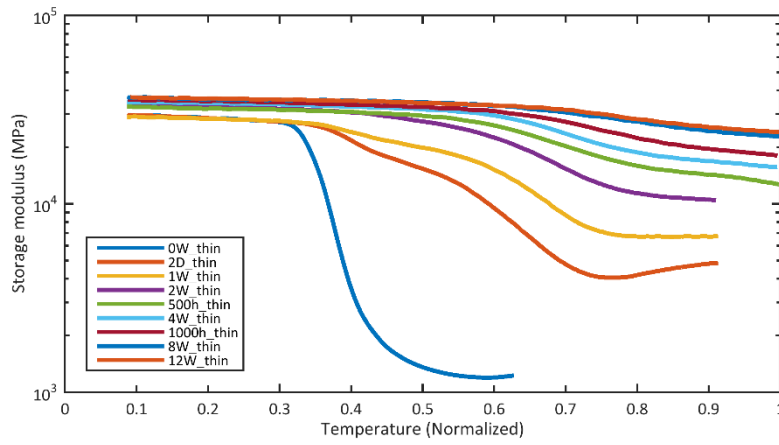
The results of the DMA measurements of aged samples under 175°C storage will be presented and discussed in this section for thick and thin samples.



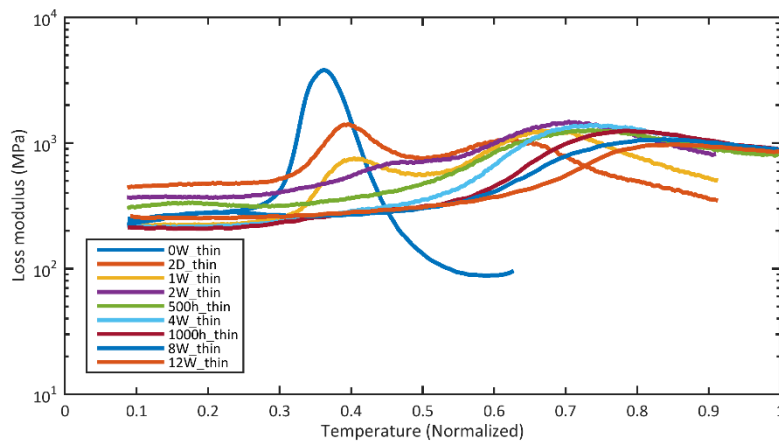
(a) Storage moduli of EMC aged at 175°C (*Thick sample*)



(b) Loss moduli of EMC aged at 175°C (*Thick sample*)



(c) Storage moduli of EMC aged at 175°C (*Thin sample*)



(d) Loss moduli of EMC aged at 175°C (*Thick sample*)

Figure 5-14: Storage and Loss moduli of EMC aged at 175°C

Figure 5-14 shows the storage and loss moduli of the thick and thin samples for different ageing times. The pictures in the first row belong to the thick samples before and after thermal ageing. The second row is from the thin samples. The ageing time ranges from 0 until 16 weeks. Here, the glass transition temperature T_g is defined as the peak value of the loss modulus at 1Hz.

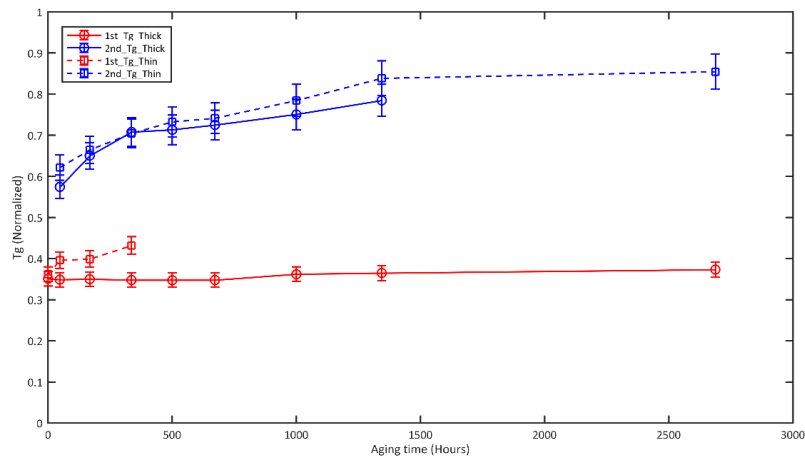


Figure 5-15: Glass transition temperature of thick and thin samples after thermal ageing

According to the above measurement results, the following conclusions can be given:

- 1) For thick samples, the storage modulus is changing significantly, in particular in the rubbery state. The difference is more than 1500% between 0 and 8 weeks of ageing. As for the glassy state, the value does not change as much as in the rubbery state. Two T_g values are observed in the loss modulus graphs. Between 0 and 8 weeks of ageing time, the first T_g value of aged EMC is always the same as for the unaged material. During HTS, the second T_g is generated due to the chemical reaction. It is shifted to a higher temperature as a function of the ageing time. However, after 8 weeks of thermal ageing, the first T_g is also starting to slowly shift to a higher temperature. This means that the core of the thick sample is also starting to oxidize. (*In Section 5.2, where the two-layer model is introduced, we will come back to this*). Meanwhile, the second T_g is continuously increasing. All the information can be found in Figure 5-15 (solid line). Unfortunately, after 16 weeks of ageing at 175°C, the aged EMC-layer was cracking at a certain temperature during the DMA-measurement. The reason could be that this thick sample is partly aged. During the DMA measurement, the temperature is increasing, then thermal stresses due to the material mismatch are added to the internal stresses between the two layers generated due to the ageing process. Once the stresses reach a critical value, the sample will crack. Therefore, only a certain part of the measurement result is shown.
- 2) For the thin samples, the storage modulus is also changing significantly in the rubbery state. The difference is more than 2700% between aged and unaged samples. However, at the glassy state, the modulus is not changed as much as in the rubbery state. Between 0 and 2 weeks of ageing, two T_g values are found in the thin samples. The first T_g is increasing with the ageing time. After 2 weeks, only one T_g value is found and continuously increasing with ageing time. When the ageing time is equal to 8 weeks, the storage modulus is almost horizontal in the temperature range of interest. After 8 weeks of ageing, the storage modulus

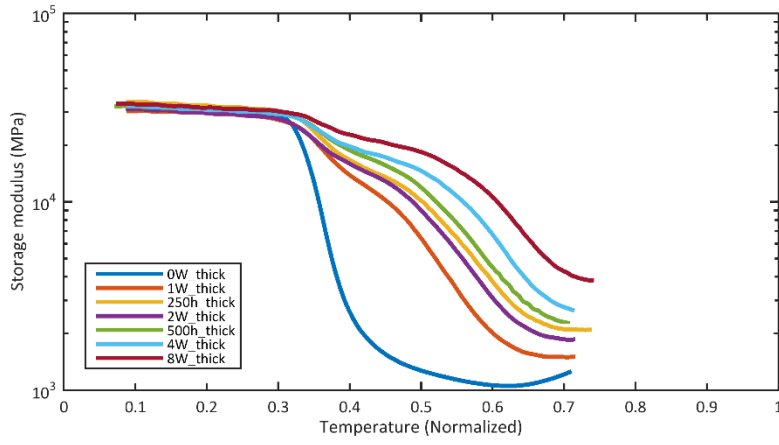
is no more changing at all and keeps stable. The similar phenomenon is also found for the T_g values. The T_g value keeps constant after 8 weeks of ageing. It indicates that the thin sample reaches the fully aged state. The changes in glass transition temperature with respect to the ageing time is shown in Figure 5-15 (dashed line).

- 3) As illustrated in Figure 5-15, the T_g values of thick and thin samples are plotted together against the ageing time. First of all, the first T_g of thick and thin samples is the same as those for an unaged sample. Once the core of the EMC is starting to age, the first T_g is shifting to a higher temperature, and the second T_g of thick and thin samples are more or less the same during HTS. Meanwhile, the second T_g is rising quickly until 500 hours of ageing. After that, the increment becomes slowly. It again has a good correlation with the curve of the oxidation layer growth (see Figure 5-11). The second T_g is generated due to the oxidation process, which is created below the surface of the EMC. However, the state of this oxidation layer is still far away from the fully aged state. As a result, the second T_g is continuously increasing with ageing time. After a long time of HTS, the oxidation layer is becoming close to that of the fully aged state. Therefore, the second T_g is than only slowly increasing. Once the oxidation layer gets fully aged, the T_g remains constant even for a prolonged ageing time as shown for a thin sample after 16 weeks of thermal ageing.

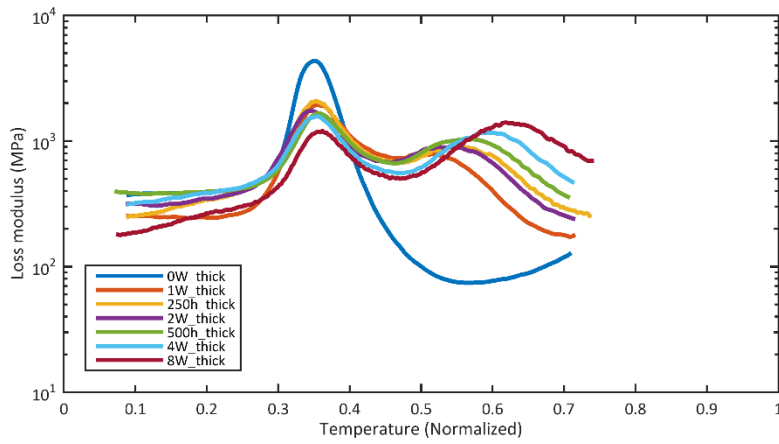
5.4.2 DMA results of Ageing at 150°C

In this section, two test conditions are considered to investigate the difference in the material property change of EMC after HTS and TC thermal ageing conditions. As shown in the cross-section micrographs, the oxidation layer thicknesses of the EMC under these two conditions are the same if the total ageing times at the higher temperature are the same. Here, the DMA testing is performed to see whether the same phenomenon can be observed from the mechanical testing.

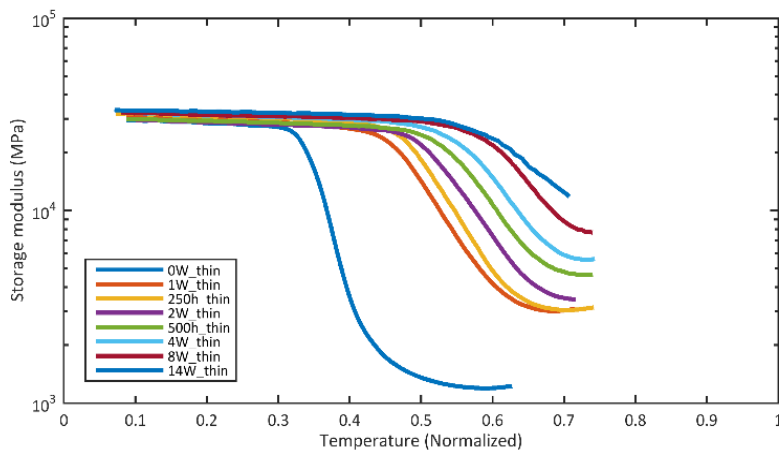
Figure 5-16 shows the DMA results of the thick and thin samples at the ageing temperature of 150°C and under HTS after several weeks. The pictures of the 1st row are from the thick samples at different ageing times. The 2nd row is from the thin samples. The ageing time ranges from 0 up to 14 weeks. The storage and loss moduli are shown in Figure 5-16 as a function of temperature. As previously defined, the glass transition temperature of aged EMC will be defined as the peak value of the loss modulus at 1Hz. Figure 5-17 presents the glass transition temperature of aged EMC after different ageing times. The solid lines are from the thick samples; the dashed line is from the thin samples.



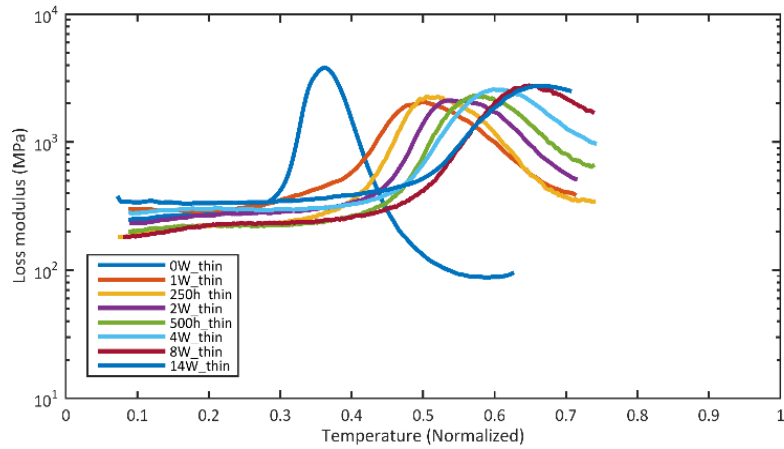
(a) Storage moduli of aged EMC at ageing temperature of 150°C (*Thick sample*)



(b) Loss moduli of aged EMC at ageing temperature of 150°C (*Thick sample*)



(c) Storage moduli of aged EMC at ageing temperature of 150°C (*Thin sample*)



(d) Loss moduli of aged EMC at ageing temperature of 150°C (*Thin sample*)

Figure 5-16: Storage and Loss moduli of aged EMC at ageing temperature of 150°C

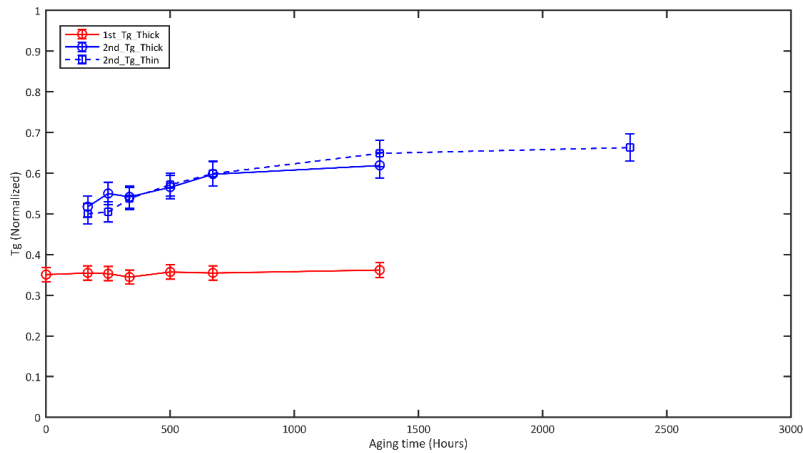


Figure 5-17: Glass transition temperature of thick and thin samples for ageing at 150°C

According to the above measurement results, the following conclusions are given:

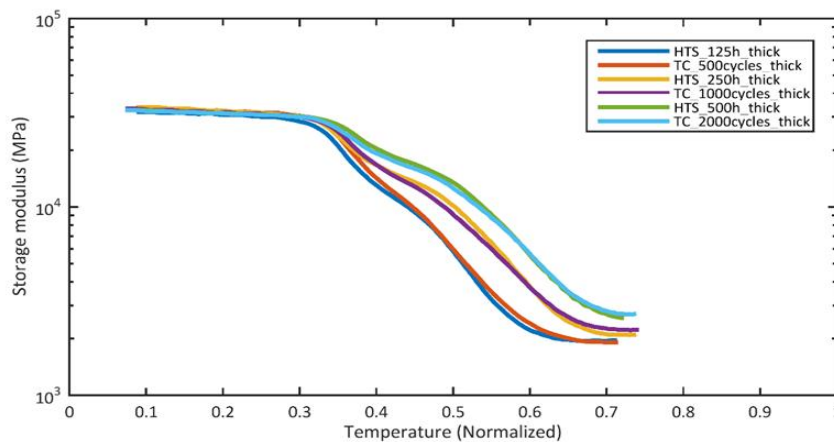
- 1) For thick samples, the storage modulus is changing significantly in the rubbery state. The difference is more than 700% between 0 and eight weeks of ageing. In the glass state, the values do not change much. Two T_g values are always observed in all thick samples during HTS. Among them, the first T_g values are always the same as for the unaged sample; only the second T_g value is increasing with ageing time.
- 2) For the thin sample, the storage modulus is changing significantly in the rubbery state, too. The difference between aged and unaged samples is more than 1600%. However, in the glassy state, the modulus does not change. After 1

week of ageing, only one T_g was found. With increasing ageing time, the T_g value is getting higher. In the end, the T_g value remains constant at a certain temperature. Therefore, only one curve is plotted in Figure 5-17 (the dashed line). The detailed explanation is presented in section 5.3.

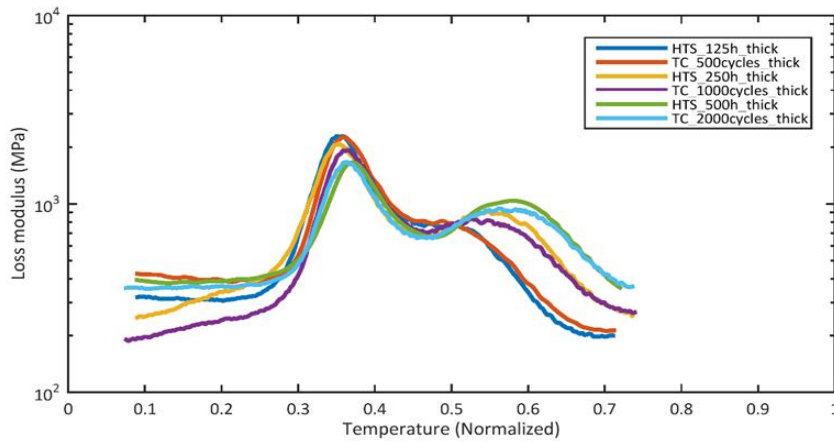
- 3) In Figure 5-17, the T_g values of thick and thin samples versus ageing times are plotted together. The T_g of the oxidation layer is similar for thick and thin samples during HTS. It means that the T_g value of the oxidation layer is thickness independent at the given ageing temperature. It only depends on the ageing time.

The thick samples aged under HTS and TC conditions are also studied and compared to see a possible difference between them while the total “equivalent ageing time” at 150°C is the same in both ageing conditions. The purpose of this measurement is to establish whether or not HTS can be used to get the same aged sample as obtained from ageing during TC. TC thermal ageing is quite time-consuming. For instance, an (equivalent) thermal ageing time of 250 hours at 150°C needs more than 1000 hours in TC.

The size of the samples is the same. They are stored in an HTS and a TC oven, respectively. The information of both ovens can be found in Chapter 3. After a certain ageing time, the samples are taken from both ovens for mechanical testing. As Figure 5-18 shows, the storage and the loss modulus are similar for three different ageing times (for both HTS- and TC-ageing conditions). It shows that ageing under TC conditions can be substituted by HTS ageing (with an “equivalent ageing time”) to get the parameters of the aged model of the EMC after TC ageing. As a result, it can save many resources and testing time. Of course, for the real package reliability testing, the HTS test cannot simply replace the TC test. The reason is that the state of stress and strain inside the package will change during TC loading and thus can trigger other damage mechanisms. The results shown here to introduce a method on how to quickly get an aged material model for EMC for TC while just applying HTS ageing.



(a) Storage moduli of aged EMC under HTS and TC ageing conditions



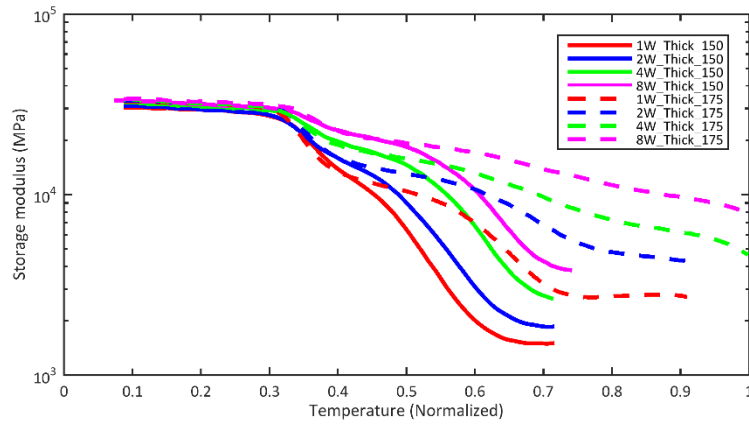
(b) Loss moduli of aged EMC under HTS and TC ageing conditions

Figure 5-18: Storage and Loss moduli of aged EMC under HTS and TC ageing conditions

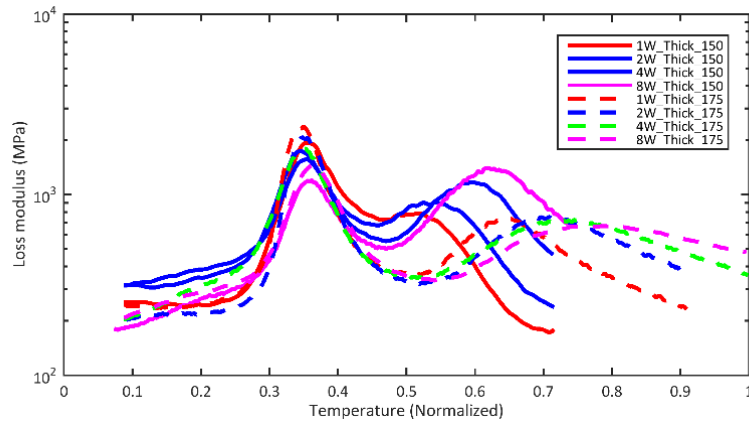
5.4.3 Comparison between 175°C and 150°C

A comparison between the thick and thin samples at the ageing temperatures of 175°C and 150°C is presented in Figure 5-19. The pictures in the first row present the storage and loss moduli of the thick samples at the ageing temperatures of 175°C and 150°C for various ageing times. The second row presents the results for the thin samples. The solid lines belong to the ageing temperature of 150°C, and dashed lines to the ageing temperature of 175°C.

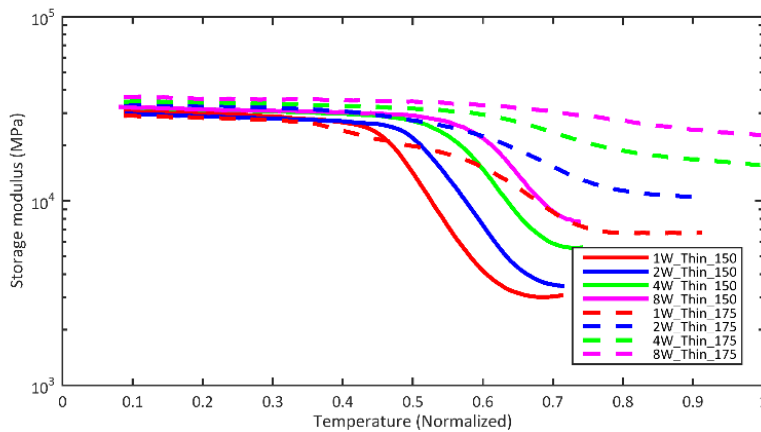
The results show that for both thick and thin samples, more cross-linking evolves at 175°C than at 150°C. As a consequence, samples are possibly more brittle and stiffer at HTS of 175°C compared to 150°C. In other words, the degree of ageing is higher at 175°C compared to 150°C after the same ageing time. As illustrated in the graphs of the loss modulus, either at 175°C or 150°C ageing temperature, the first T_g values of the thick samples are the same as for the unaged sample. However, the second T_g for ageing at 175°C is much higher than for ageing at 150°C (with the same ageing time). For the thin samples, before two weeks of ageing at 175°C two T_g values are observed and after that only one T_g value is left. It means that the thin sample has an unaged core only until two weeks of ageing at 175°C. After that, the whole volume is oxidized (as then one T_g only is found). Ageing at 150°C shows one single T_g already after one week of ageing. The pictures from the fluorescence microscopy (see Figure 5-11) confirm this phenomenon since they show that the oxidation layer growth is much higher at 150°C than at 175°C.



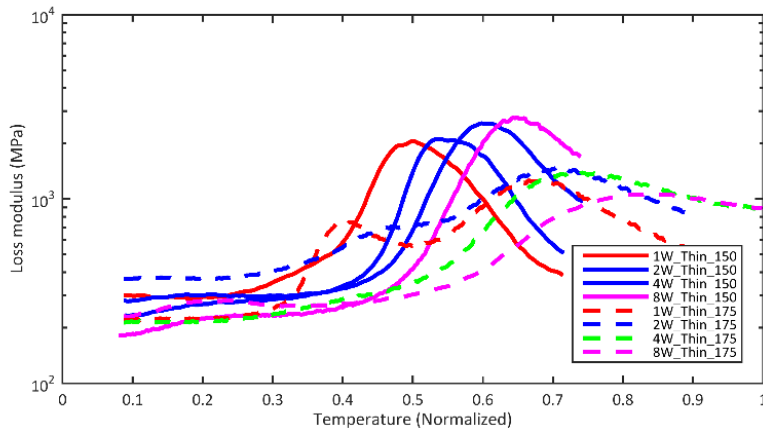
(a) Storage moduli of the *thick samples* at ageing temperature of 175°C and 150°C



(b) Loss moduli of the *thick samples* at ageing temperature of 175°C and 150°C



(c) Storage moduli of the *thin samples* at ageing temperature of 175°C and 150°C



(d) Loss moduli of the *thin samples* at ageing temperature of 175°C and 150°C

Figure 5-19: Storage and loss modulus of the thick and thin samples for various ageing times and ageing temperatures of 175°C and 150°C.

5.5 TMA measurement of aged EMC

From various findings in the past [96], [103], [104], the thermal ageing will reduce the CTE value above the glass transition temperature of about 10%-20% (of unaged material). But it only slightly reduces or has no impact on the CTE value below the glass transition temperature. However, all measurements were performed on very thick samples. Based on the previous DMA and cross-section results, the partly aged EMC consists of an aged outer layer and an unaged core. Both material properties are different. Therefore, performing a thermal expansion test on partly aged samples cannot straightforwardly result in proper CTE changes due to the ageing effect. The measured data contain two parts: thermal expansion of the (complete) partly aged sample and internal stress due to the CTE mismatch between aged and unaged EMC. Therefore, the measurement data from partly aged samples cannot be directly used for evaluation and simulation purposes. Up to now, no experimental data is available about how the CTE changes once the EMC gets fully aged. In the present thesis, only thin samples are used to monitor the CTE change during the thermal ageing process, since the thin sample can get fully aged in a short time (compared to the thick sample). The measurement results will be presented and discussed in this section. The test conditions are the same as introduced in Chapter 3 for unaged EMC. The temperature range for the CTE determination is the same above and below T_g in all measurements.

5.5.1 TMA measurement of Ageing at 175 and 150°C.

Figure 5-20 shows the CTE values of thin samples of EMC during several weeks of ageing at 175°C. Before 500 hours, there are two CTE values existing in the temperature range of interest. This indicates that the thin sample is not fully oxidised. After that, only one CTE was found. From 500 hours to 8 weeks of ageing, a slow decrease of the CTE is observed. Finally, the CTE value gets stable after 8 weeks of ageing. The first CTE reduces about 60% and the second CTE reduces around 90% compared to the unaged sample. The fact that the CTE value of aged EMC is getting stable means that the thin sample becomes fully aged after 8 weeks of ageing. It has a good correlation with the DMA measurements. Before 500 hours of ageing, there are two T_g values observed from the loss modulus. After that, only one glass transition temperature was found.

It should be noted that in Section 5.4, it was found that also the storage modulus and loss modulus remain constant after 8 weeks of ageing. In this measurement, a second T_g is expected when the measured temperature is high enough. In the present thesis, the temperature range of interest is limited.

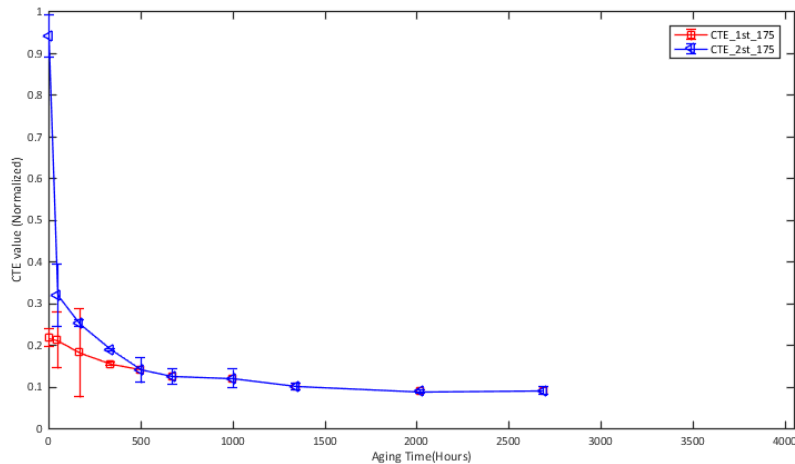


Figure 5-20: CTE of EMC during thermal Ageing at 175°C

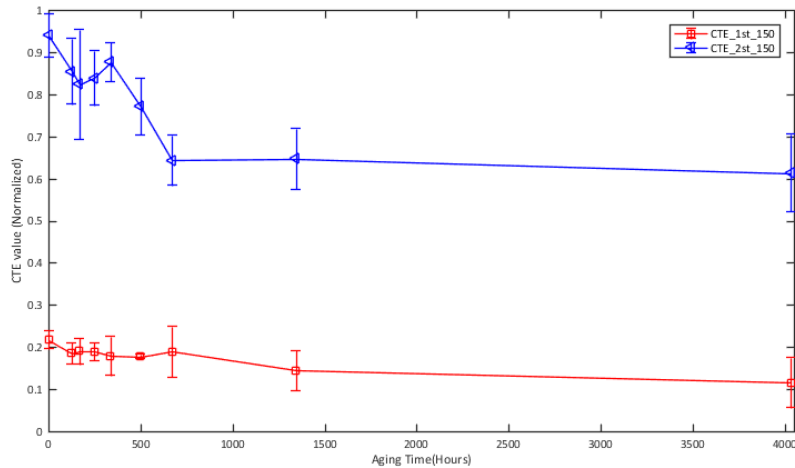


Figure 5-21: CTE of EMC during thermal Ageing at 150°C

Figure 5-21 shows the CTE versus time for ageing at 150°C. Here, different behaviour is observed compared to ageing at 175°C. Two trends of the CTE can be found in the time range of interest. During the whole ageing time, the first CTE value (below glass transition temperature) is slowly decreasing and subsequently remains constant. However, the second CTE (above glass transition temperature) shows unstable behaviour between 1 week (168 hours) and 4 weeks (672 hours) of ageing. This can result from two reasons: firstly, since the thin samples are obtained through polishing; their quality is not the same, which can lead to some differences. Secondly, as introduced at the beginning of this section, if the EMC does not reach the fully aged state, the result of the thermal expansion measurement includes two parts: thermal expansion and the CTE mismatch. In other words, the measurement result for the CTE of the partly aged sample cannot be used to indicate the material property change of aged EMC. The recorded data is mixing up the thermal expansion and the material properties mismatch. Only the homogeneously (or fully) aged and unaged EMC can be used to evaluate the CTE change. In the end, the second CTE value gets stable once the thin sample reaches the fully aged state. Compared to the unaged sample, the first CTE of aged EMC reduces 30% and the second CTE also reduces 30%. For simulation, the CTE value of fully aged EMC will be used.

The behaviour of the CTE values of aged EMC under HTS and TC thermal ageing conditions is also studied and compared to confirm that the material properties in both thermal ageing conditions are the same if the total (equivalent) ageing time is the same at the higher temperature. The results are shown in Figure 5-22. The experimental results from TC condition with 500, 1000 and 2000 cycles match very well with HTS for 125, 250 and 500 hours, respectively. It indicates that the material property changes of EMC due to thermal ageing are only dependent on the storage time at the highest temperature under TC conditions.

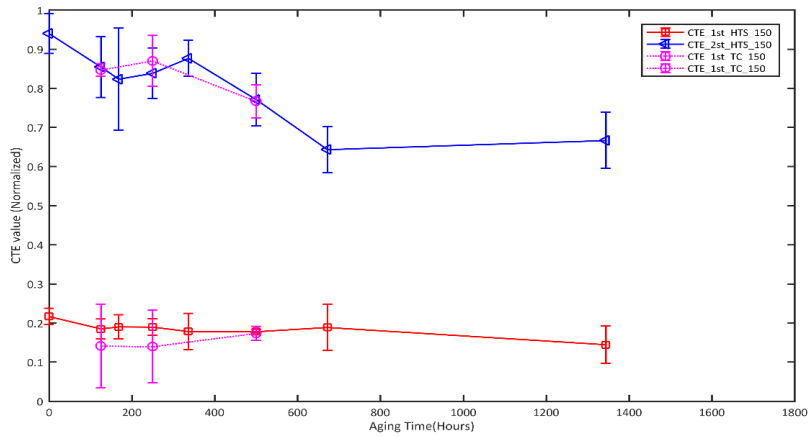


Figure 5-22: CTE of EMC during ageing at HTS and TC conditions

5.5.2 Comparison and Discussion

As illustrated in Figure 5-23, the CTE values for various ageing times and for both ageing temperatures (150°C and 175°C), are plotted together for comparison. The solid lines are from ageing at 175°C and the dashed lines from ageing at 150°C. The following results are found:

- 1) The storage temperature has a huge impact on the CTE changes during HTS, even while the difference is only 25°C. The final state of the fully aged EMC is also ageing temperature-dependent;
- 2) The CTE measurement has a good correlation with the DMA results.
- 3) Both thermal conditions show that either at 175°C or 150°C, the thin sample can become fully aged.

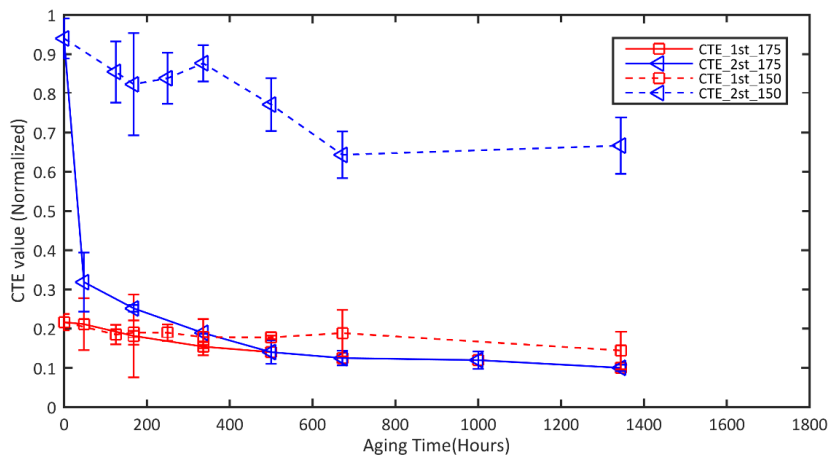


Figure 5-23: CTE comparison between 175°C and 150°C

5.6 Thermal ageing shrinkage of EMC

The EMC consists of epoxy resin, filler and other ingredients. In the epoxy resin, additional cross-linking will be formed during high-temperature storage, which leads to a denser cross-linked network. As a result, the EMC could shrink (see below) and its stiffness will increase during the ageing process. In a real package, where this shrinkage is (partly) hindered by the adjacent materials, this phenomenon will generate additional stresses or warpage, just because of ageing under HTS. In order to monitor the shrinkage as a function of the ageing time at a certain temperature, the DMA machine was used to measure the ageing shrinkage of strips of EMC with various thicknesses under isothermal conditions. The ‘force controlled’ mode was applied with a small pre-load of 0.001N under tension. The shrinkage is measured directly from the length changing of the sample itself. Firstly, the various thicknesses of samples are measured (at the same temperature). Secondly, the sample with the same thickness are also measured under different temperature conditions. The measurement results are presented and discussed in this section.

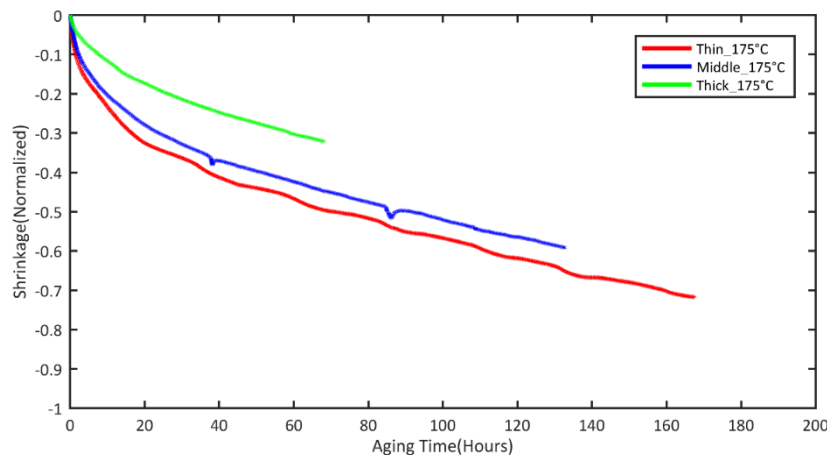


Figure 5-24: Ageing shrinkage measurement at 175°C for samples of various thickness

Figure 5-24 shows the measurement results from three samples with different thicknesses aged at 175°C. The geometry of the samples is the same but the thickness differs. The test conditions are also the same in these three measurements. The ageing shrinkage curves from three samples are plotted in Figure 5-24. They are highly thickness dependent. The reason is that the oxidation layer growth at a certain temperature is thickness independent, but the percentage of the oxidized volume to the whole sample volume is different. The same phenomenon was also found in [68], [96], [105].

Meanwhile, the shrinkage value as an input parameter for the simulation is directly affecting the accuracy of the predicted results, such as warpage. Most people use the ageing shrinkage value directly from an independent measurement and then implement it into the FE model to evaluate the stress or strain state of the real package after thermal ageing. This is not correct since the ageing shrinkage is highly dependent on

the sample size. If the size of the measured sample is not the same as in the real package, then the value cannot be directly used in the FE model. There are some jumps during the measurement. They are coming from the vibration of the external environment since the loading force is extremely small in order to avoid material creep during the measurement. Therefore, a very small vibration could make the measurement not quite stable.

Three thin samples are also measured under three different temperatures to investigate the influence of the testing temperature on shrinkage. Here, the measurement is running up to 1 week at 150°C, 175°C and 225°C, respectively. The results are plotted in Figure 5-25 for comparison. It can be seen that the ageing shrinkage is highly dependent on the ageing temperature. At 225°C, the ageing shrinkage value of EMC is much higher than for two lower temperatures. This indicates that a different chemical reaction occurs when the ageing temperature is higher.

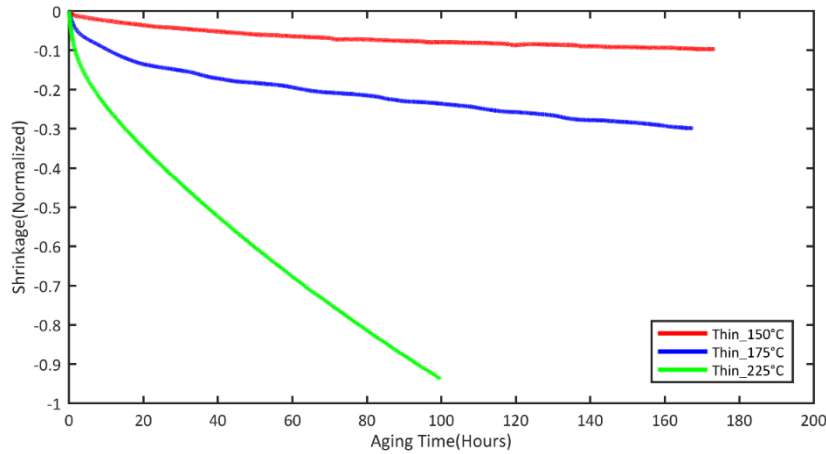


Figure 5-25: Ageing shrinkage measurement at 150°C, 175°C and 225°C with same thickness samples

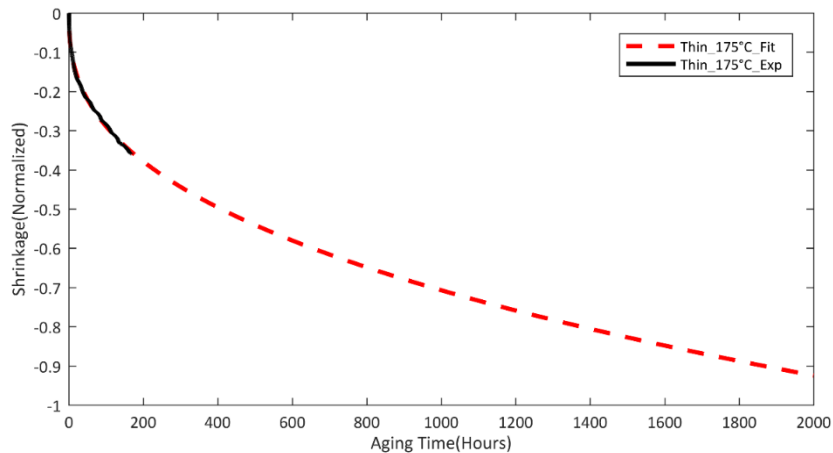


Figure 5-26: The extrapolation of ageing shrinkage measurement

For determining the ageing shrinkage of fully aged EMC at a certain ageing temperature, a mathematic fit was used to save testing time. In this manner, the curve will be extrapolated to the ageing time where the fully aged EMC is obtained for a sample with a certain thickness. Once the equivalent thickness of the oxidation layer as a function of ageing time is determined for the used ageing temperature, then the ageing time for reaching the fully aged state can be estimated (see Figure 5-26). This extrapolated value will be checked carefully in a later section.

5.7 Equivalent thickness of the Oxidation layer

As we know, the thermal ageing process inside the epoxy-based material is quite complex. In order to reduce the complexity of the ageing process in a mechanical simulation, the concept of the equivalent thickness of a fully oxidized layer of EMC is proposed. According to the experimental results of thick and thin samples, the equivalent thickness of the fully oxidized layer of EMC is established by combining the experimental results with numerical analyses. Based on DMA and TMA results, fully aged thin samples are obtained from 8 weeks ageing at 175°C and 150°C, respectively. Here, only HTS is considered, because the changes in the material properties of EMC are the same under HTS and TC if the same (equivalent) ageing times are applied. Therefore, the equivalent thickness of the oxidation layer as a function of ageing time will be established by using data from the HTS.

The 3D finite element model used in the analysis is illustrated in Figure 5-27. As illustrated in the picture, the unaged cored is uniformly covered by an aged layer according to the cross-section of aged EMC from microscopy. The material properties of unaged and fully aged EMC are used as input parameters for this analysis. Then numerical simulations are performed for various assumed outer layer thicknesses. The master curves of the partly aged sample at 120°C from 1 week up to 8 weeks ageing at 175°C as predicted by the two-layer assumption are presented (Figure 5-28). The solid lines are measurement data and the dashed lines in red are the simulation results. It can be seen that the predicted curves are fitting quite well with the experiment results.

Comparison of the overall mechanical properties with the previous measurement results finally makes it possible to obtain the proper “equivalent thickness” for a given ageing time. The obtained and normalized results of the oxidation layer thickness (or so-called equivalent thickness) versus ageing time are presented in Figure 5-29 and Figure 5-30, together with the experimental data from microscopy. The equivalent oxidation layer growth is following an empirical power law:

$$d = \left(\frac{t}{t_0}\right)^\alpha + d_0 \quad (5-2)$$

The variable t is the ageing time and t_0 , α and d_0 are fitting parameters. The fitted curve (blue dashed line) from the above equation is also plotted together in Figure 5-28. It can be seen that the empirical power law fits quite well with the predicted curve. As a result, the oxidation layer growth in dependence on the ageing time can be calculated

by this function.

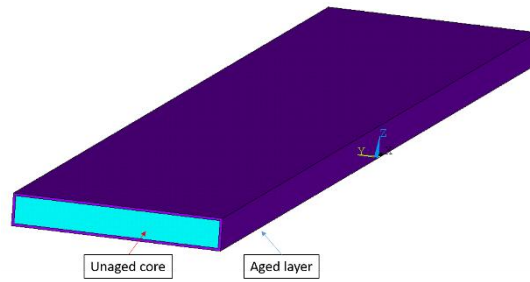


Figure 5-27: FEM model of equivalent thickness determination

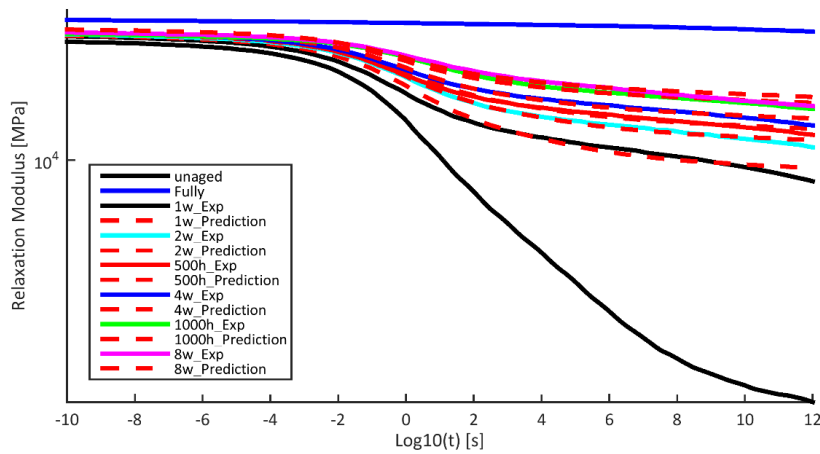


Figure 5-28: Predicted and master curves (at 120°C) of a partly aged sample (including fully and unaged sample)

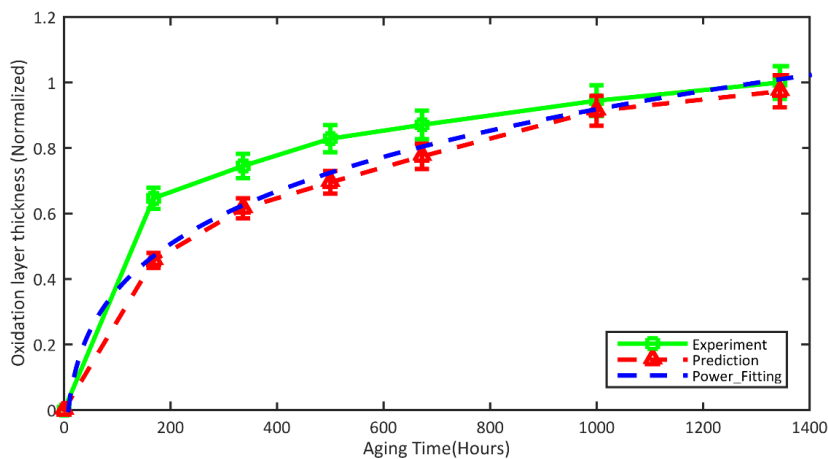


Figure 5-29: Experimental results (Green), empirical power law (Blue) and prediction (Red) results of oxidation layer growth at 175°C

Furthermore, the same procedure is applied to determine the equivalent thickness of the fully oxidized layer for the ageing temperature of 150°C. Figure 5-30 presents the

results of oxidation layer growth versus ageing time. It can be seen that the prediction curve can be fitted by the empirical power law (blue dashed line) with perfect quality

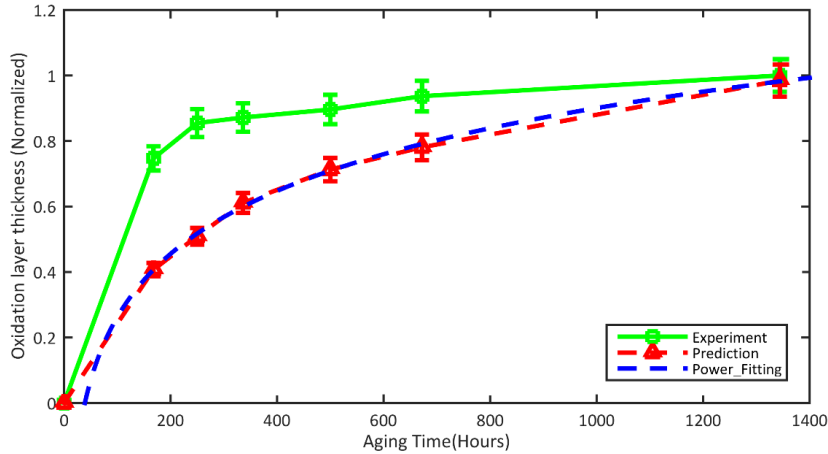


Figure 5-30: Experimental results (Green), empirical power law (Blue) and prediction results (Red) of oxidation layer growth at 150°C

Under both thermal conditions, an interesting phenomenon has been found. At the beginning of thermal ageing, the equivalent thickness of the oxidation layer is much less than the result of microscopy measurement. Afterwards, with increasing ageing time, the predicted thickness is closer to the measured result from microscopy. The reason is that at the beginning of thermal ageing, the ageing level of the EMC is very low as shown in the fluorescence microscopy. As a result, the equivalent thickness of the oxidation layer is relatively thin. While when the ageing time is higher, the ageing level of the EMC is much higher and the percentage of the reaction zone (yellow zone) becomes much smaller compared to the thickness of the aged layer (Figure 5-31).

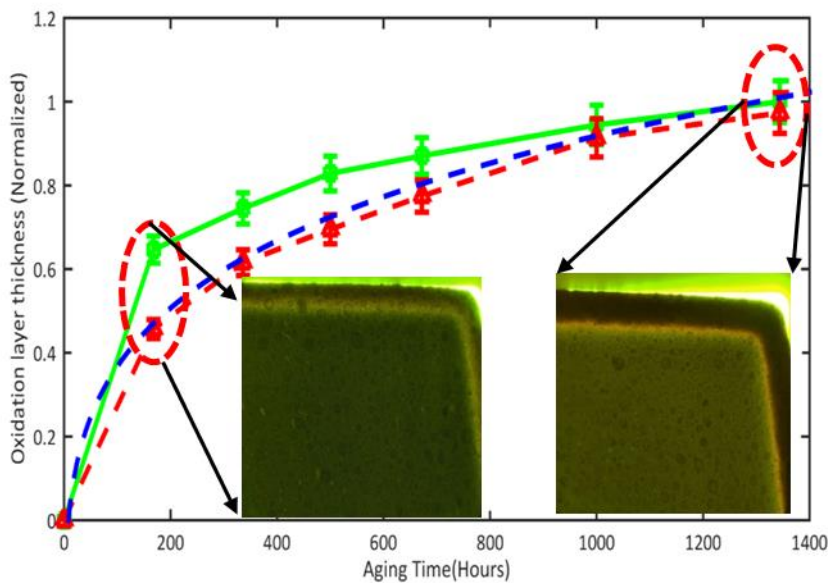


Figure 5-31: Oxidation layer at various ageing times

5.8 Model verification and simulation

5.8.1 Ageing shrinkage measurement and determination

The ageing shrinkage measurement method was previously described in Section 5.6. Below the measurement results will be shown and discussed

The DMA test results show that the thin sample becomes fully aged after at least, 8 weeks of ageing at 175°C as well as at 150°C. This means that for establishing the ageing shrinkage of a sample with a given thickness always a long-term test is necessary. Figure 5-32 shows the ageing shrinkage results obtained from thin samples which are mounted in the DMA machine under the force-controlled mode (with a very small force, see section 5.6). Two tests are performed at 175°C and 150°C, respectively. During the measurement, the axial force is kept approximately zero. The length change of the sample is measured in real-time. Figure 5-32 shows the normalized shrinkage versus the ageing time together with a power law fit of the measurement data. The fully aged state is not reached in the measurements. A longer ageing time would be needed to end up in the fully aged state. However, the equivalent thickness of the oxidation layer growth concerning ageing time is developed in section 5.7, the needed time for a certain thickness of the EMC sample under a certain ageing temperature to become fully aged state can be calculated based the equation (5-2).

It can be seen that the higher the ageing temperature, the more ageing shrinkage is obtained. This can be well observed for bi-material samples (Cu-EMC) as shown in Figure 5-33. The curvature changes are smoother at 150°C and more pronounced at 175°C. This Figure shows the curvature of the samples at room temperature after storing in two different isothermal ovens at 175°C and 150°C, respectively. The left samples are from the 175°C oven and the right samples are the from 150°C oven. As can be seen, the warpage of bi-material samples is not only temperature-dependent but also ageing time-dependent. The longer the ageing time, the more warpage is observed.

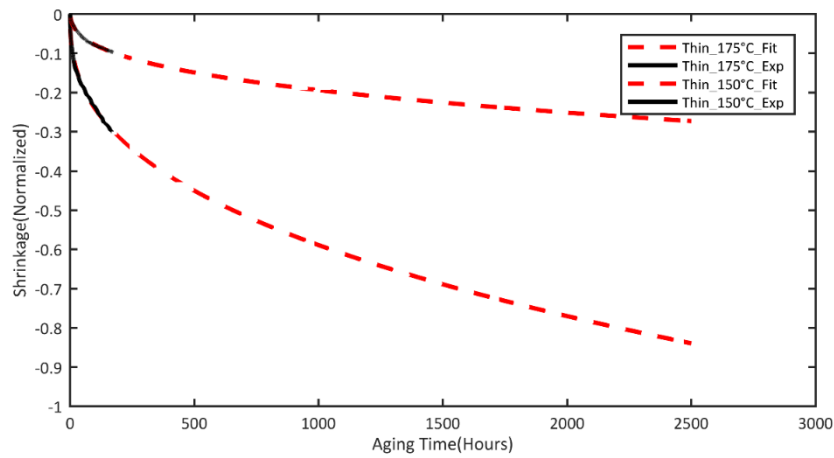


Figure 5-32: Ageing shrinkage measurement as well as fitting



Figure 5-33: Bi-material sample (at room temperature) after ageing at two different temperatures: 175°C (left) and 150°C (right)

In Chapter 4, a dummy package was used to determine the curing shrinkage of unaged EMC. Here, the dummy package is used to verify the ageing shrinkage from the above measurements. The dummy package samples are stored at 175°C for 500 hours and then the curved profile of the sample along a diagonal surface at room temperature is measured. At least three samples are measured in order to minimize the measurement errors. Before the measurement, the cross-section of the aged dummy package is prepared as shown in Figure 5-34. As illustrated in the picture, three layers exist in the aged EMC. The outer layer is the oxidized layer and the light yellow colour is the reaction zone as described in section 5.3. Considering the transition of the copper substrate and the moulding compound at a sidewall, we see that the outside of the moulding compound is oxidized without any penetration on the interface. It means that there is no delamination at the interface between EMC and the lead frame during the thermal ageing treatment. This indicates that the adhesion at the interface of LF and EMC is strong enough. However, the interface properties degradation or enhancement during thermal ageing are not taken into account here. For this more investigations should be performed in the future.

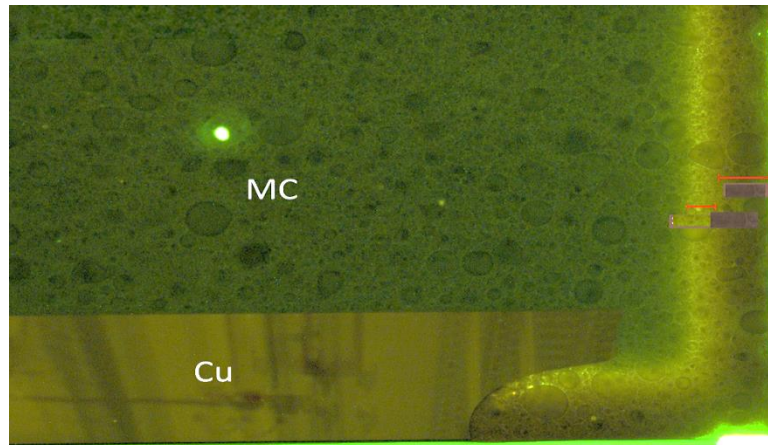


Figure 5-34: Cross section of a dummy package after 500h ageing at 175°C

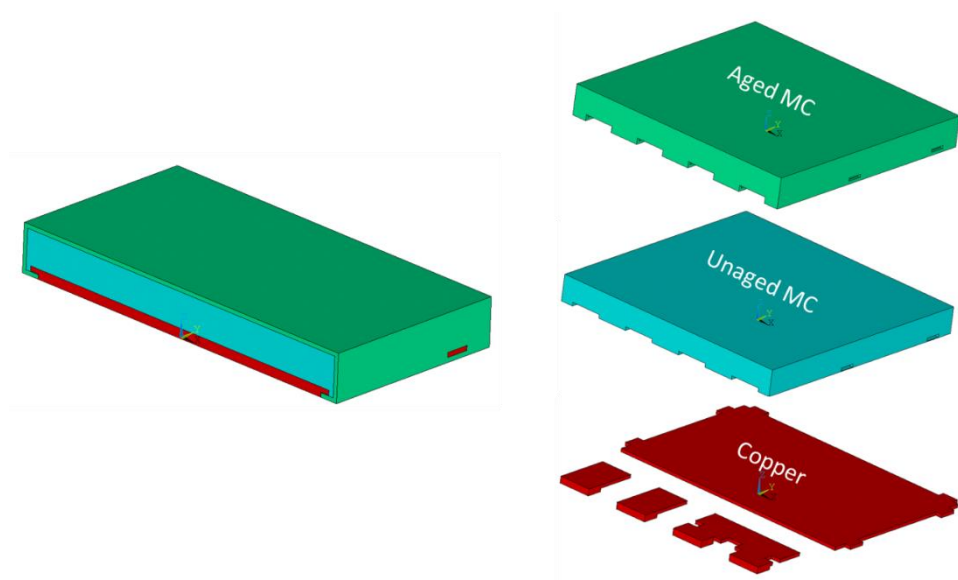


Figure 5-35: Structure of the aged dummy package (right: cross-section of the aged model, left: structure of three parts in the simulation model)

The 3D FE model of the dummy package consists of three parts as illustrated in Figure 5-35. The outer layer is the oxidation layer (fully aged EMC), and the inner part is unaged EMC. The bottom is copper. All the material properties are fully characterized in the previous and the present chapter. The material models are identified based on a large number of measurement results. The simulation process is following the temperature profile of the dummy package in the production line and the subsequent ageing process. The comparison between simulation and experiment is shown in Figure 5-36. The standard deviation is also included based on the measurement results. It can be seen that the simulation results (using the ageing shrinkage as determined from the previous measurements) show a very good agreement with the experiments. In Figure 5-37, the curvatures of the sample surface before and after thermal ageing are plotted together to see the change. More warpage in the aged sample is observed compared to the unaged sample. The reason is that 1) due to the ageing shrinkage of EMC the

dummy package gets the more smiling shape compared to the unaged dummy package. 2) Moreover, an additional oxidation layer is generated at the EMC surface which has different thermo-mechanical properties than the unaged EMC in the core. When the temperature is reduced from ageing temperature to room temperature, the CTE mismatch will also contribute to the warpage.

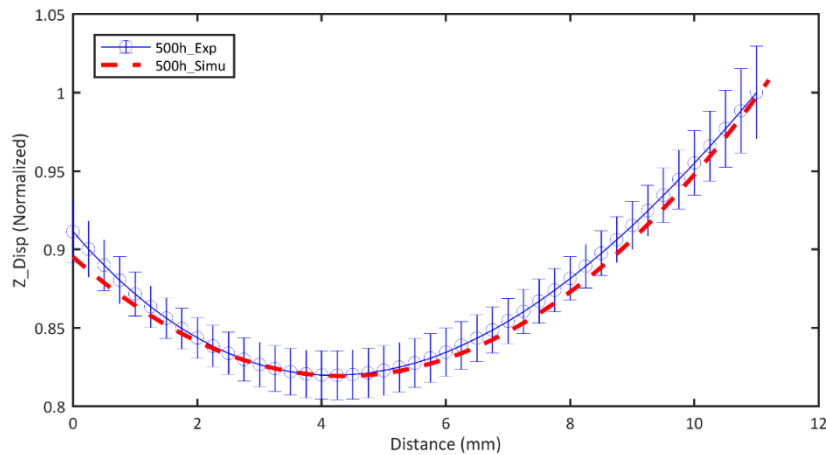


Figure 5-36: Simulation and experiment results of the curved profile of the sample along a diagonal surface at room temperature after 500h of ageing

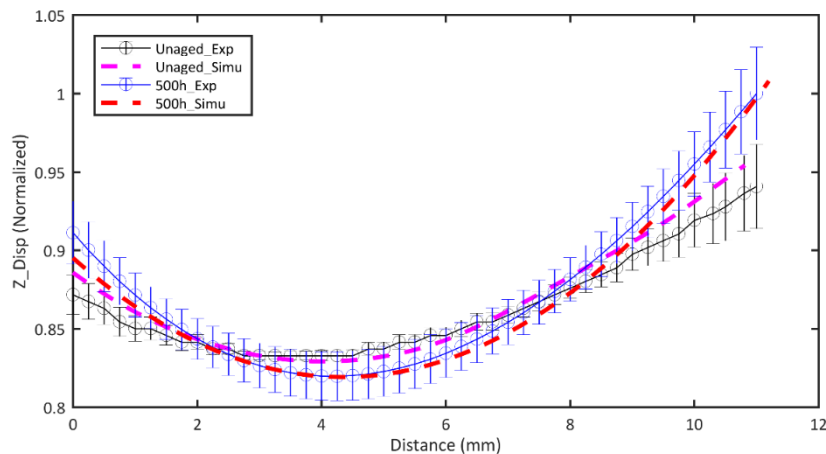


Figure 5-37: Comparison between aged and unaged samples as well as simulation results.

5.8.2 Model verification (175°C and 150°C)

The purpose of this project is to establish a modelling method to predict the thermo-mechanical behaviour of real packages after HTS and TC thermal ageing conditions. In this study, the accuracy of the identified material model as input for the simulations is the key point. Up to now, all material properties, such as the

viscoelasticity of aged and unaged EMC, the CTE values of aged and unaged EMC, the curing shrinkage and the ageing shrinkage, are fully characterized by a series of proper measurements. Based on these elements, the thermo-mechanical behaviour of selected samples under temperature loading should be predictable after thermal ageing. Therefore, in this section, the thermo-mechanical behaviour of aged bi-material samples under temperature loading is monitored first and then the corresponding simulations are performed to represent the behaviour by using the proposed modelling method.

First, the bi-material samples were stored in the HTS oven at 175°C for several weeks and in the TC oven between -55°C and 150°C for several thousands of cycles, respectively. Figure 5-38 shows the cross-section of the aged bi-material sample after several weeks of ageing at 175°C. Similar to Figure 5-34, it is clear to see that the unaged core is covered by the oxidation layer. At the interface between EMC and lead frame, the oxidation layer is not propagating to the centre location. This means that no delamination occurs at the interface during the thermal ageing process. Then, the warpage measurement under temperature loading is performed by using the 3-point bending method as developed in Chapter 4. Here, the warpage measurement of the aged bi-material samples is performed after 500 and 1000 hours of HTS at 175°C. However, for thermal ageing at 150°C, the check points are after 1000 cycles (250 hours at 150°C) and 2000 cycles (500 hours at 150°C), respectively. In the end, the simulation model using the established material model is used to compute the thermo-mechanical behaviour of the aged bi-material samples.

Based on this observation and the measurement data, a 3D model is generated in a commercial FE software as shown in Figure 5-39. The model is consisting of three parts, the copper layer, the unaged core and the oxidation layer. The material properties of the aged layer are from the fully aged EMC. The oxidation layer thickness is obtained from Figure 5-29 and Figure 5-30. The unaged core is defined as the fresh EMC.

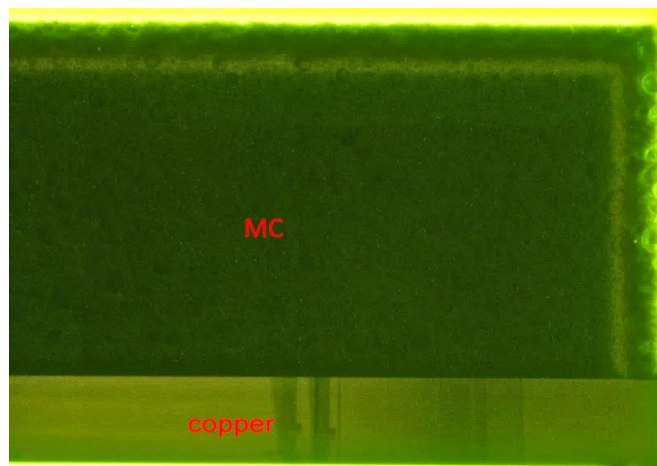


Figure 5-38: Cross-section of the bi-material sample after thermal Ageing at 175°C

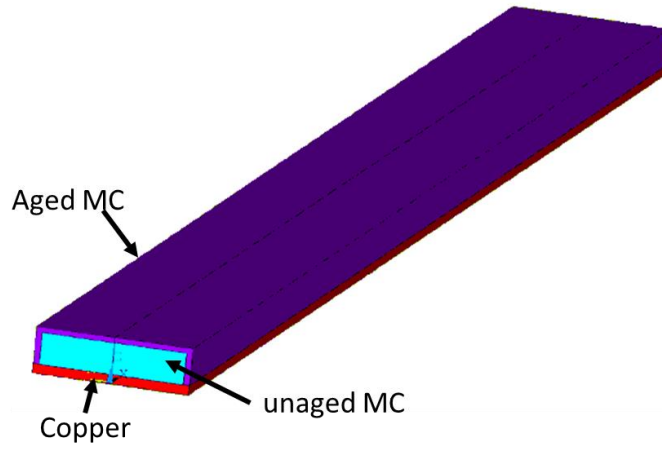


Figure 5-39: 3D model of the aged bi-material sample

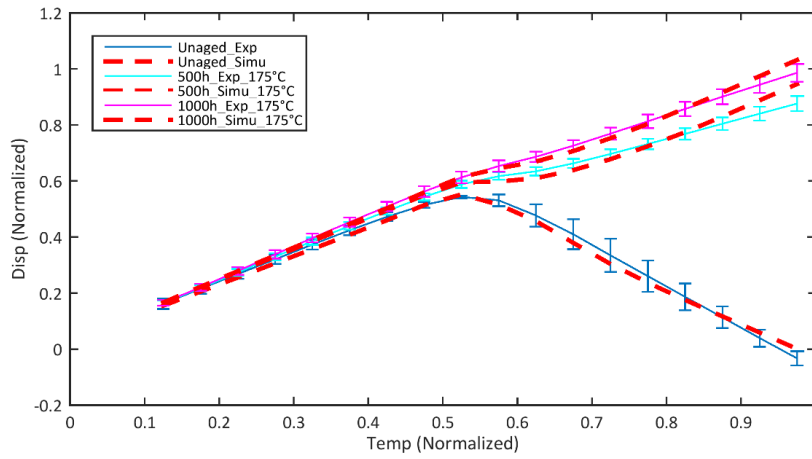


Figure 5-40: 3PB displacement-Comparison of unaged, 500h and 1000h (175°C)

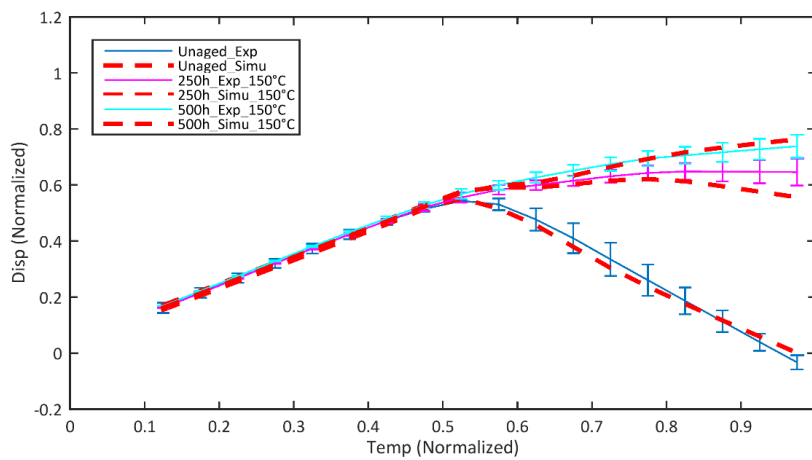


Figure 5-41: 3PB displacement-Comparison of unaged, 250h and 500h (150°C)

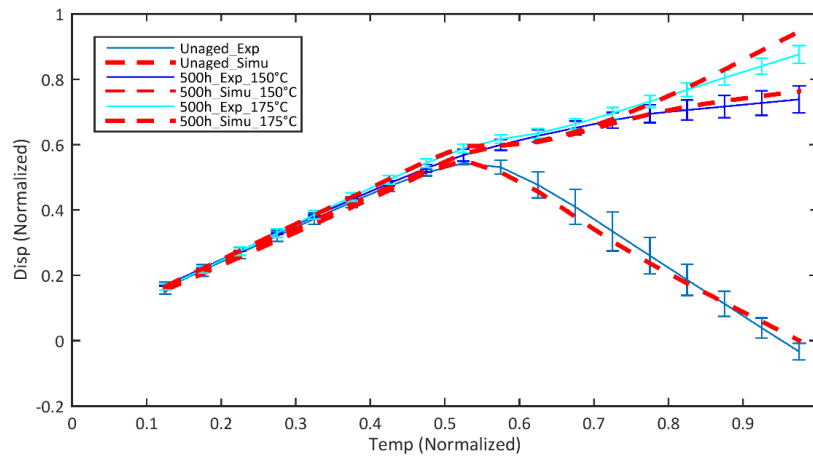


Figure 5-42: 3PB displacement-Comparison between different Ageing temperatures (150°C and 175°C) within the same ageing time

As illustrated in Figure 5-40 and Figure 5-41, the simulation model captures the thermo-mechanical behaviour of the aged bi-material samples very well during temperature loading either under HTS or in TC conditions. It confirms that the proposed modelling method is effective and that the material parameters as obtained from the developed characterization process are accurate.

Based on the above results and comparisons, the conclusion is as follows:

Firstly, before thermal ageing, the bi-material sample shows the typical thermo-mechanical behaviour of the EMC-LF sample during temperature loading (blue curve in Figure 5-40). When the loading temperature is lower than the glass transition temperature of the unaged EMC, the thermal expansion of copper is higher than that of the EMC such that the ‘smiling’ shape of the sample evolves as shown in Figure 5-43. The warpage value in Figure 5-40 is increasing. If the loading temperature is higher than the glass transition temperature of the unaged EMC, the thermal expansion of copper is lower than that of EMC so the ‘crying’ shape of the sample as shown in Figure 5-43 evolves. Therefore, the warpage as plotted in Figure 5-40 is starting to decrease once the loading temperature exceeds the glass transition temperature of the EMC.

Secondly, the aged bi-material sample shows a completely different thermo-mechanical behaviour under temperature loading. As we know, after thermal ageing an oxidized layer is generated below the EMC surface. This very thin oxidation layer has completely different material properties than fresh EMC. As a result, the warpage of aged bi-material sample depends on the properties of these three materials, lead frame, unaged EMC and aged EMC. Figure 5-40 and Figure 5-41 present the warpage measurements from bi-material samples after a certain ageing time at 175°C and 150°C, respectively. Before the glass transition temperature of the unaged EMC, the curves are only slightly different compared to the curves of the unaged bi-material samples. The reason is that below T_g the CTE values of fully aged EMCs are quite similar to those of unaged EMC but lower than that of copper as shown in Figure 5-44. If the loading

temperature is higher than T_g of the unaged EMC, the curves of aged bi-material samples show a completely different warpage change. The warpage is continuously increasing in the whole temperature range. The only difference is the slope of the growth, because the thickness of the oxidation layer is depending on ageing time. The longer the thermal ageing time, the thicker is the oxidation layer. As a consequence, the warpage of aged bi-material samples is also depending on the ageing time.

Thirdly, Figure 5-42 shows the curves for different ageing temperatures (150°C and 175°C) and the same ageing time. The difference can be seen clearly from the picture. As we know from the previous measurements, the material property of fully aged EMC is also ageing temperature-dependent. At the same ageing time, the higher ageing temperature will make the EMC stiffer and leads to a lower CTE. As a result, the slope of the warpage growth is different in both cases.

The proposed modelling method can predict the thermal-mechanical behaviour of the bi-material sample before and after thermal ageing very well. Such as in Chapter 4, the real structure of a package without a chip, a so-called called dummy package, will be used to perform a final check of the modelling method as well. This is carried out because the established modelling method and material model will be used to evaluate the reliability of a real package after long-term thermal ageing treatment. The unaged model and sample were shown before in Chapter 4. The cross-section of the samples aged under different conditions are shown in Figure 5-45.

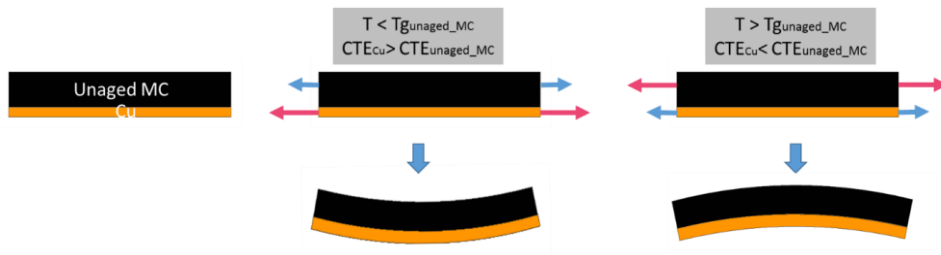


Figure 5-43: Bending mechanism of bi-material before thermal ageing

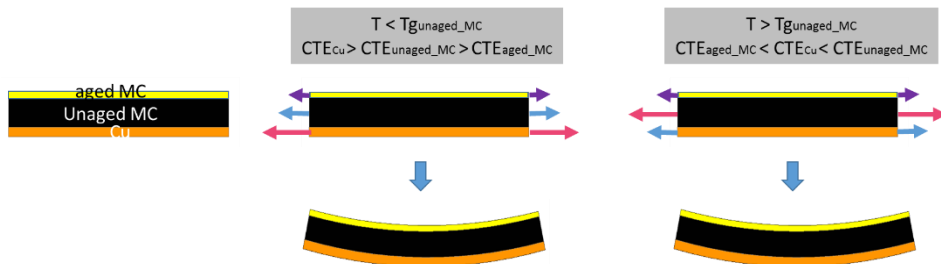


Figure 5-44: Bending mechanism of bi-material after thermal ageing

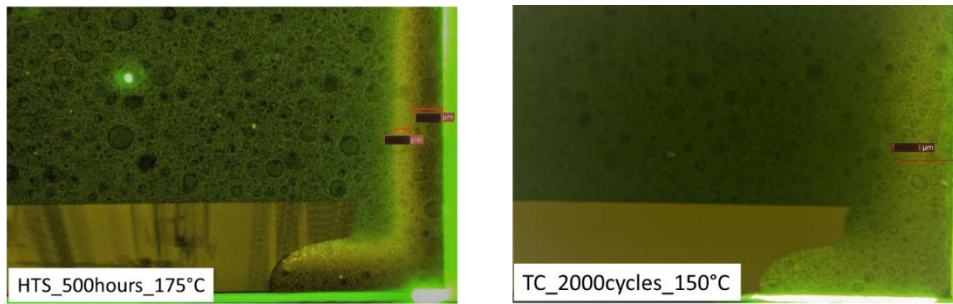


Figure 5-45: Cross-section of two dummy package strips aged at HTS_175°C and TC_150°C

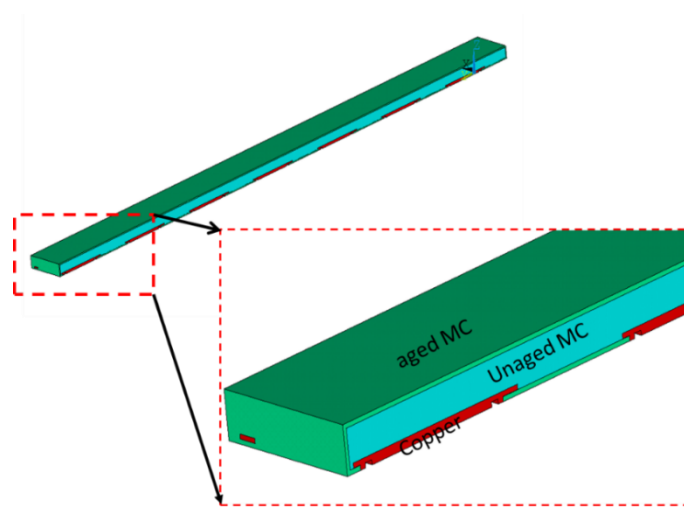


Figure 5-46: 3D model of the sample after thermal ageing

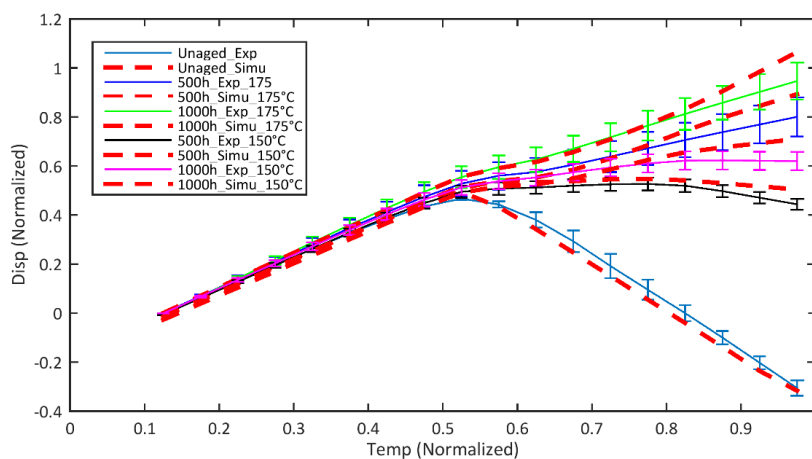


Figure 5-47: Experiment and Simulation results of dummy package before and after thermal treatment

The 3D model of the aged dummy package is shown in Figure 5-46, as well as an enlargement of a part of the strip. The dummy strip samples are stored in a normal oven

(175°C and 150°C, respectively) or a TC oven (with cycles between -55°C and 150°C). After the long-term isothermal and TC treatment, warpage measurements are performed to monitor the warpage changes during temperature loading. The simulation process is performed after the measurements. Figure 5-47 plots the simulation results as well as the measurement results. As expected, the simulation can predict the measurement results very well.

5.9 Conclusion

In this chapter, a simple and efficient modelling method based on the “two-layer” assumption is proposed based on the observations from the measurements. A series of measurements is designed and performed to verify the proposed modelling method. After that, a systematical characterization method and procedure are used to obtain an accurate material model and its parameters for simulation purposes. In the end, a bi-material sample as well as dummy package samples are used to verify the modelling method and the material parameters. The simulations show quite a good agreement with the measurements.

- 1) A two-layer model based on an “equivalent thickness” assumption for the aged layer is proposed to simulate the ageing process of EMC. The mechanism of thermal ageing of EMC is found by performing DMA tests on samples stored in a vacuum and a normal air oven. Thermal ageing occurs when oxygen exists.
- 2) The fluorescence microscopy technology is used to measure the oxidation layer growth during the thermal ageing treatment. It was found that the oxidation layer growth is not only ageing time-dependent but also ageing temperature-dependent. Furthermore, the oxidation layer growth is following the empirical power law.
- 3) A systematical characterization is performed to obtain the material properties of fully aged EMC, such as for thermal expansion, viscoelasticity and ageing shrinkage. The CTE is reduced quite a lot not only above the glass transition temperature but also below. The ageing shrinkage of EMC during HTS is not only temperature-dependent but also thickness dependent.
- 4) The material property changes of EMC under HTS and TC conditions are the same once the “equivalent thermal ageing time” in both conditions is the same.
- 5) In order to simplify the simulation method, an “equivalent thickness” of the oxidation layer dependent on the ageing time is established. It is based on measurement results and numerical analyses. The equivalent thickness can be used to evaluate the “overall material properties” of a strip of moulding compound at any ageing time.
- 6) Two different types of samples are selected to verify the proposed model method. Both samples are aged at 175°C and 150°C for several weeks. After that, warpage measurements are performed to monitor the thermo-mechanical behaviour of the aged samples under temperature loading. The measurements

show that the warpage behaviour of the aged sample is not only ageing time-dependent but also ageing temperature-dependent. Comparing unaged bi-material samples and aged bi-material samples, it is found that the warpage behaviour shows significant changes if the loading temperature is higher than the glass transition temperature of the unaged EMC.

- 7) The simulations match all experimental results, either under different ageing conditions, such as different ageing temperatures and times or for different sample types.

6 Conclusion of project

EMCs are polymer-based materials, which include various ingredients to comply with various requirements. In order to limit the material mismatch induced stresses and/or strains inside the electronic package and to reduce the cost, a high percentage (70%~90%) of silica filler is present in these encapsulation materials (EMC). The silica filler is bonded together by an epoxy matrix and some additive ingredients. Because of the epoxy matrix, the mechanical behaviour of filled EMC is exhibiting viscoelasticity.

When the packages are exposed to a harsh environment such as to high-temperature storage or temperature cycling, various reliability issues in the packages can take place, such as delamination at the interface between EMC and lead frame, chip cracking and bond pad cracking. Among these, the EMC plays an essential role in the reliability of the electronic package. As we know, the material properties of the silica filler are stable during the application of HTS and TC conditions. However, the epoxy matrix can change significantly when the temperature exceeds a specific value and while exposed to air. These changes can be attributed to chemical processes such as thermo-oxidation and degradation. In the experimental measurements, a very thin skin layer or oxidized layer is observed at the outer surface of the EMC material after the thermal ageing process. This layer has different properties compared to the original EMC. The thickness of this thin layer is growing as a function of ageing time as well as of ageing temperature. As a result, the (mean) thermomechanical properties of the whole EMC structure change significantly. Finally, it leads to changes in the stress and/or strain state in an electronic package and consequently it affects the reliability of the package under the application of HTS or TC conditions. Due to the impact on the long-term reliability of the electronic packages, the characterization and modelling of the ageing process in EMCs are becoming an important issue since more and more electronic products are working under HTS and TC conditions. In the past, many researchers are focusing on this topic, but unfortunately, a systematic characterisation method is still not available for EMCs during thermal ageing processes. Up to now, there is even no efficient and straightforward modelling method available to describe the mechanical behaviour changes of the EMC during HTS and TC conditions.

Based on the above issues, this thesis is starting with a basic understanding of the thermo-mechanical behaviour of the fresh EMC, such as viscoelasticity, thermal expansion and curing shrinkage. Firstly, based on DMA experimental results, the viscoelastic material model of the fresh EMC is established by using the time-temperature superposition principle. Validation tests, to verify the identified viscoelastic model, are performed based on relaxation experiments. By using the FE method, simulations can predict the viscoelastic behaviour of EMC at various temperature quite well. Secondly, the coefficient of thermal expansion is established by TMA experiments. Two CTE values are found for above and below the glass transition temperature of fresh EMC, respectively. Thirdly, combining the viscoelastic material model and the determined CTE values, the curing shrinkage is determined by an

indirect method. Simulations of a dummy package are performed with and without curing shrinkage included in the simulation model. Without curing shrinkage the simulation cannot predict the out-of-plane deformation of the dummy package. Besides that, the warpage of a defined bi-material sample is measured during temperature loading by using a newly developed measurement method. Simultaneously, the simulation is performed by including all established material parameters, such as for the viscoelasticity, the CTEs and the curing shrinkage of the EMC. The simulations can predict the mechanical behaviour of the bi-material sample under temperature loading very well.

For modelling thermal ageing of EMC, a two-layer model based on an ‘‘equivalent thickness’’ assumption for the aged layer is introduced. The thermo-mechanical property changes in the EMC during the thermal ageing process are due to thermal oxidation. The (mean-) thermo-mechanical properties of EMC during thermal ageing are characterised based on the established characterisation process. During the thermal ageing process, the modulus of EMC increases and the CTEs decrease. The values will approach a stable state once the EMC becomes ‘‘fully aged’’. The thermo-mechanical property changes for HTS at 150°C and TC from -55°C to 150°C are equal if the ‘‘equivalent thermal ageing time’’ in both conditions is the same. An ‘‘equivalent thickness’’ of the oxidation layer depending on the ageing time is established based on mechanical measurement results and numerical analyses. The oxidation layer growth is following an empirical power law. The established equivalent thickness can be used to evaluate the ‘‘overall material properties’’ of the EMC for arbitrary ageing time. In the end, according to the two-layer model, the mechanical behaviour for two types of validation samples after HTS and TC are simulated under temperature loading. The simulation results show a very good agreement with the experimental results.

All in all, this thesis provides an efficient and straightforward modelling method to describe the mechanical property changes during the thermal ageing process of epoxy-based EMC. Besides, a systematic characterisation process to obtain the material model and its parameters for simulation purposes is developed, applied and presented. After that, a number of validation tests are performed to check the reliability of the material model including the established model parameters.

6.1 Limitations and Recommendations

In this thesis, only two ageing temperatures, 150°C and 175°C, are applied and modelled. More temperature points would be interesting to study the vernal applicability of the proposed modelling method. In the future, more material properties of aged EMC should be characterized, such as the ultimate strength. It could be hugely attractive to use the measurement data to predict the EMC cracking during thermal ageing. Further investigation is advisable to explore how thermal ageing is effecting the interface properties between EMC and lead frame since the delamination issue at this interface is one of the most interesting topics in the semiconductor industry.

7 Appendix

7.1 List of Figures

Figure 1-1: Typical structure of semiconductor product.....	1
Figure 2-1: (a) Stress-Strain curve of a linear elastic material and (b) Stress-Strain curve of a viscoelastic material.....	12
Figure 2-2: (a) Applied step strain ϵ_0 at time t_0 (b) Induced stress as a function of time.....	13
Figure 2-3: (a) Applied step stress σ_0 at time t_0 (b) Induced strain as a function of time.....	14
Figure 2-4: Stress relaxation response of a linear viscoelastic material to multi-step loading.....	14
Figure 2-5: (a) spring and (b) dashpot element.....	16
Figure 2-6: simple models: (a) Maxwell model; (b) Kelvin-Voigt model; (c) the standard linear model; (d) the Burgers model.....	16
Figure 2-7: Generalized Maxwell model.....	18
Figure 2-8: Applied dynamic strain (dashed, Black) and responded stress (Red).....	19
Figure 2-9: Curve of the <i>1Hz Storage</i> modulus vs. Temperature.....	20
Figure 2-10: Schematic illustration of time-temperature shift.....	21
Figure 2-11: Schematic illustration of specific volume vs. temperature.....	23
Figure 3-1: cross-section of aged EMC.....	27
Figure 3-2: Diamond saw and polishing machine.....	29

Figure 3-3: Four types of EMC samples	29
Figure 3-4: Mold Map and strip; single dummy package and strip dummy package....	30
Figure 3-5: DMA machine and clamp systems	31
Figure 3-6: TMA machine.....	33
Figure 3-7: temperature cycling oven, isothermal oven and vacuum oven	34
Figure 3-8: Profilometer.....	35
Figure 3-9: Microscope	36
Figure 3-10: Embedded sample and cross-section of aged sample.....	37
Figure 4-1: Schematic of detecting system	42
Figure 4-2: Comparison between “Sample Temperature” (= chamber temperature plus temperature compensation value) according to the DMA-machine and according to the thermocouple. <i>Heating rate = 2°C/min.</i>	43
Figure 4-3: Comparison between “Sample Temperature” (= Chamber temperature) according to the DMA-machine and according to the thermocouple. <i>Heating rate = 1°C/min.</i>	43
Figure 4-4: DMA test at 1HZ: Storage modulus (a) and Loss modulus (b) as functions of Temperature	44
Figure 4-5: Storage modulus as a function of temperature and frequency	45
Figure 4-6: Loss modulus as a function of temperature and frequency	45
Figure 4-7: Tan delta values as a function of temperature and frequency	46
Figure 4-8: Constructed master curve after TTS.....	47
Figure 4-9: Master curve fitted by Generalized Maxwell model.....	48
Figure 4-10: Shift factors fitted by the defined functions	49
Figure 4-11: Schematic of three-point bending Relaxation test (setup and FE model) .	49

Figure 4-12: Results of simulations and relaxation tests	50
Figure 4-13: CTE measurements of EMC and copper.....	51
Figure 4-14: Total shrinkage of EMC	53
Figure 4-15: Sample structure and measured paths	54
Figure 4-16: Data processing for measurement data and simulation results	54
Figure 4-17: The structure of a dummy package	55
Figure 4-18: Simulation procedure and out-of-plane deflection of the dummy package	55
Figure 4-19: Deformation with and without curing shrinkage of EMC compared with experiment result.....	56
Figure 4-20: The schematic of warpage measurement by three-point bending	57
Figure 4-21: Setup and Bi-material Sample.....	58
Figure 4-22: Setup for calibration measurements	59
Figure 4-23: Expansion and contraction calibration result of the clamping system.....	59
Figure 4-24: Test result of the (simple) bi-material sample	60
Figure 4-25: 3D models of bi-material samples.....	61
Figure 4-26: Comparison between experiment and simulation	61
Figure 5-1: Thermal ageing temperature profiles for HTS and TC	64
Figure 5-2: (Fluorescence microscopy-) Cross-section of unaged EMC.....	67
Figure 5-3: (Fluorescence microscopy-) Cross-section of aged EMC.....	67
Figure 5-4: The principle of a two layers model.....	68
Figure 5-5: Samples of two different thicknesses are prepared for mechanical testing.	68
Figure 5-6: DMA test results of thick and thin EMC samples before and after ageing at 175°C: 1 st row: unaged (0w); 2 nd row: aged (2w); 3 rd row: aged (4w)	69

Figure 5-7: Storage and loss moduli of EMC before and after thermal Ageing under air and under vacuum environment 72

Figure 5-8: The Cross-section of EMC before and after thermal Ageing in the air and vacuum oven 72

Figure 5-9: Cross-section of aged EMC after thermal Ageing at 175°C 73

Figure 5-10: Cross-section of samples after thermal ageing at 150°C 74

Figure 5-11: Oxidation layer growth as a function of ageing time 75

Figure 5-12: Cross-section of EMCs after thermal ageing at HTS and TC at 150°C.... 76

Figure 5-13: Oxidation layer growth after HTS and TC thermal ageing at 150°C..... 76

Figure 5-14: Storage and Loss moduli of EMC aged at 175°C 78

Figure 5-15: Glass transition temperature of thick and thin samples after thermal ageing 79

Figure 5-16: Storage and Loss moduli of aged EMC at ageing temperature of 150°C . 82

Figure 5-17: Glass transition temperature of thick and thin samples for ageing at 150°C 82

Figure 5-18: Storage and Loss moduli of aged EMC under HTS and TC ageing conditions 84

Figure 5-19: Storage and loss modulus of the thick and thin samples for various ageing times and ageing temperatures of 175°C and 150°C. 86

Figure 5-20: CTE of EMC during thermal Ageing at 175°C 87

Figure 5-21: CTE of EMC during thermal Ageing at 150°C 88

Figure 5-22: CTE of EMC during ageing at HTS and TC conditions 89

Figure 5-23: CTE comparison between 175°C and 150°C 89

Figure 5-24: Ageing shrinkage measurement at 175°C for samples of various thickness 91

Figure 5-25: Ageing shrinkage measurement at 150°C, 175°C and 225°C with same

thickness samples	92
Figure 5-26: The extrapolation of ageing shrinkage measurement.....	92
Figure 5-27: FEM model of equivalent thickness determination.....	94
Figure 5-28: Predicted and master curves (at 120°C) of a partly aged sample (including fully and unaged sample)	94
Figure 5-29: Experimental results (Green), empirical power law (Blue) and prediction (Red) results of oxidation layer growth at 175°C	94
Figure 5-30: Experimental results (Green), empirical power law (Blue) and prediction results (Red) of oxidation layer growth at 150°C	95
Figure 5-31: Oxidation layer at various ageing times	95
Figure 5-32: Ageing shrinkage measurement as well as fitting	97
Figure 5-33: Bi-material sample (at room temperature) after ageing at two different temperatures: 175°C (left) and 150°C (right)	97
Figure 5-34: Cross section of a dummy package after 500h ageing at 175°C.....	98
Figure 5-35: Structure of the aged dummy package (right: cross-section of the aged model, left: structure of three parts in the simulation model).....	98
Figure 5-36: Simulation and experiment results of the curved profile of the sample along a diagonal surface at room temperature after 500h of ageing.....	99
Figure 5-37: Comparison between aged and unaged samples as well as simulation results.	99
Figure 5-38: Cross-section of the bi-material sample after thermal Ageing at 175°C.	100
Figure 5-39: 3D model of the aged bi-material sample	101
Figure 5-40: 3PB displacement-Comparison of unaged, 500h and 1000h (175°C)	101
Figure 5-41: 3PB displacement-Comparison of unaged, 250h and 500h (150°C)	101
Figure 5-42: 3PB displacement-Comparison between different Ageing temperatures (150°C and 175°C) within the same ageing time.....	102

Figure 5-43: Bending mechanism of bi-material before thermal ageing	103
Figure 5-44: Bending mechanism of bi-material after thermal ageing	103
Figure 5-45: Cross-section of two dummy package strips aged at HTS_175°C and TC_150°C	104
Figure 5-46: 3D model of the sample after thermal ageing	104
Figure 5-47: Experiment and Simulation results of dummy package before and after thermal treatment	104

7.2 List of Table

Table 1-1: Typical ingredient of EMC as well as their benefits.....	3
Table 2-1: Relation between elastic constants	26
Table 3-1: Technical data of Q800 DMA.....	32
Table 3-2: Technical data of TMA	33

7.3 Symbols

σ	Stress
ε	Strain
k	Material parameter
t	Time
T	Temperature
Q	Moisture concentration
E	Modulus
D	Compliance
ξ	Application time
η	Viscosity
τ	Characteristic time
ε_m	Amplitude of the strain
ω	Radial frequency
f	Natural frequency
δ	Phase lag
E'	Storage modulus
E''	Loss modulus
a_T	Shift factor
C_1	Constant
C_2	Constant
V_0	Occupied volume
V_f	Free volume
f	Fractional free volume
T_g	Glass transition temperature of polymer materials
A	Constant
B	Constant
ΔH	Activation energy
T_{ref}	Reference temperature
T_∞	Constant temperature

G	Shear modulus
K	Bulk modulus
D_{ij}	Deviatoric coefficient matrices
V_{ij}	Volumetric coefficient matrices
ε_v^{eff}	Effective volumetric strain
ε_{ij}^d	Deviatoric strain
ε_{ii}^*	Initial strain

7.4 Abbreviation

FEM	Finite Element Method
EMC	Epoxy Moulding Compound
HTS	High-Temperature Storage
TC	Temperature Cycling
IC	Integrated Circuit
DMA	Dynamical Mechanical Analysis
TMA	Thermal Mechanical Analysis
CTE	Coefficient of Thermal Expansion
HTC	High-temperature Cycling
TTS	Time-temperature Superposition
WLF	Williams–Landel–Ferry
3PB	Three-Point Bending
CT100	Cyber Technology 100
PMC	Post-Mould Curing

8 Reference

- [1] X. J. F. G.Q. Zhang, W.D. van Driel, *Mechanics of Microelectronics*. 2006.
- [2] R. R. Tummala and E. J. Rymaszewski, *Microelectronics packaging handbook*. Van Nostrand Reinhold, 1989.
- [3] W. J. Greig, *Integrated circuit packaging, assembly and interconnections*. 2007.
- [4] I. C. Cheng, *Materials for advanced packaging* . 2016.
- [5] R. W. Johnson, J. L. Evans, P. Jacobsen, J. R. Thompson, and M. Christopher, "The changing automotive environment: High-temperature electronics," *IEEE Trans. Electron. Packag. Manuf.*, vol. 27, no. 3, pp. 164–176, 2004.
- [6] A. Teverovsky, "Effect of environments on degradation of moulding compound and wire bonds in PEMs," *Proc. - Electron. Components Technol. Conf.*, vol. 2006, pp. 1415–1424, 2006.
- [7] A. Teverovsky, "Effect of vacuum on high-temperature degradation of gold/aluminum wire bonds in PEMs," *IEEE Int. Reliab. Phys. Symp. Proc.*, vol. 2004-Janua, no. January, pp. 547–556, 2004.
- [8] A. Teverovsky, "NASA Electronic Parts and Packaging Program (NEPP) Reliability of COTS PEMs Effect of Environments on Degradation of Moulding Compound and Wire Bonds in PEMs October 2005," no. October, pp. 1–21, 2005.
- [9] D. G. Yang et al., "Effect of high temperature aging on reliability of automotive electronics," *Microelectron. Reliab.*, vol. 51, no. 9–11, pp. 1938–1942, 2011.
- [10] G. Dandong, C. C. Meng, K. L. K. Ian, and M. Walter, "A comparison study of thermal aging effect on mold compound and its impact on leadframe packages stress," in *Proceedings - International Symposium on Advanced Packaging Materials*, 2011, pp. 403–409.
- [11] P. Lall, S. Deshpande, Y. Luo, M. Bozack, L. Nguyen, and M. Murtuza, "Degradation mechanisms in electronic mold compounds subjected to high temperature in neighborhood of 200°C," *Proc. - Electron. Components Technol. Conf.*, pp. 242–254, 2014.
- [12] T.-K. Lee, H. Ma, K.-C. Liu, and J. Xue, "Impact of Isothermal Aging on Long-Term Reliability of Fine-Pitch Ball Grid Array Packages with Sn-Ag-Cu Solder Interconnects: Surface Finish Effects," *J. Electron. Mater.*, vol. 39, no. 12, pp. 2564–2573, 2010.
- [13] J. Zhang et al., "AGING EFFECTS ON CREEP BEHAVIOURS OF LEAD-FREE SOLDER JOINTS AND Reliability in Lead Free Solder Joints," *SMTA J.*, vol. 25, no. 3, pp. 19–28, 2012.
- [14] J. Zhang et al., "Thermal aging effects on the thermal cycling reliability of lead-free fine pitch packages," *IEEE Trans. Components, Packag. Manuf. Technol.*, vol. 3, no. 8, pp. 1348–1357, 2013.
- [15] R. Pufall, R. Dudek, "Degradation of moulding compounds during highly accelerated tests," pp. 2–6, 2011.
- [16] M. Goroll and R. Pufall, "Determination of adhesion and delamination prediction for semiconductor packages by using Grey Scale Correlation and Cohesive Zone Modelling," *Microelectron. Reliab.*, vol. 52, no. 9–10, pp. 2289–2293, Sep. 2012.

Reference

- [17] V. N. N. T. Rambhatla, D. Samet, S. R. McCann, and S. K. Sitaraman, "A Characterization Method for Interfacial Delamination of Copper/Epoxy Mold Compound Specimens under Mixed Mode I/III Loading," *Proc. - Electron. Components Technol. Conf.*, pp. 1888–1893, 2017.
- [18] R. Schmidt, P. Alpern, ... K. P.-P. of 2nd, and undefined 1998, "Investigation of the adhesion strength between moulding compound and leadframe at higher temperatures," ieeexplore.ieee.org.
- [19] C. L. Struik Elisa, "Physical aging in amorphous polymers and other materials door," *Polym. Eng. Sci.*, vol. 17, no. 3, pp. 1–230, 1977.
- [20] J. Verdu, *Oxidative Ageing of Polymers*. 2013.
- [21] Y. I. I. Kitagawa, M. Yoshikawa, K. Kobayashi, Y. Imakura, K. S. Im, "Thermoviscoelastic analysis of residual stresses in a thermosetting resin/metal laminated beam casused by cooling," *Chem. Pharm. Bull.*, vol. 28, no. 1, pp. 296–300, 1980.
- [22] R. B. R. Van Silfhout, J. G. J. Beijer, K. Zhang, and W. D. Van Driel, "Modelling methodology for linear elastic compound modelling versus visco-elastic compound modelling," *Proc. 6th Int. Conf. Therm. Mech. Multi-Physics Simul. Exp. Micro-Electronics Micro-Systems - EuroSimE 2005*, vol. 2005, pp. 483–489, 2005.
- [23] W. D. Van Driel, J. H. J. Janssen, G. Q. Zhang, D. G. Yang, and L. J. Ernst, "Packaging induced die stresses - Effect of chip anisotropy and time-dependent behaviour of a moulding compound," *J. Electron. Packag. Trans. ASME*, vol. 125, no. 4, pp. 520–526, 2003.
- [24] R. Keunings, "Theory of Viscoelasticity: An Introduction," *J. Nonnewton. Fluid Mech.*, vol. 13, no. 2, pp. 233–235, 1983.
- [25] J. D. Ferry, *Viscoelastic properties of polymers*. 1980.
- [26] P. Hiemenz, T. L.-N. (News & I. for Chemical, and undefined 2007, "Polymer Chemistry 2nd Edition," papersearch.net.
- [27] S. H. Chae, J. H. Zhao, D. R. Edwards, and P. S. Ho, "Characterization of viscoelasticity of moulding compounds in time domain," *Proc. ASME InterPack Conf. 2009, IPACK2009*, vol. 1, no. 4, pp. 435–441, 2010.
- [28] G. Hu, A. A. O. Tay, Y. Zhang, W. Zhu, and S. Chew, "Characterization of viscoelastic behaviour of a moulding compound with application to delamination analysis in IC packages," *Proc. Electron. Packag. Technol. Conf. EPTC*, no. 1, pp. 53–59, 2006.
- [29] L. J. Ernst, G. Q. Zhang, K. M. B. Jansen, and H. J. L. Bressers, "Time- and temperature-dependent thermo-mechanical Modelling of a packaging moulding compound and its effect on packaging process stresses," *J. Electron. Packag. Trans. ASME*, vol. 125, no. 4, pp. 539–548, 2003.
- [30] N. Srikanth, "Warpge analysis of epoxy molded packages using viscoelastic based model," *J. Mater. Sci.*, vol. 41, no. 12, pp. 3773–3780, 2006.
- [31] W. Lin and M. W. Lee, "PoP/CSP warpge evaluation and viscoelastic Modelling," *Proc. - Electron. Components Technol. Conf.*, pp. 1576–1581, 2008.
- [32] K. M. B. Jansen, "Thermomechanical modelling and characterisation of polymers, 'Course book, Delft University of Technology, WB1433,'" no. March, 2007.
- [33] V. H. Kenner, B. D. Harper, and V. Y. Itkin, "Stress relaxation in moulding compounds," *J. Electron. Mater.*, vol. 26, no. 7, pp. 821–826, 1997.
- [34] M. Lee, M. Pecht, X. Huang, and S. W. R. Lee, "Stress relaxation in plastic moulding

- compounds,” Proc. 4th Int. Symp. Electron. Mater. Packag. EMAP 2002, vol. 00, no. C, pp. 37–42, 2002.
- [35] P. J. Gromala, A. Prisacaru, M. Jeronimo, H. S. Lee, Y. Sun, and B. Han, “Non-linear Viscoelastic Modelling of Epoxy Based Moulding Compound for Large Deformations Encountered in Power Modules,” Proc. - Electron. Components Technol. Conf., vol. 1, pp. 834–840, 2017.
- [36] P. Gromala, B. Muthuraman, B. Öztürk, K. M. B. Jansen, and L. Ernst, “Material characterization and nonlinear viscoelastic modelling of epoxy based thermosets for automotive application,” 2015 16th Int. Conf. Therm. Mech. Multi-Physics Simul. Exp. Microelectron. Microsystems, EuroSimE 2015, pp. 1–7, 2015.
- [37] Daoguo Yang, “Cure-dependent viscoelastic behaviour of electronic packaging polymers : Modelling , characterization , implementation and applications,” 1999.
- [38] R. K. Lowry, K. Hanley, and R. Berriche, “Effects of temperatures above the glass transition on properties of plastic encapsulant materials,” no. Table 1, pp. 57–62, 2002.
- [39] W. L. Schultz and S. Gottesfeld, “Reliability Considerations for Using Plastic-Encapsulated Microcircuits in Military Applications,” 1994.
- [40] Y. Yao, G. Q. Lu, D. Boroyevich, and K. D. T. Ngo, “Survey of high-temperature polymeric encapsulants for power electronics packaging,” IEEE Trans. Components, Packag. Manuf. Technol., vol. 5, no. 2, pp. 168–181, 2015.
- [41] A. A. Gallo, “Effectors of high temperature reliability in epoxy encapsulated devices,” 43rd Electron. Components Technol. Conf., vol. v, pp. 356–366, 1993.
- [42] V. Ruppenthal, “Reliability of commercial plastic encapsulated microelectronics at temperatures from 125°C to 300°C,” in The Third European Conference on. IEEE, 1999, pp. 125–132.
- [43] Y. Mecheri, L. Boukezzi, a. Boubakeur, and M. Lallouani, “Dielectric and mechanical behaviour of cross-linked polyethylene under thermal aging,” 2000 Annu. Rep. Conf. Electr. Insul. Dielectr. Phenom. (Cat. No.00CH37132), vol. 2, pp. 560–563, 2000.
- [44] Y. Yao, Z. Chen, G. Q. Lu, D. Boroyevich, and K. D. T. Ngo, “Characterization of Encapsulants for High-Voltage , High-Temperature Power Electronic Packaging Characterization of Encapsulants for High-Voltage , High-Temperature Power Electronic Packaging,” vol. 26, no. 4, pp. 4–6, 2010.
- [45] E. Nguengang, J. Franz, A. Kretschmann, and H. Sandmaier, “Aging effects of epoxy moulding compound on the long-term stability of plastic package,” 2010 11th Int. Conf. Therm. Mech. Multi-Physics Simulation, Exp. Microelectron. Microsystems, EuroSimE 2010, pp. 1–6, 2010.
- [46] X. Ma et al., “Effect of aging of packaging materials on die surface cracking of a SiP carrier,” EuroSimE 2008 - Int. Conf. Therm. Mech. Multi-Physics Simul. Exp. Microelectron. Micro-Systems, pp. 5–8, 2008.
- [47] K.-F. Becker, R. , Thomas, T., Bauer, J., Kahle, R., Braun, T., Aschenbrenner, and K.-D. Schneider-Ramelow, M., Lang, “Smart power module moulding advances : Evaluating high temperature suitability of moulding compounds,” 46th Annu. IMAPS Int. Symp. Microelectron., no. Imaps, pp. 177–182, 2013.
- [48] T. Thomas, K. F. Becker, T. Braun, M. Van Dijk, O. Wittler, and K. D. Lang, “Assessment of high temperature reliability of molded smart power modules,” Proc. 5th Electron. Syst. Technol. Conf. ESTC 2014, pp. 1–7, 2014.
- [49] N. Lakhera, S. Shantaram, and A. K. Singh, “Resolution of extreme warpage in ultra-thin molded array packages under High Temperature Storage Life,” Proc. - Electron. Components

- Technol. Conf., vol. 2015-July, no. JULY 2015, pp. 380–387, 2015.
- [50] S. Manoharan, C. Patel, S. Dunford, C. Morillo, and P. McCluskey, “Aging characteristics of green mold compound for use in encapsulation of microelectronic devices,” *Proc. - Electron. Components Technol. Conf.*, vol. 2018-May, pp. 1768–1773, 2018.
- [51] X. Buch and M. E. R. Shanahan, “Thermal and thermo-oxidative ageing of an epoxy adhesive,” *Polym. Degrad. Stab.*, vol. 68, no. 3, pp. 403–411, 2000.
- [52] X. Colin and J. Verdu, “Strategy for studying thermal oxidation of organic matrix composites,” *Compos. Sci. Technol.*, vol. 65, no. 3–4, pp. 411–419, 2005.
- [53] X. Colin, C. Marais, and J. Verdu, “A new method for predicting the thermal oxidation of thermoset matrices: Application to an amine crosslinked epoxy,” *Polym. Test.*, vol. 20, no. 7, pp. 795–803, 2001.
- [54] X. Colin, C. Marais, and J. Verdu, “Thermal oxidation kinetics for a poly(bismaleimide),” *J. Appl. Polym. Sci.*, vol. 82, no. 14, pp. 3418–3430, 2001.
- [55] X. Colin, A. Mavel, C. Marais, and J. Verdu, “Interaction between cracking and oxidation in organic matrix composites,” *J. Compos. Mater.*, vol. 39, no. 15, pp. 1371–1389, 2005.
- [56] L. Olivier, C. Baudet, D. Bertheau, J. C. Grandidier, and M. C. Lafarie-Frenot, “Development of experimental, theoretical and numerical tools for studying thermo-oxidation of CFRP composites,” *Compos. Part A Appl. Sci. Manuf.*, vol. 40, no. 8, pp. 1008–1016, 2009.
- [57] J. Decelle, N. Huet, and V. Bellenger, “Oxidation induced shrinkage for thermally aged epoxy networks,” *Polym. Degrad. Stab.*, vol. 81, no. 2, pp. 239–248, 2003.
- [58] K. V. Pochiraju and G. P. Tandon, “Modelling thermo-oxidative layer growth in high-temperature resins,” *J. Eng. Mater. Technol. Trans. ASME*, vol. 128, no. 1, pp. 107–116, 2006.
- [59] G. P. Tandon, K. V. Pochiraju, and G. A. Schoeppner, “Modelling of oxidative development in PMR-15 resin,” *Polym. Degrad. Stab.*, vol. 91, no. 8, pp. 1861–1869, 2006.
- [60] S. S. Wang and X. Chen, “Computational Micromechanics for High-Temperature Constitutive Equations of Polymer-Matrix Composites With Oxidation Reaction, Damage, and Degradation,” *J. Eng. Mater. Technol.*, vol. 128, no. 1, p. 81, 2006.
- [61] S. Roy, S. Singh, and G. A. Schoeppner, “Modelling of evolving damage in high temperature polymer matrix composites subjected to thermal oxidation,” *J. Mater. Sci.*, vol. 43, no. 20, pp. 6651–6660, 2008.
- [62] M. Gigliotti, L. Olivier, D. Q. Vu, J. C. Grandidier, and M. Christine Lafarie-Frenot, “Local shrinkage and stress induced by thermo-oxidation in composite materials at high temperatures,” *J. Mech. Phys. Solids*, vol. 59, no. 3, pp. 696–712, 2011.
- [63] O. Zienkiewicz, R. Taylor, and J. Z. Zhu, *The Finite Element Method: its Basis and Fundamentals: Seventh Edition*. 2013.
- [64] R. Li, “Time-temperature superposition method for glass transition temperature of plastic materials,” *Mater. Sci. Eng. A*, vol. 278, no. 1–2, pp. 36–45, Feb. 2000.
- [65] M. L. Williams, R. F. Landel, and J. D. Ferry, “The Temperature Dependence of Relaxation Mechanisms in Amorphous Polymers and Other Glass-forming Liquids,” *J. Am. Chem. Soc.*, vol. 77, no. 14, pp. 3701–3707, 1955.
- [66] I. M. (Ian M. Ward and J. (John) Sweeney, *Mechanical properties of solid polymers*. .
- [67] H. Lu, X. Zhang, and W. G. Knauss, “Uniaxial, shear, and poisson relaxation and their conversion to bulk relaxation: Studies on poly(methy methacrylate),” *Polym. Eng. Sci.*, vol. 37,

- no. 6, pp. 1053–1064, 1997.
- [68] J. De Vreugd, “The effect of aging on moulding compound properties,” no. March, 2011.
- [69] K. M. B. Jansen et al., “Modelling and characterization of moulding compound properties during cure,” *Microelectron. Reliab.*, vol. 49, no. 8, pp. 872–876, Aug. 2009.
- [70] H. Roberts, D. Leonard, K. Vandewalle, M. C.-D. Materials, and undefined 2004, “The effect of a translucent post on resin composite depth of cure,” Elsevier.
- [71] M. Mengel, J. Mahler, and W. Schober, “Effect of Post-mold Curing on Package Reliability,” *journals.sagepub.com*, vol. 23, no. 16, pp. 1755–1765, 2004.
- [72] D. Yang, K. Jansen, L. Ernst, ... G. Z.-M., and undefined 2007, “Numerical Modelling of warpage induced in QFN array moulding process,” Elsevier.
- [73] J. De Vreugd et al., “Advanced viscoelastic material model for predicting warpage of a QFN panel Thermal cycling of Fibre Metal Laminates View project Interface properties of Copper and Moulding Compound View project Advanced Viscoelastic Material Model for Predicting Warpage of a QFN Panel,” *ieeexplore.ieee.org*, 2008.
- [74] K. M. B. Jansen et al., “Constitutive Modelling of moulding compounds [electronic packaging applications] Semiconductor reliability View project Prognostics and Health Management of safety relevant electronics for future application in autonomous driving View project Constitutive Modelling of Moulding Compounds,” *ieeexplore.ieee.org*, 2004.
- [75] J. Park, J. Kim, M. Yuen, ... S. L.-K. E., and undefined 1998, “Thermal stress analysis of a PQFP moulding process: Comparison of viscoelastic and elastic models,” *repository.ust.hk*.
- [76] G. Kelly, C. Lyden, W. Lawton, J. B.-... T. P. B, and undefined 1996, “Importance of moulding compound chemical shrinkage in the stress and warpage analysis of PQFPs,” *ieeexplore.ieee.org*.
- [77] G. Hu, J. Luan, S. C.-J. of, and undefined 2009, “Characterization of chemical cure shrinkage of epoxy moulding compound with application to warpage analysis,” *asmedigitalcollection.asme.org*.
- [78] J. H. Aklonis, W. J. MacKnight, M. Shen, and W. P. Mason, *Introduction to Polymer Viscoelasticity*, vol. 26, no. 5. 1973.
- [79] K. Oota and M. Saka, “Cure shrinkage analysis of epoxy moulding compound,” *Polym. Eng. Sci.*, vol. 41, no. 8, pp. 1373–1379, Aug. 2001.
- [80] Y. Wang and P. Hassell, “Measurement of Thermally Induced Warpage of BGA Packages/Substrates Using Phase-Stepping Shadow Moiré.”
- [81] K. Verma, D. Columbus, and B. Han, “Development of Real Time/Variable Sensitivity Warpage Measurement Technique and its Application to Plastic Ball Grid Array Package,” 1999.
- [82] Noriyuki KinjoMasatsugu OgataKunihiko NishiAizou KanedaK. Dušek, “Epoxy Moulding Compounds as Encapsulation Materials for Microelectronic Devices.” .
- [83] S. Murali, N. Srikanth, C. V. I.-M. research bulletin, and undefined 2003, “An analysis of intermetallics formation of gold and copper ball bonding on thermal aging,” Elsevier.
- [84] D. D. Lu and C. P. Wong, *Materials for advanced packaging*. Springer US, 2009.
- [85] C. J. Hang, C. Q. Wang, M. Mayer, Y. H. Tian, Y. Zhou, and H. H. Wang, “Growth behaviour of Cu/Al intermetallic compounds and cracks in copper ball bonds during isothermal aging,” 2007.

Reference

- [86] J. De Vreugd, K. Jansen, ... L. E., M. & Multi, and undefined 2010, "High temperature storage influence on moulding compound properties," ieeexplore.ieee.org.
- [87] M. Johlitz, "On the representation of ageing phenomena," *J. Adhes.*, vol. 88, no. 7, pp. 620–648, Jul. 2012.
- [88] Z. Cui, M. Cai, R. Li, P. Zhang, X. Chen, and D. Yang, "A numerical procedure for simulating thermal oxidation diffusion of epoxy moulding compounds," *Microelectron. Reliab.*, vol. 55, no. 9–10, pp. 1877–1881, Aug. 2015.
- [89] R. Li, D. Yang, P. Zhang, F. Niu, M. Cai, and G. Zhang, "Effects of high-temperature storage on the elasticity modulus of an epoxy moulding compound," *Materials (Basel)*, vol. 12, no. 4, Feb. 2019.
- [90] D. G. Yang et al., "Effect of high temperature aging on reliability of automotive electronics," in *Microelectronics Reliability*, 2011, vol. 51, no. 9–11, pp. 1938–1942.
- [91] R. Pufall, M. Goroll, ... M. B.-3rd E., and undefined 2010, "Adhesion of moulding compounds on various surfaces. A study on moisture influence and degradation after high temperature storage," ieeexplore.ieee.org.
- [92] D. Leveque, A. Schieffer, A. Mavel, J. M.-C. science and, and undefined 2005, "Analysis of how thermal aging affects the long-term mechanical behaviour and strength of polymer–matrix composites," Elsevier.
- [93] B. Dippel, M. Johlitz, and A. Lion, "Ageing of polymer bonds: A coupled chemomechanical modelling approach," *Continuum Mechanics and Thermodynamics*, vol. 26, no. 3. Springer New York LLC, pp. 247–257, 2014.
- [94] B. Musil, M. Johlitz, ... A. L. the 9th E. conference on, and undefined 2015, "Chemical ageing of polymers-experiments and modelling," books.google.com.
- [95] X. Ma, K. Jansen, ... L. E.-... and M.-P., and undefined 2008, "Effect of aging of packaging materials on die surface cracking of a SiP carrier," ieeexplore.ieee.org.
- [96] N. Lakhera, ... S. S.-2015 I. 65th E., and undefined 2015, "Resolution of extreme warpage in ultra-thin molded array packages under High Temperature Storage Life," ieeexplore.ieee.org.
- [97] E. Nguegang, J. Franz, ... A. K.-, M. & Multi, and undefined 2010, "Aging effects of Epoxy Moulding Compound on the long-term stability of plastic package," ieeexplore.ieee.org.
- [98] A. Mavinkurve, ... L. G.-2013 E., and undefined 2013, "Epoxy moulding compounds for high temperature applications," ieeexplore.ieee.org.
- [99] K.-F. Becker et al., "Smart Power Module Moulding Advances: Evaluating high temperature suitability of Moulding Compounds," *Int. Symp. Microelectron.*, vol. 2013, no. 1, pp. 000177–000182, Jan. 2013.
- [100] S. Kuroda, I. M.-E. polymer journal, and undefined 1989, "Degradation of aromatic polymers—II. The crosslinking during thermal and thermo-oxidative degradation of a polyimide," Elsevier.
- [101] X. Colin, C. Marais, J. V.-P. Testing, and undefined 2001, "A new method for predicting the thermal oxidation of thermoset matrices: application to an amine crosslinked epoxy," Elsevier.
- [102] J. Decelle, N. Huet, V. B.-P. D. and Stability, and undefined 2003, "Oxidation induced shrinkage for thermally aged epoxy networks," Elsevier.
- [103] S. Manoharan, C. Patel, ... S. D.-2018 I. 68th, and undefined 2018, "Aging characteristics of green mold compound for use in encapsulation of microelectronic devices," ieeexplore.ieee.org.

- [104] A. T.-56th E. C. and Technology and undefined 2006, “Effect of environments on degradation of moulding compound and wire bonds in PEMs,” ieeexplore.ieee.org.
- [105] S. Watzke, P. A.-W.-2014 15th International, and undefined 2014, “Degradation of silicone in white LEDs during device operation: a finite element approach to product reliability prediction,” ieeexplore.ieee.org.

